AN ABSTRACT OF THE DISSERTATION OF

Kate C. Fickas for the degree of Doctor of Philosophy in Forest Ecosystems and Society presented on July 25, 2018.

Title: The Benefits of Time: Characterizing Intra-and Inter-Annual Variability in Oregon Wetland Ecosystems Using the Landsat Spectral-Temporal Domain.

Abstract approved: _____

Warren B. Cohen

The use of Landsat data has historically been constrained to spectral and spatial information derived from a carefully selected image or set of images. However, free and open access to Landsat imagery combined with advances in data storage and computing are revolutionizing how the Landsat temporal domain is used to map and monitor land surface properties and land cover change. Since the opening of the USGS archives in 2008, many different time series analysis approaches have been developed without a unified framework for characterizing information extracted from dense time series of Landsat imagery.

In Chapter 1, we define Spectral-Temporal Features (STFs) as discrete or continuous features derived from time series of remotely sensed observations. Like spectral indices, STFs represent a transformation of the original image data and can provide new information about land surface properties and other biophysical parameters. STFs offer a number of improvements over conventional spectral or spatial inputs, including seamless coverage over large extents, more consistent and stable feature sets for classification through time, and new information on both spectral and temporal variability in reflectance that can be related to biophysical parameters.

To demonstrate how STFs can be applied in practice, we present a series of case studies spanning a range of geographic locations within different ecosystem types, and study objectives. These case studies illustrate relationships between different STFs and various biophysical

parameters and yield insight into the specific ecological metrics that can be discovered and characterized with the spectral-temporal domain.

With the release of collection-style Landsat products and continued advances in pre-processing algorithms, as well as availability of tiled Analysis Ready Data and improved access to cloud- and cluster-based computing resources such as Google Earth Engine, the Australian Data Cube, and Sentinel Hub, time series approaches are becoming increasingly prevalent. We argue that STFs provide new information on both spectral and temporal variability in reflectance in different ecosystems that can be related to biophysical parameters. Thus, there is a critical need to continue to review and standardize the discussion and application of STFs for locally-accurate mapping and monitoring of forested ecosystem dynamics.

In Chapter 2, we test the utility of primary STFs derived from time series of all available Landsat TM/ETM+ observations, including Global Surface Water (GSW) features, for discriminating among wetlands at different categorical resolutions within the National Wetlands Inventory (NWI) classification taxonomy. We examine two key types of primary STFs, 1) reflectance STFs, which characterize reflectance values of spectral indices used, and 2) day of year (DOY) STFs, which quantify the timing of their associated reflectance STFs. As an exploratory measure, we also abstract and evaluate spatial-temporal climate features, such as the per-pixel annual maximum of daily maximum temperature, to yield insight into potential drivers of wetland characterization. Using an NWI reference dataset from two Oregon ecoregions in distinctly different eco-hydrological climate zones, we test classification agreement and examine relative performance of different classification inputs across ecoregions and wetland categories. We test an array of classifications that use consistent training and testing datasets, but vary the features and feature-sets used as model inputs. Beyond classification performance, we also explore categorical-level agreement and the importances of different features for differentiation within different wetland categories. Our aim is not to estimate the accuracy of the reference NWI map or monitor wetland change over time and space, but rather to build a framework for multi-level wetland classification across climate gradients.

We found that STFs feature-sets consistently produced high overall accuracies and were able to accurately delineate wetland habitats across climate gradients and wetland categorical

resolutions even further when combined with other features. Additionally, accuracies decreased with increasing categorical resolution in both energy-and water-limited ecosystems. Evaluation of individual feature importance for distinguishing between different wetland habitats showed that different features are more important for different climate gradients and categorical resolutions. However, GSW Occurrence was consistently valuable for both ecoregions across all categorical resolutions, exemplifying the value of utilizing the GSW dataset for wetland classification. Further, although not all types of features were found to be important in overall classification, in quantifying correlations between individual features and individual wetland habitat classification probabilities, we found that all feature types were had and strong positive and negative correlations with individual habitats. This indicates the importance of using the various features as inputs for wetland classification.

In Chapter 3, we use all available Landsat imagery from 1985 - 2017 to explore how Pacific Northwest wetland ecosystems are changing over time in different climate zones and at varying categorical resolutions. Additionally, we investigate the long term changes in abstracted Landsat spectral-temporal features that are closely associated with different aspects of wetland hydro-ecological processes. We found that our annual classification model built from Landsat spectral-temporal features, climate-temporal features, and ancillary datasets performs well in showing change in wetland habitat. Individual STFs also display distinct changes in intra-annual wetland dynamics in the context of wetland land use change. In terms of long term wetland change, Willamette Valley wetlands are trending toward more non-vegetated wetlands, fewer vegetated wetlands, and extreme annual-conditions with the lower extrema occurring earlier in the year. In addition to other drivers, this change may be attributed to increased precipitation and increased temperature. In contrast North Basin wetlands are trending towards more vegetated wetlands, fewer non-vegetated wetlands, and extreme annual-conditions with the lower extrema occurring earlier in the year, except for max TCW which is trending towards later annual occurrence. Timing and persistence are key for wetland habitats and this study begins the work to examine change in both occurrence of wetland habitat type and timing of key hydrologic and phenological features and ecosystem drivers.

The Benefits of Time: Characterizing Intra-and Inter-Annual Variability in Oregon Wetland Ecosystems Using the Landsat Spectral-Temporal Domain

by
Kate C. Fickas

A DISSERTATION

submitted to

Oregon State University

in partial fulfillment of
the requirements for the
degree of

Doctor of Philosophy

Presented on July 25, 2018
Commencement June 2019

Doctor of Philosophy dissertation of Kate C. Fickas presented on July 25, 2018

APPROVED:

Major Professor, representing Forest Ecosystems and Society

Head of the Department of Forest Ecosystems and Society

Dean of the Graduate School

I understand that my dissertation will become part of the permanent collection of Oregon State University libraries. My signature below authorizes release of my dissertation to any reader upon request.

Kate C. Fickas, Author

CONTRIBUTION OF AUTHORS

Chapter 1: Dr. Valerie Pasquarella[1,2,3] contributed a significant portion of effort towards the chapter design, writing, data processing, literature review, result interpretation, and development, refinement, and editing of the chapter. Dr. Warren Cohen[4,5], Dr. Zhiqiang Yang[4], and Dr. Curtis Woodcock[3,6] contributed to the conceptual development of and provided significant guidance and editing support for the chapter. Paulo Arevalo[6] contributed data processing and graphics of the South American case study design and conceptual support of the case study text as well as conceptual support and editing of the chapter. Eric Bullock[6] contributed data processing and graphics of the Southeast Asian case study design and conceptual support of the case study text as well as conceptual support and editing of the chapter. Shijuan Chen[6] and Yingtong Zhang[6] contributed data processing and graphics of the Canadian case study design and conceptual support of the case study text. Dr. Pontus Olofsson[3,6] and Christopher Holden[6] contributed conceptual insight in the chapter. All contributors listed here are also co-authors on a manuscript in-progress that incorporates work from this chapter.

Chapter 2: Dr. Warren Cohen[4,5] contributed to the development of and provided editing support for the chapter. Dr. Zhiqiang Yang[4] provided processing of time series Landsat products for comparative analysis (which were not included in the final version of the dissertation) as well as assistance in Google Earth Engine code development for data processing used in this chapter. Dr. Valerie Pasquarella[1,2,3] provided python code which assisted in the classification of Landsat time series analytics as well as support and guidance on data processing techniques used in this chapter.

Chapter 3: Dr. Warren Cohen[4,5] contributed to the development of the chapter and editing support.

[1] Department of Environmental Conservation, University of Massachusetts Amherst, Amherst, MA

[2] DOI Northeast Climate Adaptation Science Center, Amherst, MA

[3] Center for Remote Sensing, Boston University, Boston, MA

[4] Department of Forest Ecosystems & Society, Oregon State University, Corvallis, OR

[5] USDA Forest Service, Pacific Northwest Research Station, Forestry Sciences Laboratory, Corvallis, OR

[6] Department of Earth and Environment, Boston University, Boston, MA

TABLE OF CONTENTS

LIST OF FIGURES

LIST OF TABLES

CHAPTER 1
THE BENEFITS OF TIME: CHARACTERIZING THE LANDSAT SPECTRAL-TEMPORAL DOMAIN

Introduction

The land surface properties and dynamics that can be distinguished from remotely sensed imagery are largely determined by the spectral, spatial and temporal characteristics of available images and image collections. In its most basic form, an image acquired by an optical remote sensing instrument is a collection of digital numbers recorded for each pixel over a continuous area at a given time (Cracknell 1998; Strahler et al. 1986). Although these observations--which are typically corrected to measures of top of atmosphere and/or surface reflectance--may serve as direct inputs for land surface characterization and change detection, observed values can also be transformed to enhance information content and highlight particular patterns and properties (Wulder et al. 2016). There is a long-standing use of image data transformation in the spectral and spatial domains and these transforms have been, and continue to be, utilized in a broad range of applications (e.g. Cohen and Goward 2004; Pettorelli et al. 2005). However, we argue that the integration of the spectral and temporal domains has lacked a formalized characterization.

Unlike spectral and spectral-spatial analyses, which maximize the information content of individual images, spectral-temporal analyses rely on information extracted from multi-date image stacks. While the use of spectral-temporal transforms has been more prevalent for sensors with a high temporal resolution, such as the Advanced Very High Resolution Radiometer (AVHRR) and the Moderate Resolution Imaging Spectrometer (MODIS), the opening of the Landsat archive in 2008 (Woodcock et al.

2008) has resulted in a dramatic increase in the use of dense time series of Landsat imagery. With continued advances in automated pre-processing algorithms (e.g. Loveland and Dwyer 2012; Markham and Helder 2012; Masek et al. 2008; Zhu and Woodcock 2012) and improved access to cloud- and cluster-based computing resources (e.g. Gorelick et al. 2017), combined with the reorganization of the Landsat archive into tiered collections designed to "provide a consistent archive of known data quality to support time-series analyses and data 'stacking', while controlling continuous improvement of the archive and access to all data as they are acquired" (USGS 2017), more researchers and end-users are able to work directly with multi-temporal observations. Furthermore, with the Landsat and European Space Agency's Sentinel programs both providing free access to their complementary data streams, we expect both the use and density of Landsat and Landsat-like time series will only continue to increase going forward. Thus, there is a critical need to formalize a description of the spectral-temporal domain within the context of other remote sensing domains, e.g. spectral and spectral-spatial, and to provide practical examples of spectral-temporal products and applications.

In this paper, we first review the use of the spectral, spectral-spatial, and spectral-temporal domains and present a conceptual framework that generally applies to both spatial and temporal analysis of remotely sensed imagery. We then focus on recent advances in the use of the Landsat spectral-temporal domain and provide a series of case studies illustrating the information content of various spectral-temporal

combinations. Our goals are to (1) support efforts to generate, utilize and discuss spectral-temporal products or "features", as well as to (2) display the breadth of applications that could benefit from the evolving use of the spectral-temporal domain, especially for Landsat data .

Background

Spectral, Spectral-Spatial, and Spectral-Temporal Transforms

The spectral domain is the foundation of optical remote sensing. Analysis of spectral data assumes that surface materials can be distinguished based on distinct reflectance profiles (Jordan 1969; Ollinger 2010; Price 1994). Though the use of data from individual spectral bands from both broadband and hyperspectral sensors remains common in image processing and classification (e.g. Chang et al. 1999; Cohen et al. 2018), a long history of spectral analysis has resulted in development of numerous spectral indices and transformations that can be applied to individual images to further emphasize particular land surface properties.

Broadly defined, *spectral indices* are transformations of two or more spectral bands constructed to augment various components of landscapes. These indices are computed directly, without any bias or assumptions regarding cover class or climate conditions (Huete et al. 2002). With the continued advancement of civilian remote sensing instruments programs, many spectral indices that highlight general landscape components such as vegetation and soil properties have been developed such as the

normalized difference vegetation index (NDVI), the normalized burn ratio (NBR), and the normalized difference water index (NDWI). This basic spectral information can then be further extended by characterizing the spatial and temporal context of spectral observations.

The spatial context of spectral observations describes the structure of the imaged landscape (Woodcock and Strahler 1987). Thus, *spectral-spatial* analysis characterizes spectral properties in relation to their spatial arrangement, and typically is conducted for individual images (i.e. bands x rows x columns). Given the tendency to work with single-date imagery, the use of spatial-spectral domain is relatively well-established (Adams et al. 1986, Keshava and Mustard 2002, Asner et al. 2011). However, space-borne remote sensing platforms, as well as some regular aerial surveys, also offer a unique opportunity to analyze time series of imagery (Gómez et al. 2016).

The temporal context of spectral observations describes the spectral variability of the imaged landscape, revealing both short- and long-term patterns and processes (Coppin 2004, Kennedy et al. 2014). *Spectral-temporal* analysis transforms spectral information-based temporal relationships, and utilizes stacks of imagery, resulting in a time series of observations for each pixel (i.e. bands x time). As more applications integrate spectral-temporal analysis, there is a need to describe the use of the spectral-temporal domain in the context of existing remote sensing approaches.

We have identified a set of methods used to generate analogous spectral-spatial and spectral-temporal features. These methods, *rescaling*, *moving window*, and *segmentation*, can be applied to both image data (e.g. arrays of pixels) and time series (e.g. repeated observations for an individual pixel) (Figure 1). Though the focus of this paper is on the use of the spectral-temporal domain, we find extending concepts from the spatial to the temporal domain provides a sound foundation for analysis in both of these core dimensions.

Rescaling

Rescaling operations, as we consider them here, depend on a fixed user-specified spatial or temporal interval size. When observations are spatially rescaled or aggregated, spectral values within non-overlapping n-by-n pixel neighborhoods are used to calculate spectral-spatial features, which could include block statistics (Chavez et al. 1991) as well as texture metrics (Blan and Butler 1999; Hamunyela et al. 2016; Irons and Petersen 1981; Reiche et al. 2018; Wolock and Price 1994). Similarly, when observations are temporally rescaled, spectral values are grouped by a user-specified temporal interval, such as calendar year or season. The result of re-scaling operations are images or time series with a reduced number of values that summarize information content over discreet areas or intervals (Al-Bakri and Suleiman 2004; Hansen et al. 2002; Helldén and Tottrup 2008; Ricotta et al. 1999) (Figure 1).

Moving Window

Moving window operations are another type of neighborhood method used to smooth or "filter" observed data. Unlike rescaling, which is based on discrete, non-overlapping spatial or temporal intervals, a single spectral observation can contribute to multiple estimates produced by moving window approaches (Figure 1). In the spectral-spatial domain, moving windows can be used to generate block statistics, texture metrics (Arai, 1993; Chica-Olmo and Abarca-Hernández 2000; Miranda et al. 1992) and measures of autocorrelation (Anselin 1995; Getis and Ord 1992; Paez and Scott 2004; Qi and Wu 1996; Wulder and Boots 1998). In the temporal domain, smoothing operations can also be used to generate summary statistics, such as moving averages or variance (Archibald and Scholes 2007; Beck et al. 2006; Chen et al. 2004; Hird and McDermid 2009; Ma and Veroustraete 2006; Reed et al. 1994; Velleman 1980; White et al. 2009), as well as more complex interpolated values such as splines (Bradley et al. 2007; Fan and Yao 2008; Hermance et al., 2007; Jonsson and Eklundh 2002), filters (Chen et al. 2004;), and LOWESS (Cleveland 1979; Nagendra 2010).

Segmentation

A final methods for calculating spectral-spatial and spectral-temporal features is segmentation (Figure 1). In spatial segmentation, spectral-spatial information is used to automate the assignment of pixels to larger objects and features (Benz et al. 2004; Dey et al. 2010; Ryherd et al. 1996; Woodcock and Harward 1992). Similarly,

in the spectral-temporal domain, temporal segmentation is used to automatically partition time series of observations into a set of segments and breaks (e.g. Chance et al. 2016; Kennedy et al. 2010; Keogh 2001; Hermosilla et al. 2015 a.,b.; Zhu et al. 2014). Properties of objects and segments, as well as differences between adjacent boundaries and segment-based spectral values provide new information about landscape properties and dynamics.

Primary and Secondary Spectral-temporal Features (STFs)

Having established a general set of methods that can be applied across both spatial and temporal dimensions, we further explore the features produced by these methods specifically for the temporal domain. Rescaling, moving window, and segmentation methods may be applied to a time series of spectral observations in any number of ways. For example, a re-scaling approach could be applied to generate a time series of annual means, then a model could be fit to these means to identify breaks and segments. Alternatively, segments could be identified from all observed data, then means could be generated for each segment. Because of the ability to utilize and chain multiple methods in feature creation, there is a need to further differentiate between different categories of spectral-temporal features based on the characteristics of the data they are generated from.

To distinguish these different types of features, we use the terms *primary* and *secondary* features. Specifically, we consider spectral-temporal features (STFs)

calculated directly from observed time series of spectral observations, indices or transforms to be "primary" STFs (Table 1). These STFs include standard population summary metrics such as the minimum, maximum, mean, median and range, and can be computed for any temporal interval or segment. Though some assumptions must be made regarding the underlying distribution of observed spectral values, primary STFs are the result of a direct transformation of an observed spectral time series.

An additional category of "secondary" STFs can be produced when parametric or non-parametric smoothing functions or models are fit to observed data. Secondary STFs include modeled interval/segment attributes, as well as land cover change features. A variety of different modelling approaches for extracting spectral-temporal information have been developed (Table 2). For example, many change detection approaches rely on regression models to fit a series of breaks and segments to dense time series of reflectance observations. Coefficients from these models, including model intercepts, trends, and harmonic amplitudes and phases, would be considered secondary STFs. The use of fitted models also enables the production of additional STFs that estimate model error/residuals, such as RMSE and correlation coefficients, which can be used to characterize model uncertainty as well as stochasticity in reflectance dynamics. Thus, through the use of model fitting, secondary STFs can provide a second tier of information on land surface properties and change.

Synthetic images

An added benefit of generating model-based secondary STFs is the ability to produce interpolated or "synthetic" spectral observations, essentially upsampling or increasing the frequency of observed values. Unlike true primary and secondary STFs, which are a transformation of the spectral-temporal domain over a given interval (e.g. the mean of a single year or range over a segment), synthetic observations are predicted values for a particular date or point in time (e.g. predicted NDVI for a given day of year). By predicting spectral values from a continuous fitted curve, synthetic images eliminate issues of cloud cover, reduce noise in the temporal signal, and enable the production of images for days between overpasses (Gao et al. 2006).

Synthetic images tend to provide more stable estimates of long-term reflectance patterns (Kennedy et al. 2010), and provide greater flexibility in the choice of image dates used for analysis (Zhu et al. 2014). For example, Cohen et al. (2017) use both observed time series and time series of synthetic Landsat imagery to evaluate different change detection products, while Pasquarella et al. (2017) difference observed and synthetic images to characterize short-term changes in ecosystem condition. We include synthetic images in our discussion of STFs as they are closely associated products and offer an alternative to compositing approaches for producing cloud-free images (e.g. White et al. 2014). With improved access to time series of moderate resolution broad-band imagery combined with advances in

computing and modeling approaches, continued development and utilization of synthetic images is expected.

Case Studies in the Landsat Spectral-Temporal Domain

Use of the spectral-temporal domain is primarily limited by the availability of regularly acquired, high quality calibrated imagery. The launch of the first Landsat satellite (formally known as ERTS-1) marked the advent of space-based Earth observing systems and a significant advance in the collection of regularly repeated observations of the global land surface (Lauer et al. 1997; Williams et al. 2006; Loveland and Dwyer 2012). However, prior to the opening of the Landsat archive in 2008, time series analysis of remotely sensed imagery tended to focus on sensors with high temporal resolution and open data access policies (Wulder et al. 2016).

AVHRR imagery (1981-present) has been used for decades to characterize land surface phenology (Heumann et al. 2007; Jonsson and Eklundh 2002, 2004; White et al. 2009). More recently, time series of MODIS observations have been used to map global land cover using spectral-temporal features such as EVI phenology (Friedl et al. 2002), forest composition using features calculated from harmonic models (Wilson et al. 2012), and disturbance processes using maximum land surface temperature and EVI (Mildrexler et al. 2009) and thermal anomalies (Mildrexler et al. 2018). These studies clearly demonstrate the utility of the spectral-temporal domain

for a variety of applications; however, the coarse spatial resolution of AVHRR and MODIS presents a significant challenge for monitoring highly heterogeneous ecosystems and landscapes (Wulder et al. 2016).

While interest in the Landsat spectral-temporal domain has increased over time (Collins and Woodcock 1994; Collins and Woodcock 1996; Oetter et al. 2001; Schroeder et al. 2007; Song et al. 2002, 2007), prohibitive costs and processing requirements historically limited how many Landsat images could be included in any given analysis, resulting in both restricted use of STFs and a more limited concept of change (Coppin et al. 2004; Kennedy et al. 2014). Today, with free and open access to Landsat imagery, it is now possible to generate STFs from dense time series of all clear Landsat observations (Kennedy et al. 2014).

The evolving use of the Landsat spectral-temporal domain has recently been discussed in other reviews, particularly in the context of large-scale land cover and land cover change mapping (Gomez et al. 2016; Wulder et al. 2016) and change detection (Zhu 2017). Our conceptual framework, including methods for generating spectral-temporal features, characterization of primary and secondary STFs and description of synthetic imagery produced from interpolated models, provides a more generalized overview of the use of the spectral-temporal domain. We support the application of our framework with a series of case studies to illustrate how STFs calculated from Landsat time series can be used for land surface mapping and monitoring.

We begin with a general example of how STFs are calculated and visualized (New England, USA). We then present examples of STF applications for representing diverse geographies and a range of ecosystem processes, including identifying plantation species (Southern Thailand), mapping forest recovery and floodplain forest variability (Colombia Amazon), characterizing forest disturbance (Western Canada) and monitoring wetland dynamics (Pacific Northwest, USA) (Figure 2). Our goal is to highlight the evolving suite of STFs that can be calculated from Landsat and Landsat-like datasets, as well as the detailed information content these STFs can be used to explore and characterize.

Selecting And Visualizing STFs (New England, USA)

A time series of observations for an individual pixel (or group of pixels) can be used to calculate any number of spectral-temporal features. The features ultimately selected for analysis will depend on the application and objectives. To illustrate our approach to exploring and visualizing STFs, we will use a classic example of "before-after" land cover change, i.e. an abrupt change from one relatively stable land cover to another. Specifically, we will consider an example of urban development where forested area in the Northeastern United States was converted from temperate mixed-deciduous forest to impervious surface cover, in this case, a shopping mall (Figure 3).

The change in land cover from forest to impervious surface results in a distinct change in spectral-temporal attributes of the example pixel across all Landsat bands. More conventional before-after approaches that compare images acquired on two different dates could suffice for identifying this step-like pattern of change, and observed values (those not obscured by clouds or shadows) could possibly be used to assign before and after land cover labels (e.g. Coppin 2004). However, even in the case of "simple" before-after change, the use of the full record of observations enhances information content while reducing reliance on any individual observation and associated uncertainty (e.g. Kennedy et al. 2014; Pasquarella et al. 2016).

We calculated annual STFs, specifically the mean and 90th percentile, for a time series of Tasseled Cap Greenness (TCG) observations. We also fit a harmonic break detection model (CCDC; Zhu et al. 2014) to the same time series to illustrate differences in the resulting characterizations of the spectral-temporal trajectory for this pixel (Figure 3). We chose to show time series of TCG because the land cover change of interest involves the removal of vegetation; however, similar features could be calculated for any spectral band, index or transform.

In general, we find that annual STFs are more sensitive to year-to-year variability in the reflectance signal. As would be expected, the deciduous vegetation shows a larger range of TCG values annually than the impervious surface, which is consistently near zero for both the mean and range. These patterns are also well-characterized by the harmonic break detection model. In this case, the time

series has been divided into two temporal segments, each with an associated set of secondary STFs, such as the model intercept and amplitude of the annual (12-month) harmonic. Individual STF values may be used to characterize land cover at a particular point in time. Fitted models can also be used to predict reflectance values at any given point in time (i.e. points along curve in bottom panel of Figure 3).

When change processes are of interest, the differences in values of annual and segment-based STFs can be calculated across years to produce a set of secondary change features. For example, we define a set of "delta-Tasseled Cap" or "dTC" features that represent the different in TC values from one harmonic model segment to another. These dTC features provide information on the magnitude and direction of spectral change, and have great potential for use in change process attribution.

While single-band, single-pixel visualizations are a useful starting point for exploring the spectral-temporal domain, multi-band RGB rasters and scatter plots provide additional tools for examining spectral-temporal patterns across pixels. STF values for each pixel can be assigned to the Red, Green and Blue channels of a raster image to show both spatial patterns and the relative values of multiple STFs. In some cases, it may be desirable to examine the same STF, e.g. annual mean, calculated for different spectral bands or transforms, e.g. TCB, TCG and TCW (Figure 4, d-f). It may also be useful to compare different features for the same transform, e.g. segment-based harmonic model intercept, annual amplitude and RMSE for TCG (Figure 4, g-i). Difference features, such as the aforementioned dTC

features (Figure 4, j-l), and predicted values, e.g. synthetic images (Figure 4, m-o), can also be displayed as multi-band rasters.

In visualizing our development example as a series of STF rasters (Figure 4), we see spatial, spectral, and temporal variability in the calculated values, and there are notable differences across the various methods and combinations of spectral values. For example, the annual features for 2007 likely include areas just being cleared, therefore early signs of development are evident in the raster visualization. In the segment-based features, a more linear feature, likely a road, is detected as having changed by 2007, and results in a somewhat different spatial pattern than that shown by the annual features. The annual features also suggest a greater range of variability when comparing the developed areas in the 2015 rasters, which makes sense given the more stable nature of model parameters. It is worth noting that the range of variability is greater for the dTC visualization, which includes multiple TC bands, compared to the harmonic visualization that only includes TCG features, suggesting the benefit of utilizing a variety of STFs.

To further examine the separability of different surface attributes and processes spectral-temporal feature space, we can produce series of two-dimensional scatterplots for STF values. Like the Tasseled Cap planes presented by Kauth and Thomas (1976), these plots allow us examine pairwise comparisons of the three STFs used to create the RGB image. By coloring data points to match corresponding colors in the RGB image, we can see clustering in land cover types and/or surface processes.

In the following case studies, we visualize different STFs first through RGB images, where different STFs are mapped to the red, green, and blue channels individually, and then through two-dimensional scatterplots for STF values to show the spectral separability of different STFs in classification and change detection.

Using harmonic STFs to map plantation species (Thailand)

Forest plantations represent special case of forest type mapping, as they typically represent systematically arranged monocultures of a single species. Yet despite their relatively homogeneous composition, the identification of specific plantation species can be difficult due to the similarity in their canopy structure to that of a primary forest (*Global Forest Resources Assessment,* 2015). While this spectral similarity makes single-date imagery of limited use, differences in the spectral-temporal characteristics of primary forest and various plantation species can aid in their distinction. For example, the seasonal defoliation of rubber trees during the monsoon season gives them a unique phenological profile (Dong et al., 2013).

Secondary STFs generated from harmonic models are particularly well-suited for forest mapping applications because maturing forests typically exhibit relatively stable seasonal cycles and long-term dynamics. Thus, harmonic features characterize long-term patterns while remaining relatively robust to noise. We fit harmonic (CCDC) models to Landsat time series stacks covering the Southern Thailand (Figure 5). Exploratory analysis indicated that short-wave indices showed the greatest

differences among native forest, palm plantations and rubber plantations, therefore, we chose to visualize the model intercept for first Short-wave band (SWIR1), which characterizes a long-term baseline reflectance, as well as sine and cosine coefficients for the Normalized Difference Moisture Index (NDMI), which characterize phenological patterns (timing of seasonal events) (Figure 5).

We find that native forest and the two types of plantations show visually distinct spectral-temporal patterns. The NDMI sine and cosine terms of the native forest are close to zero, whereas palm has negative cosine and positive sine, and rubber has the opposite--a negative NDMI sine and positive NDMI cosine. This difference in the sine and cosine STFs across plantation types and between plantation and native forest suggests improved discrimination is possible. Additionally, both cloud cover and data availability are significant limiting factors in many tropical areas where plantation agriculture is most extensive. Therefore, the use of harmonic models aids in minimize noise and fill temporal gaps, resulting in secondary STFs like those used in this case study that can be generated for any date and used as inputs for any number of classification methods.

Using Trend STFs To Map Forest Regrowth (Colombia)

Secondary STFs that characterize trends are particularly useful for examining gradual change processes (Vogelmann et al. 2012; Vogelmann et al. 2016). In many countries, attempting operational deforestation monitoring,

monitoring forest regrowth is also an important goal. Trend analysis can be performed directly on time series of observations (e.g. Czerwinski et al. 2014), and segment-based change detection approaches typically include a trend term as part of regression modeling (Zhu et al. 2014, Kennedy et al. 2010, Brooks et al.).

We extracted model slope terms from harmonic (CCDC) models fit to time series of NIR and two SWIR bands for an actively disturbed forested landscape in the Colombian Amazon (Figure 6). When the slope terms of these three STFs are combined into an RGB image, we find that pixels with near-zero trends in all three bands are mapped in gray tones, while regrowth is mapped in shades of green, indicating a positive slope in the NIR and negative slopes in the SWIR bands (Figure 6). This matches well with the expected spectral-temporal pattern of regrowth, with increasing vegetation cover and density making the land surface brighter in the NIR and darkers in the SWIR.

This relatively simple secondary STF approach enables first-level visual identification of potential areas of regrowth. The spatial coherence of trend patterns is encouraging, and fits the expectation that disturbances and subsequent recovery have a patchy distribution on this landscape. Given the ongoing development of time-series-based change detection and validation methods for tropical deforestation monitoring (e.g. DeVries et al. 2016), information on spectral-temporal trends is becoming more readily available and, as shown in this

case study, trend-based secondary STFs reveal interesting new perspectives on long-term forest dynamics.

Using Harmonic Change STFs For Forest Change Agent Attribution (Western Canada)

While exploring spectral-temporal trends for individual bands is useful for examining specific types of gradual change, many different change agents may be acting on a particular landscape at a given point in time, with resulting changes occurring at a range of spatial and temporal scales (Kennedy et al 2014). At a most basic level, time series change detection algorithms typically produce binary maps of changed and unchanged areas, often with additional information on the timing of change. However, temporal segmentation results can also be used to estimate spectral-temporal trajectories and extract secondary change or "delta" STFs that provide information on the magnitude and direction of change.

We use synthetic image generated from harmonic break detection models (CCDC; Zhu et al. 2014) to calculate change in the three Tasseled Cap (TC) components between two anniversary dates (1985-1999). Different forest change processes common to the landscapes of Western Canada, including fire, logging and regrowth, show distinct patterns in associated delta TC or "dTC" features (Figure 7). As would be expected, disturbance processes (fire, logging) show opposite trends across all three TC components compared to recovery processes (regrowth). Logging appears to result in a larger increase in TCB and decreased in TCW than fire or

regrowth, with each process forming distinct clusters in spectral-temporal feature space (Figure 7).

Using Primary STFs To Map Wetland Condition (Pacific Northwest, USA)

Most work in wetland ecological characterization and classification using satellite imagery has employed single-date classification, two-date change detection, or short-term (0–5 years) change detection using annual images (e.g. Baker et al. 2007; Frohn et al. 2009; Johnston and Barson 1993; Lunetta and Balogh 1999; Wright and Gallant 2007). However, with the augmented availability of Landsat data, time-series analysis for detailed characterization of both inland and coastal wetlands has increased as researchers recognize the power of the temporal domain for identifying key wetland dynamics (Fickas et al. 2016; Halabisky et al. 2016; Hermosilla 2018; Pasquarella 2016; Sagar et al. 2017, 2018). Although continuous, modeled STFs have been found to be more robust than single and multi-date image stacks in forest type classification (Pasquarella et al. 2018), intra-annual freshwater wetland dynamics can display too much natural variability to be fit to a spectral harmonic model or time series segmentation. Sinusoidal harmonic models, such as CCDC (Zhu et al. 2014), are most accurate in characterizing ecosystems that have predictable intra-annual cycles (such as forests) and less ecologically defensible and accurate when fitting curves to habitats with inter-annual and/or intra-annual

variability. Therefore, wetland time series data may not contain enough spectral consistency to fit a robust sinusoidal curve.

Here, we utilize a conceptually and computational simple primary STF, the statistical range of the Tasseled Cap Transformation (TC) spectral index, to characterize wetlands in the Pacific Northwest, USA, based on their annual spectral variability (Figure 8). The annual statistical range is derived by differencing the maximum and minimum values from individual TC B,G, and W bands for each year. Broadly, this STF uses observed (rather than modeled) data to represent the within period variability of a given wetland pixel. The pixels chosen to demonstrate the power of the statistical range are from wetland areas in the Malheur National Wildlife Refuge (MWR) of Eastern Oregon.

We visualize STF data from two Palustrine National Wetland Inventory (NWI) wetland hydroperiods in the MWR: semipermanently Flooded and seasonally flooded wetlands. The statistical range of TCB, TCG, and TCW for the year 1995 are mapped to the red, green, and blue channels respectively (Figure 8). Semipermanently flooded wetlands show high annual variability in TCB and TCW but relatively low variability in TCG. In contrast, seasonally flooded wetlands show relatively higher variability in TCG and lower variability in TCB and TCW. The TC range exemplifies the ability of computationally simply STFs to highlight separability in fine categorical classification, such as wetland hydroperiods.

Discussion

The use of Landsat data has historically been constrained to spectral and spatial information derived from a carefully selected image or set of images. However, free and open access to Landsat imagery combined with advances in data storage and computing are revolutionizing how the Landsat temporal domain is used to map and monitor land surface properties and land cover change. In addition to the availability of tiled Analysis Read Data (ARD) products, continued advances in pre-processing algorithms, improved access to cloud-and cluster-based computing resources such as Google Earth Engine, the Australian Data Cube, and Sentinel Hub, time series approaches are becoming increasingly prevalent. However, many different time series analysis approaches have been developed without a unified framework for characterizing information extracted from dense time series of Landsat imagery.

We argue that STFs provide new information on both spectral and temporal variability in reflectance in various ecosystems that can be related to biophysical parameters. Thus, there is a critical need to continue to review and standardize the discussion and application of STFs for locally-accurate mapping and monitoring of forested ecosystem dynamics. Our conceptual framework builds on the long traditions of spatial and spectral analysis of remotely sensed imagery and aims to provide a unified means of describing methods for generating STFs. STFs offer a number of improvements over conventional spectral or spatial inputs, including seamless

coverage over large extents, more consistent and stable feature sets for classification through time, and new information on both spectral and temporal variability in reflectance that can be related to biophysical parameters.

STFs in Practice

Our case studies emphasize several important aspects of STFs to consider when utilizing features for classification or change detection of remotely sensed time series imagery. First, the breadth of features that we employ in our case studies demonstrates that many different STFs can be generated from the same time series of observations. However, the selection of which spectral transform(s) and spectral-temporal analysis methods will depend on the process the user is trying to characterize. Temporal segmentation approaches and associated secondary STFs work well for land cover with relatively stable reflectance signatures, like forests. Use of temporal segmentation and/or model fitted features has additional benefit of change detection features through predicted spectral-temporal trajectories. More dynamic systems, like wetlands, require STFs with a finer temporal grain. In these systems, primary STFs tend to offer more flexibility and can be used to characterize changes in reflectance for shorter time steps. However, these features are more subject to ephemeral noise and natural variability than modeled features, therefore additional filtering/QA may be required during exploratory phase.

In addition to careful consideration for which type of STF to use in a given system based on spectral-temporal variation, STF users must also recognize

limitations in data density. More robust primary and secondary STFs can be produced for pixels with a greater number of high quality, cloud free observations. However, the number of observations per pixel varies geographically as a function of acquisition strategies, downlink capabilities, and atmospheric conditions/cloud cover (Wulder et al. 2016). In places with fewer cloud-free observations, shorter summary periods (e.g. seasonal, annual) may not be suitable. Attention must also be given to periods of missing data, which are common in places served from non-US receiving stations. The total number of cloud-free observations also varies substantially depending on whether one or two Landsat satellites are in operation, and more stable primary STFs and more accurate time series models can generally be produced following the launch of Landsat 7 in 1999. Thus, an important consideration for any study utilizing STFs will include the features that can reliably be calculated given the data density.

Spectral-Temporal Features and Spectral Composites

In considering STF visualization, it is important to note that STF images are distinct from best-available-pixel (BAP) image composites (Roy et al. 2010; White et al. 2014; Hermosilla et al. 2015; Hermosilla et al. 2016). Here, we distinguish the two categories by data-utilization objectives and purposes. Many STFs, such as the mean, variance or modeled annual amplitude, represent a new transformation of the existing reflectance values, while other STFs, such as the maximum and minimum, are existing values from individual images chosen using a selection criteria. The

objective of STFs, therefore, is to abstract new information from an existing dataset for the purpose of characterizing land surface properties. BAP composites, on the other hand, are generated and scored from rule-based algorithms to eliminate cloud, shadow, snow, water or other cover, maximize phenological criteria (such as peak NDVI), and target specific acquisition timestamps or image overlaps (White et al. 2014). Under this categorization, the objective of composites is to construct the first step in land cover classification by creating high-quality, seamless, large-area images that are free of clouds (or other masked categories/contamination) for the purpose of further image analysis. While composite imagery is becoming increasingly common in land cover and land cover change mapping applications (e.g. Huang et al. 2010, Kennedy et al. 2010), composited pixel values from different images could potentially influence higher-level analysis products such as classification results (Pasquarella et al. 2018).

The Future of STFs

Simple visualization techniques applied to the case studies presented here indicate separability of land surface types and processes that go beyond what would have been possible using only the spectral or spectral-spatial domain. We believe this is just the beginning for STFs. With improved access to time series analysis code, image collections, and cloud-based computing resources, we expect to see increased availability and use of STF datasets as well as the development of new models for characterizing the spectral-temporal domain. Specifically, to increase the potential for

future, high quality time series data analysis, it is essential that data that are consistently processed to the highest scientific standards and level of processing required for direct use in applications. Further, the ability to reduce the burden of processing on data users, could yield a path towards dense time series as the standard in classification and change detection. We believe that dense time series analysis and products will advance at unprecedented rates with global ARD data products. Tiled ARD datasets integrate reflectance observations at a pixel (rather than scene) level, facilitating analysis of time series of all available Landsat observations for a given location. ARD will help users, who currently have to download and process large amounts of Landsat image-based data for time series analysis, consistently analyze time series data faster and with greater repeatability. Though ARD data was not necessarily used for all of the case studies presented in this paper, in developing the framework presented here, we assume that STFs can (and should) be calculated from time series of all available high-quality surface reflectance (and brightness temperature) observations, and that ARD (and the Collection data used to produce it) will become the standard data source for generate STF datasets going forward.

In addition to ARD and ARD-like products, Landsat integration with other sensors will augment time series observation density creating more robust STFs and STF products. The Sentinel-2A satellite was successfully launched in summer of 2015, as part of the European Copernicus program. Sentinel-2 carries a wide-swath, high-resolution, multispectral imager (MSI) with 13 spectral bands (Drusch et al.

2012). The minimum five-day global revisit time (with two satellites in concurrent orbit) creates the beginning of a very dense remote sensing time series. Similar to Landsat, Sentinel data are freely available at the global scale and also have comparable spectral resolutions and the same geographic coordinate system as the Landsat data; this creates an important opportunity to fuse the two types of satellite sensor data together. Together, these two sensors can collect more frequent observations and be utilized for continuous monitoring. Landsat and Sentinel data integration creates a very high temporal resolution data stream that reduces limitations of STF use in areas that can be frequently obscured by clouds or processes, such as fine scale phenology, that require high temporal resolution for observation and detection.

Spectral-Temporal-Spatial Features

Though we do not wish to conflate our spectral-temporal feature conceptual model with the addition of the spatial domain, we do want to note that spectral-temporal-spatial features (STSFs) are the next step in merging the separate remote sensing data domains (i.e. spatial, spectral, and temporal). One example of an early STSF is the Healey et al. 2005 Disturbance Index (DI). The DI was developed to emphasize the un-vegetated spectral-temporal responses associated with forest disturbance and isolate them from all other forest features. Specifically, the DI is a linear combination of the three TC indices and applies the theory that recently cleared forest systems exhibit high TCB and low TCG and TCW in relation to undisturbed

forests. To employ the DI transformation, for every pixel, each TC index value is re-scaled to its standard deviation above or below the entire image's mean forest value. For example

$TCB_r = (TCB - TCB_\mu)/ TCB_\sigma$ where TCB = pixel TCB value, TCB_r = rescaled TCB, TCB_μ = mean forest TCB, and TCB_σ = standard deviation of forest TCB. Once the three TC indices are normalized, they are transformed linearly to create DI: $DI = TCB_r - (TCG_r + TCW_r)$. A single image DI transformation is a distinct example spectral-spatial feature, where the TC indices act as the spectral features and rescaling based on image-wide statistics operates as the spatial domain component. However, the DI can, theoretically, be applied consistently to any image date *or* be re-scale based on both spatial and temporal statistics of any image size or temporal interval. Adding the temporal domain to the spectral-spatial feature then creates a spectral-temporal-spatial feature. This is only one example of spectral-temporal-spatial features but, as spatial, spectral, and temporal image boundaries disappear with ARD, multi-sensor integration, and cloud-based data processing, we expect a conceptual model of the spectral-temporal-spatial domain as the next step in dense time-series analysis.

CHAPTER 1 FIGURES

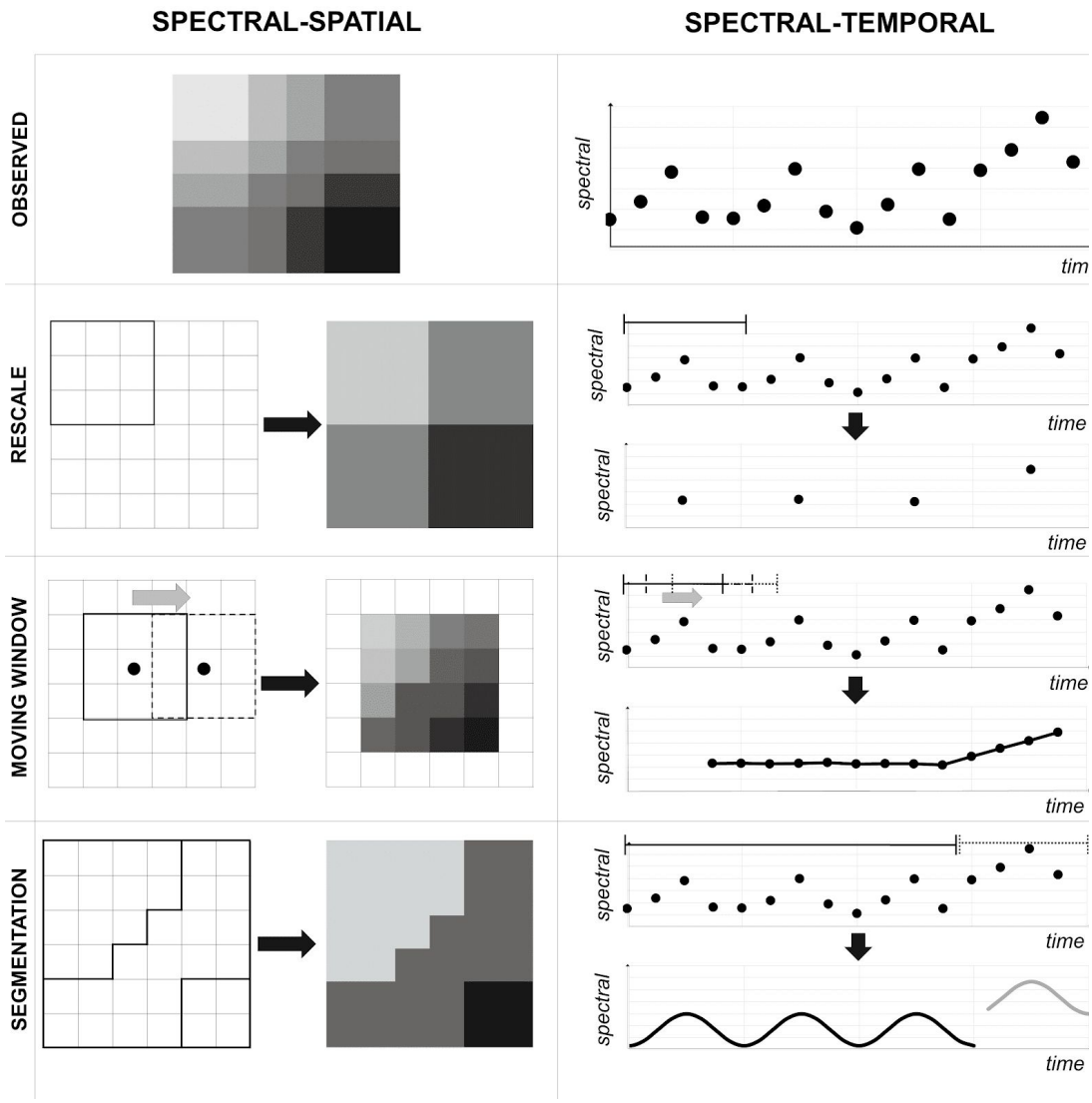

Figure 1.1: Analogue methods for extracting information from the spectral-spatial and spectral-temporal domains.

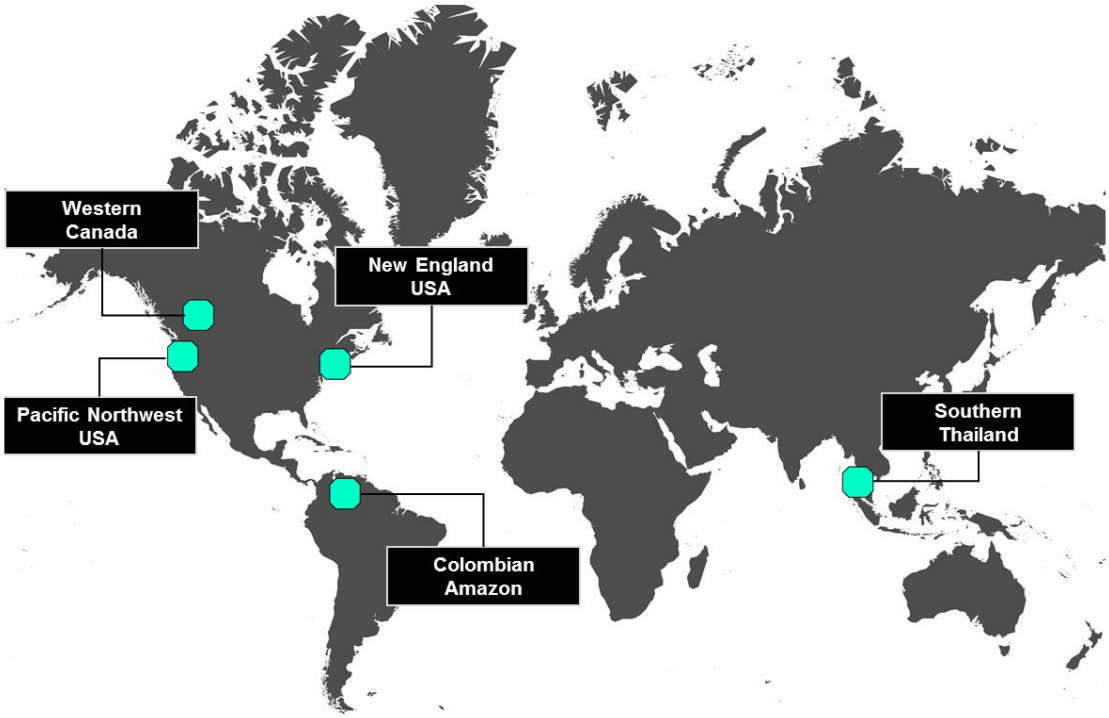

Figure 1.2: Global locations of case studies.

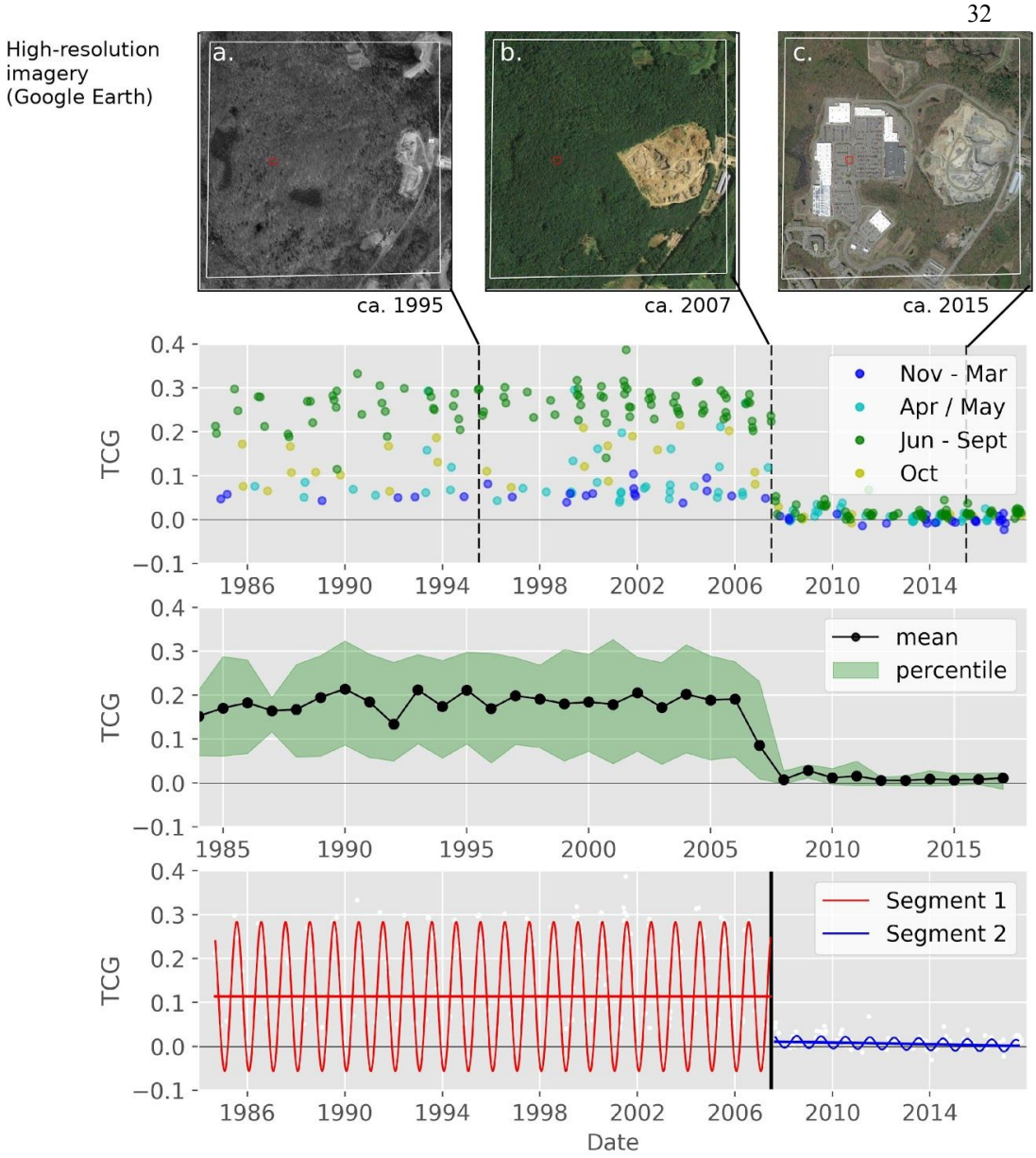

Figure 1.3: Examples of different STFs calculated for a Landsat time series of Tasseled Cap Greenness.

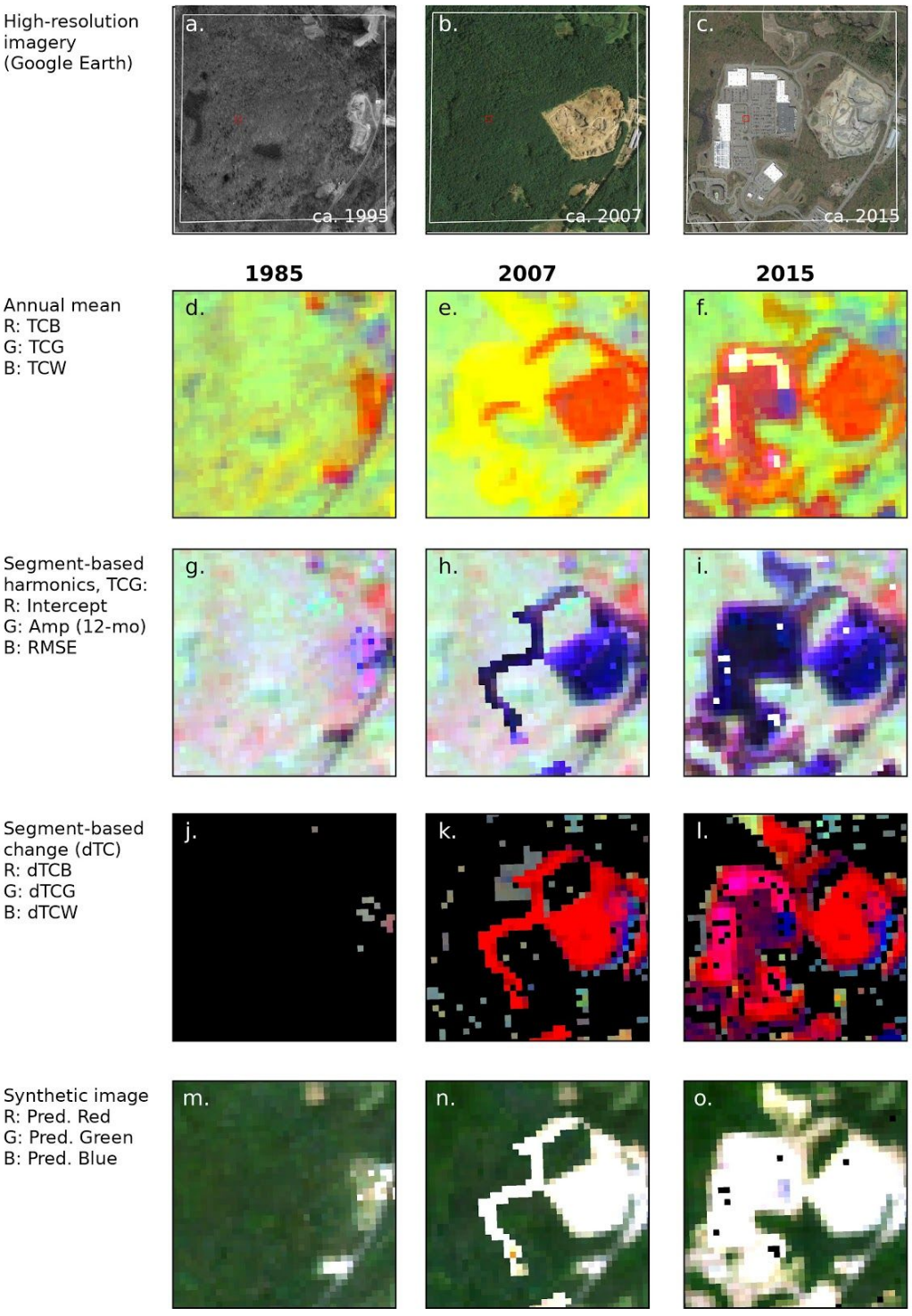

Figure 1.4: Examples of STF rasters that help display the spatial, spectral, and temporal variability in the calculated STF values.

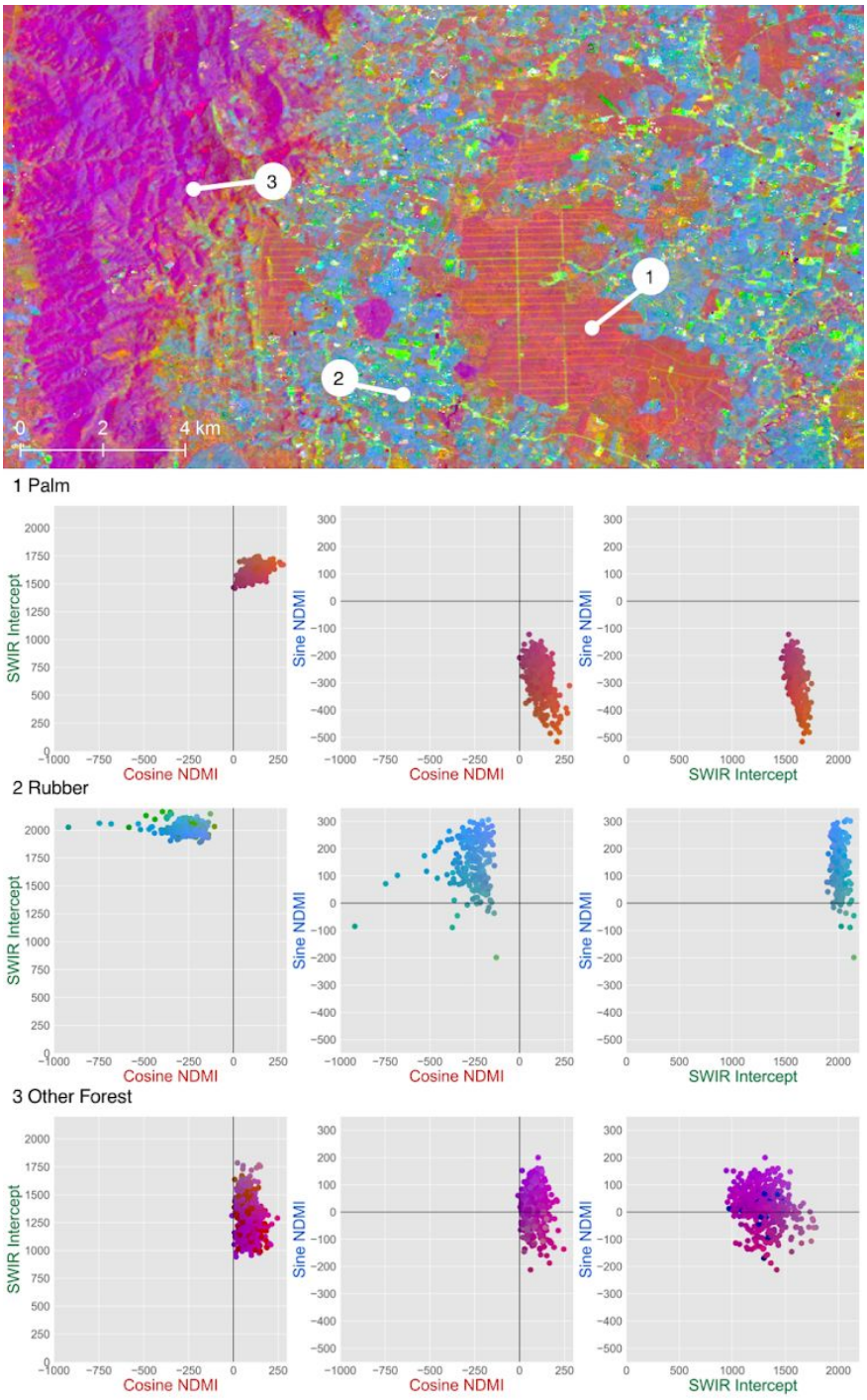

Figure 1.5: Examples of harmonic STFs for plantation species in Southern Thailand

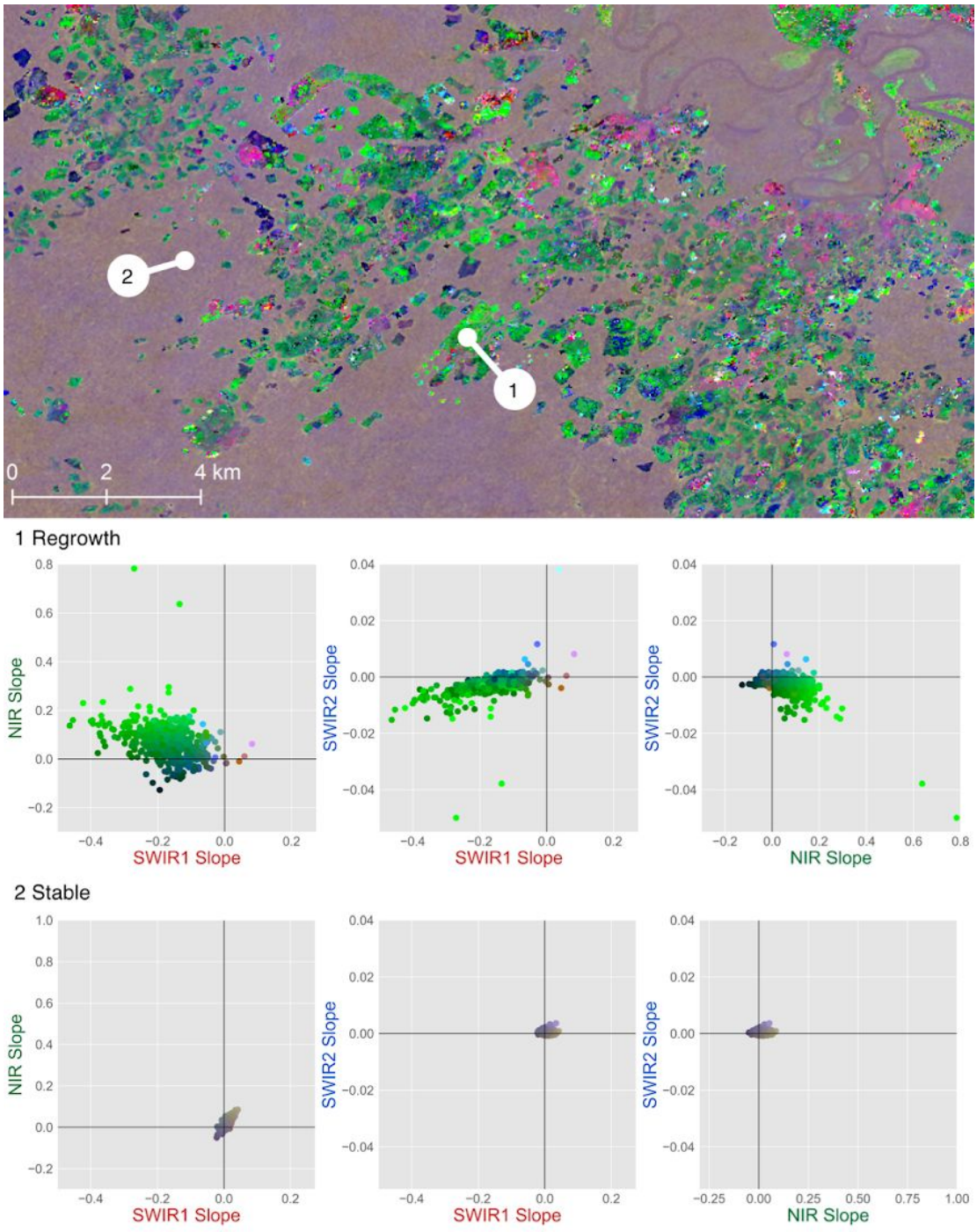

Figure 1.6: Examples of trend STFs for forest regrowth in the Columbian Amazon.

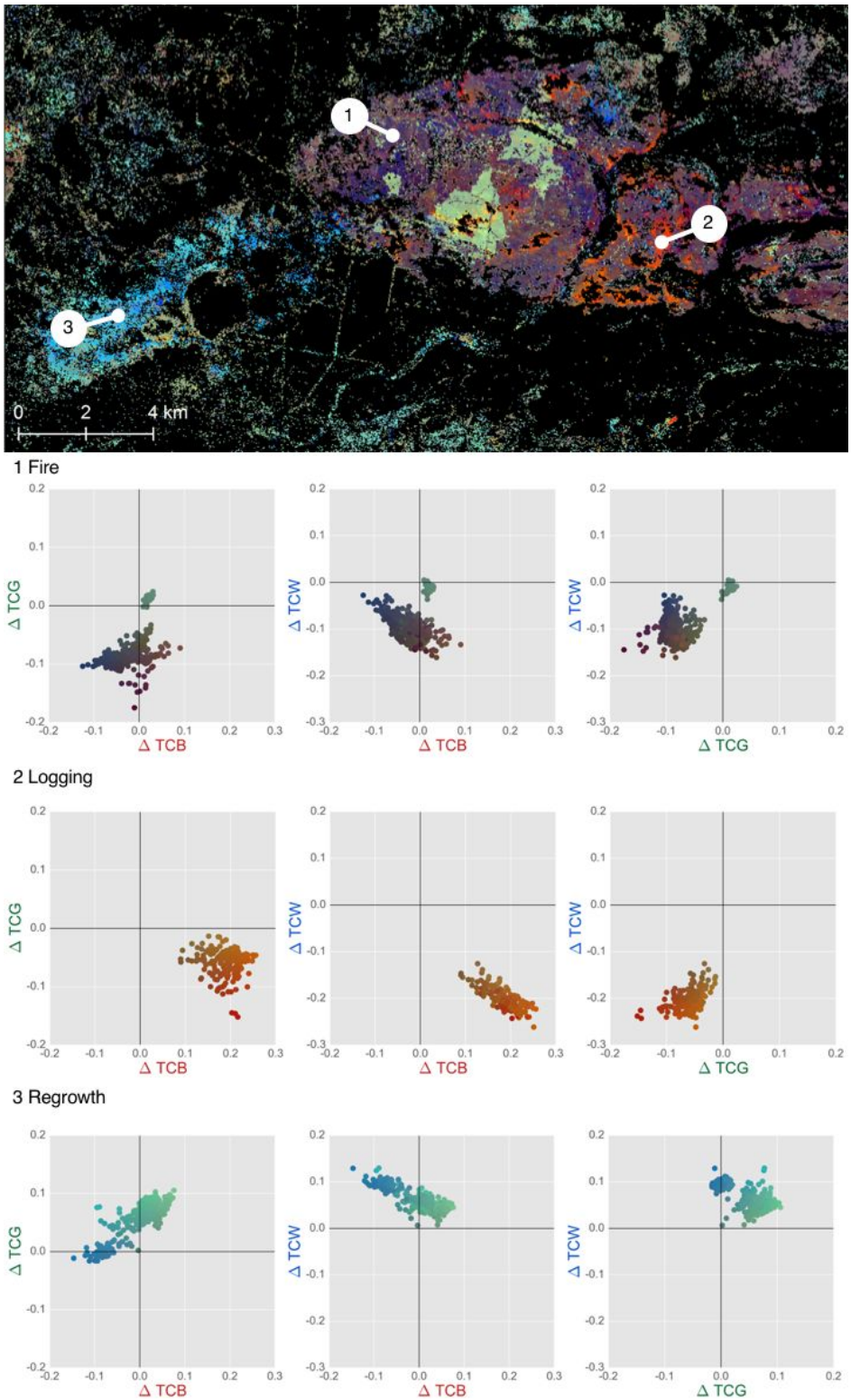

Figure 1.7: Examples of harmonic change STFs for forest change agent attribution in Western Canada.

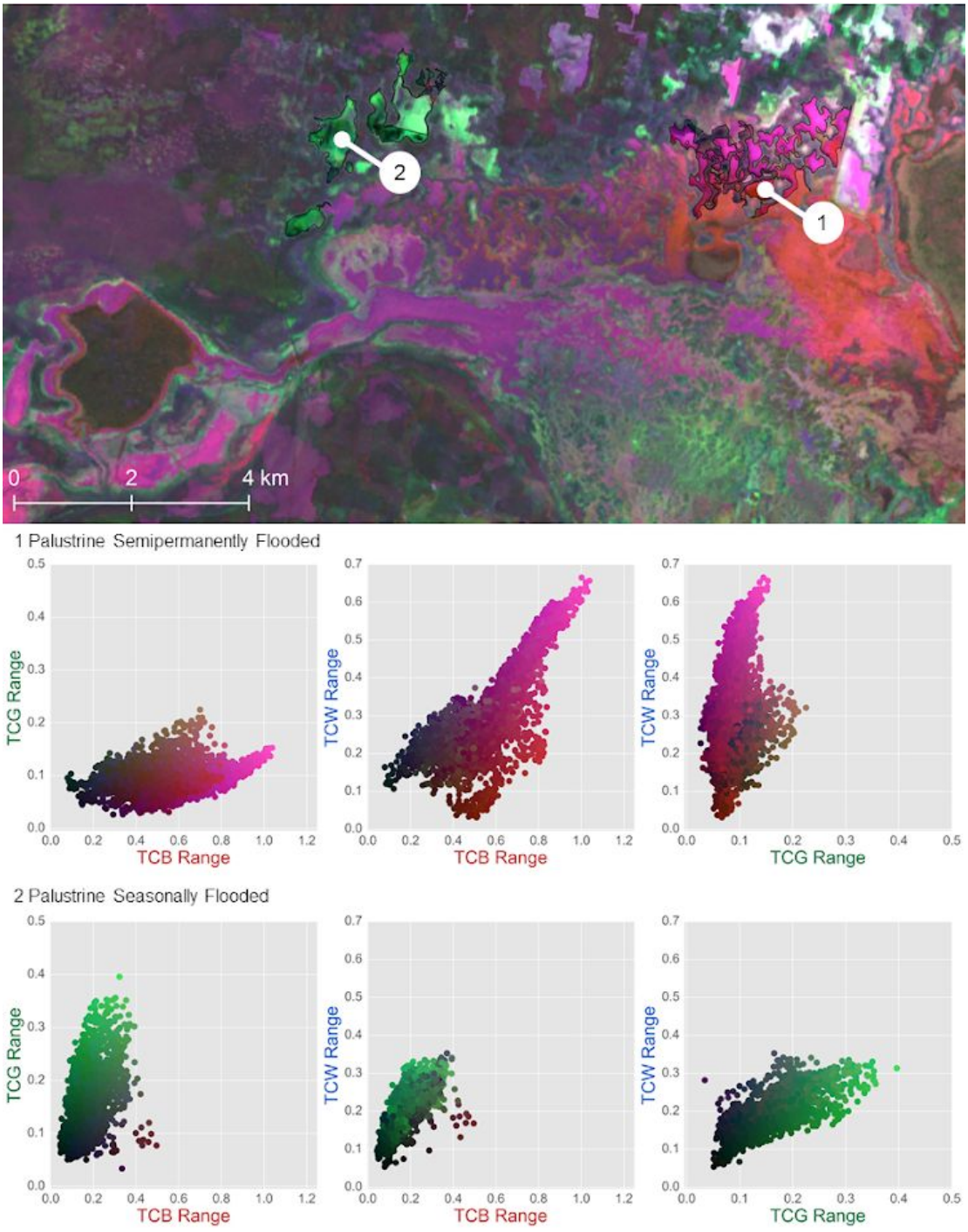

Figure 1.8: Examples of primary STFs to map wetland condition in the Pacific Northwest, USA

CHAPTER 1 TABLES

Feature	Description	Example Applications
Maximum (Max), Minimum (Min)	Measures of ordered extremes in reflectance	Maximum annual NDVI (DeFries et al. 1995)
Mean, Median, Medoid	Measures of reflectance averages and central tendency	Mean reflectance values for observations between selected percentiles (Potapov et al. 2012)
Range, Variance, Quantiles, Percentiles	Measures of variability in reflectance	Forest z-score (FZ) and integrated forest z-score (IFZ) (Huang et al. 2010) Normalized Spectral Index (NSD) (Jin et al. 2013) Spectral Vegetation Variability Index (SVVI) (Coulter et al. 2016).

Table 1.1: Examples of primary STFs. These metrics are calculated directed from time series of remotely sensed observations

Feature	Description	Algorithm
Intercept	Long-term reflectance	Image Trends from Regression Analysis (Vogelmann et al. 2012) LandTrendr (Kennedy et al. 2010,2012) BFAST (Verbesselt et al. 2010) Exponentially Weighted Moving Average Change Detection (Brooks et al. 2014) CCDC (Zhu et al. 2014) VerDET (Hughes et al. 2017)
Slope (Trend)	Long-term trend in reflectance	
Amplitude (Seasonal)	Strength of signal in a given frequency, e.g. annual	BFAST (Verbesselt et al. 2010) EWMACD (Brooks et al. 2014) CCDC (Zhu et al. 2014)
Phase (Seasonal)	Temporal offset of harmonic in a given frequency	
Start of season	Long-term mean timing of spring	Melaas et al. 2013
End of season	Long-term mean timing of autumn	
Growing season length	Days between start and end of season	
DOY of peak greenness (e.g. EVI)	Timing of maximum vegetation greenness	
Model error (e.g .RMSE, r)	Measure of model goodness-of-fit,	Melaas et al. (2013) CCDC (Zhu et al. 2014)
Number of changes	How many times a change was detected	LandTrendr (Kennedy et al. 2010, 2012)

Date of change	Timing of each change	BFAST (Verbesselt et al. 2010) EWMACD (Brooks et al. 2014) CCDC (Zhu et al. 2014) VCT (Huang et al. 2010) MIICA (Jin et al. 2013) VerDET (Hughes et al. 2017)
Magnitude of change	Before-after change in reflectance values	
Synthetic images	Model-generated values for any band, any date	CCDC (Cohen et al. 2017; Pasquarella et al. 2016; Zhu et al. 2015) Splines (Bullock et al. 201X)

Table 1.2: Examples of secondary STFs. These metrics are estimated from models fit to time series of remotely sensed observations, and examples of algorithms that can be used to generate each feature are provided.

CHAPTER 2

CHARACTERIZING INTRA-ANNUAL VARIABILITY IN WETLAND ECOSYSTEMS USING THE LANDSAT SPECTRAL-TEMPORAL DOMAIN: A FRAMEWORK FOR MULTI-LEVEL CLASSIFICATION ACROSS CLIMATE GRADIENTS

Introduction

As key ecosystems across the planet, Wetlands are found on every continent except Antarctica (Fraser and Keddy 2009). Providing a wide variety of ecosystem services, wetlands are known to cleanse polluted waters, protect shorelines, recharge groundwater aquifers, buffer flood and drought severity, and provide unique habitat to a wide variety of plants and animals (Mitsch and Gosselink 2000). A wetland ecosystem occurs when inundation by water produces soils dominated by anaerobic processes that force the biota to adapt to flooding (Keddy 2014). Bridging the gap between terrestrial and aquatic ecosystems, wetlands have both coastal (saltwater) and interior (freshwater) areas with the global majority characterized as freshwater (Lehner and Doll 2004). Despite their ubiquity and importance, the planet has lost roughly 50% of its wetlands since 1900 (Nicholls 2004). In the United States, nearly half of all states have lost more than 50% of their wetland area between the 1780s and the 1980s (Dahl 1997) with losses continuing into the present (Dahl and Stedman 2013, Fickas et al. 2015).

The National Wetlands Inventory

To protect and conserve the nation's remaining wetlands, it is essential to know and understand where, how, and when wetland resources are changing. To help answer these questions, the U.S. Fish and Wildlife Service (USFWS) began the

National Wetland Inventory (NWI) in 1974 as an endeavor to map and monitor the nation's wetlands. The NWI utilizes digital delineation of single-date aerial photography, remote sensing data, field work, and other ancillary cover class maps such as soils and land use (Wilen and Bates 1995). The NWI has been the workhorse for U.S. wetland mapping and monitoring for three decades, providing five reports to congress on the Status and Trends of Wetlands and Deepwater Habitats of the Conterminous United States (FGDC 2013). However, the NWI is a federal program with an enormous task and limited budget and must balance detail and accuracy with precision. NWI products are slow to update, with some maps over two decades old (Gibbs 2000). Priorities for mapping have been centered on the data needs of the USFWS and partners and the availability of funding and high-quality aerial photographs. Nationally, work has been focused on coastal zones, prairie wetlands, playa lakes, flood plains of major rivers, and areas of importance to the nation's waterfowl (Wilen et al. 1996). While many individual wetland mapping and monitoring products and projects exist in the peer-reviewed and grey literature across the country at finer scales and higher accuracies, the NWI is still the most widely available and suggested tool for monitoring wetlands in the U.S. (Stolt and Baker 1995, Kudray and Gale 2000, Johnson 2013).

Ideally, NWI wetland aerial-photo interpretation delineation methodology calls for a late-spring image to capture both wetland hydrology and vegetation but, often, images available are from summer, when vegetation in other ecosystems, such

as forests, is most robust (Beeri et al. 2007). Summer imagery is particularly problematic for wetland delineation as wetlands are usually driest in the summer months and it can be hard to distinguish between wetlands and similar upland ecosystems such as grasslands (Daniels 2006, Schroeder et al. 2011, Fickas et al. 2015). Beyond issues with date of acquisition, the concerns with single-date wetland classification have far-reaching consequences. Wetlands are fundamentally transient and transitional in nature with ecological morphologies based on both allogenic and autogenic factors that can shift in influence throughout the year and from year to year or decade to decade (Mitsch and Gosselink 2015).

In particular, wetland hydroperiod – the seasonal pattern of the water level of a wetland and a wetland's hydrologic signature (Snodgrass et al. 1996) – cannot, by definition, be distinguished with single-date imagery. Some wetlands, such as prairie potholes, vary considerably from year to year depending on climate and a wet-dry cycle of 10 to 20 years may be observed. Other wetlands, such as alluvial swamps in the southeastern U.S., may react distinctly to precipitation events rather than observe a general seasonal pattern (Brinson et al. 1980). Hydrology is considered one of the single most important determinant characteristics of establishment and persistence of wetlands and wetland processes (Zhang et al. 2012, Todd et al. 2010) and forms the specific ecological conditions that make wetland habitats distinct from upland terrestrial systems. If wetlands are only observed at a snapshot in time with varying map recurrence, it is hard to distinguish seasonal, yearly, or decadal spatial,

hydrological, and ecological patterns from variability in imagery acquisition date. Consequently, robust categorical classification of wetlands compared to uplands and within wetland categories themselves, is dependent on a high-temporal resolution of data to capture intra-annual hydrologic and vegetation variability.

Remote Sensing of Wetlands

In 1992, the Federal Geographic Data Committee determined that the use of remote sensing satellite imagery (including Landsat) to aid in federal wetland mapping lacked the required spatial resolution for classification detail and wetness designation that aerial photography provided (FGDC 1992). However, with the launch of a free and open Landsat archive in 2008 and there is now over 45 years of freely available, high quality annual imagery, offering the longest running time series of systematically collected remote sensing data (Cohen and Goward 2004). Additionally, development of algorithms for deriving information from Landsat time series (e.g. Zhu and 2012; Melaas et al., 2013; Zhu and Woodcock, 2014; Brooks et al., 2014; DeVries et al., 2015) has advanced opportunities to use the Landsat temporal domain to improve classification of many different land use types. Rather than using single images or image sets to distinguish land use and land cover classes, it is now possible to characterize both spectral and temporal variability from dense time series of all available observations (Kennedy et al., 2014; Pasquarella et al., 2016, Pasquarella et al. 2018). Although challenging, it is essential to begin to

understand how to utilize the power of the entire Landsat archive to classify and monitor both U.S. and global wetlands.

Global Surface Water

Similar to wetland ecosystems, un-vegetated surface water dynamics present a classification and delineation challenge when using a limited temporal scope for mapping and characterization. River course changes, loss and gain of lakes and reservoirs, and intra-annual inundations and flood–irrigation cycles all require at least two dates of image data to capture. Recognizing the need for a global surface water dynamics characterization and map, Pekel et al. 2016 employed the entire Landsat 5, 7 and 8 archive from 1984 and 2015 to map the spatio-temporal variability of global surface water and subsequently monitor its long term changes. First, utilizing the dense time series data, each 30m Landsat pixel was was classified as water or land and returned classification results with less than 5% error of commission and less than 1% error of omission for surface water pixels. Second, intra-and inter-annual variability of classified pixels were used to create a thematic map of surface water dynamics. These maps include several pixel-level, spatio-temporal water-dynamic features. First, Global Surface Water (GSW) Occurrence, the frequency with which water was present over the 32 year study-period, is calculated by summing water detections (WD) and valid observations (VO) from the same months and then dividing the sum of WD by the sum of VO for each month. Averaging the results of monthly Occurrence values then gives the long-term overall surface water

Occurrence. The second feature, GSW Recurrence, is the frequency with which water reappears inter-annually across the time-series. Recurrence is calculated as the ratio of the number of 'water years' to 'observation years' where a 'water year' is a year with at least one water observation, while an 'observation year' is a year with at least one valid observation within the 'water season'; the water season is defined as the months of the year that have water. GSW Seasonality yields information relevant to the intra-annual dynamics of water surfaces for a single year for both permanent and seasonal water and is calculated as the number of months water was present for a given time period. With these features, Pekel et al. 2016 was then able to observe and document both spatial and temporal trends in global surface water dynamics over a 32 year period.

Dense Time-Series Remote Sensing of Wetlands

As wetlands could be simplistically defined as areas of global surface water that also incorporate vegetation dynamics, following in Pekel et al. 2016's path and creating thematic maps of spatio-temporal wetland dynamics using all available Landsat imagery emerges is a logical progression in remote sensing of water-dependent ecosystems. However, it is not as simple as adding vegetation dynamics to surface water maps. The ecological variability of wetlands makes them difficult to detect and classify with remote sensing imagery and it is difficult to discriminate the boundaries between vegetation habitat types (Schmidt and Skidmore 2003, Zomer et al. 2008, Adam et al. 2010). This variability, combined with the

recurrent spectral obstruction of wetland vegetation by soil, atmospheric, and hydrologic patterns associated with wetland habitats, classification becomes even more complicated (Guyot 1990, Yuan and Zhang 2006). Identifying and characterizing freshwater wetland habitats using satellite imagery has many challenges and accurate and reliable remotely sensed products of wetland locations and intra-and inner-annual dynamics have remained elusive.

Prior to the 2008 opening of the Landsat archive, most work in wetland ecological characterization and classification using satellite imagery used single-date classification, two-date change detection, or short-term (0–5 years) change detection using annual images (e.g. Baker et al. 2007; Frohn et al. 2009; Johnston and Barson 1993; Lunetta and Balogh 1999; Wright and Gallant 2007). However, with the augmented availability of Landsat data, time-series analysis for detailed characterization of both inland and coastal wetlands has increased as researchers recognize the power of the temporal domain for identifying key wetland dynamics (Fickas et al. 2015; Halabisky et al. 2016; Hermosilla et al. 2018; Pasquarella et al. 2016; Sagar et al. 2017, 2018).

Free, publically available dense time series data from multiple sensors has allowed researchers to develop and users to employ new analysis strategies to augment the quality of time series interpretation and application. One methodology that uses all available imagery to both classify and detect land use change is Continuous Change Detection and Classification (CCDC). Zhu and Woodcock 2014

developed CCDC (adapted from Zhu et al. 2012's Continuous Monitoring of Forest Disturbance Algorithm (CMFDA)) as an algorithm that uses the statistical boundary method with all available Landsat data. Algorithms using statistical boundary assume the time series temporal trajectory to follow a given statistical boundary and any deviation from the boundary (at a given threshold) is classified as change. This algorithm utilizes all available imagery, Landsat bands 2–5 and 7 as the change indices, and has the spatial resolution of a single Landsat pixel (30 m).

While CCDC takes advantage of the full temporal depth of Landsat data, yielding information about intra-annual changes and the potential for new, temporally defined cover classes, this algorithm, and ones like it, present several limiting factors for their use in wetland characterization. First, they are most accurate in characterizing ecosystems that have predictable intra-annual cycles (such as forests) and less ecologically defensible and accurate when fitting curves to habitats with inter-annual and/or intra-annual variability. Therefore, wetland time series data may not contain enough spectral consistency to fit a robust sinusoidal curve. Second, a key ecosystem feature of wetlands is the presence of water (Cole et al. 1997). Some wetland hydrology is driven exclusively by precipitation (Brinson 1993) and with precipitation, there are often clouds occluding the ground surface at the time when wetlands are most saturated. This means the availability of clear observations may be particularly limited in wetland habitats, further constraining harmonic-fit model utility in characterizing wetland habitats. Pengra et al. 2016 used CCDC to map

wetland cover at one categorical scale (i.e. no further categorical refinement beyond the 'wetlands' class) in the Land Change Monitoring, Assessment, and Projection (LCMAP) project and found that wetlands were hardest to map in areas with a high percentage of wetland area (i.e. areas where wetlands are not generally isolated ecosystems) with the greatest confusion coming from forest and wetlands at ecotonal gradients and areas with mixed class pixels. In some areas, overall accuracy was as low as 35%.

STFs

To utilize dense time-series of remotely sensed imagery for wetland classification and characterization, a methodology that efficiently captures and recognizes the importance intra-annual variability in wetland ecosystems must be developed. Spectral-temporal features (STFs) have been identified as a powerful way to extract individual, meaningful features from multi-date image stacks at the pixel-level (e.g. DeFries et al. 1995, Potapov et al. 2012, Huang et al. 2010, Jin et al. 2013, Coulter et al. 2016, Vogelmann et al. 2012, Verbesselt et al. 2010, Melaas et al. 2013). In the spectral domain, an individual spectral index is the transformation of two or more spectral bands constructed to augment various components of the landscape (Huete et al. 2002). Similarly, a spectral-temporal feature is a transformation of spectral information-based temporal relationships and, by utilizing stacks of imagery, results in a time series of spectral-temporal calculations for an individual pixel (Pasquarella et al. 2018).

STFs can be further distinguished into two categories: primary and secondary STFs. Primary STFs are the result of a direct transformation of an observed spectral time series. These STFs include standard population summary metrics and statistics such as the minimum, maximum, mean, median and range, and can be computed for any temporal interval or segment (Pasquarella, Fickas et al. 2018 in prep). Secondary STFs can be extracted when smoothing functions or models are fit to observed data. These features include modeled interval/segment attributes, as well as land cover change features. For example, CCDC, discussed above, is a modeling approach that produces a set of sinusoidal model coefficients, intercepts, trends, and harmonic amplitudes and phases, which are all considered to be secondary STFs. The use of these models also yields the production of additional secondary STFs that estimate model error and residuals, such as RMSE and can be used to estimate model uncertainty as well as stochasticity in reflectance dynamics.

In detailed classification, analysis and comparison against single and multi-date image stacks, Pasquarella et al. 2018 found that transformed Landsat secondary STFs such as annual amplitude, RMSE, and day of year of modeled phenological metrics to be to be effective and superior in forest type classification. However, for wetlands, these features contain the same issues and limiting factors as their originating models. Intra-annual freshwater wetland dynamics may display too much natural variability to be fit to a spectral harmonic model or time series segmentation and their associated STFs will not be representative of wetland

variability or as effective in classification (Pengra et al. 2016). Primary STFs, on the other hand, have been overlooked in most land-use and land-cover classification in favor of their more complex, secondary counterparts, but should be considered for and tested in wetland ecosystems because they preserve real intra-annual wetland dynamics though direct transformation of observed (rather than modeled) time series data .

In the study presented here, we build on the work by Pasquarella et al. 2018 and Pekel et al. 2016 and test the utility of primary STFs derived from time series of all available Landsat TM/ETM+ observations, including Global Surface Water (GSW) features, for discriminating among wetlands at different categorical resolutions within the NWI classification taxonomy. In addition to GSW features, we examine two key types of primary STFs, 1) reflectance STFs, which characterize reflectance values of spectral indices used, and 2) day of year (DOY) STFs, which quantify the timing of their associated reflectance STFs. As an exploratory measure, we also abstract and evaluate spatial-temporal climate features, such as the per-pixel annual maximum of daily maximum temperature, to yield insight into potential drivers of wetland characterization. As far as we are aware, this is the first time primary STFs derived from all available Landsat TM/ETM+ observations have been utilized for detailed wetland classification. Using an NWI reference dataset from two Oregon ecoregions in distinctly different eco-hydrological climate zones, we test classification agreement and examine relative performance of different classification

inputs across ecoregions and wetland categories. We test an array of classifications that use consistent training and testing datasets, but vary the features and feature-sets used as model inputs. Beyond classification performance, we also explore categorical-level agreement and the importances of different features for differentiation within different wetland categories. Our aim is not to estimate the accuracy of the reference NWI map or monitor wetland change over time and space, but rather to build a framework for multi-level wetland classification across climate gradients.

Specifically, at different categorical resolutions and ecoregional climate zones, our objectives are to:

1) Systematically explore and quantify feature-set accuracies and wetland classification performance,

2) Evaluate individual feature importance for distinguishing between different wetland habitats,

3) Quantify correlations between individual features and individual wetland habitat classification probabilities, and

4) Describe a new framework for annual wetland classification that captures intra-annual variability with spectral-temporal and related features.

Methods

Study Area

Given the manner in which wetland dynamics vary among different wetland categories, it is important to consider specific temporal-climatic features that drive and influence wetland ecosystems. Two key, abiotic ecological drivers in wetland habitats are hydrology (water) and energy (light) (Cole et al. 2007). Across its geographic boundaries, the State of Oregon has a wide spatial and quantitative gradient in temperature (Figure 1A), precipitation (Figure 1(B), and solar irradiance, making it an ideal location to explore spatio-temporal dynamics across different climate regions.

To capture the spatio-temporal climate gradient in Oregon when evaluating wetland intra-annual characteristics and categorization, we chose two distinct Level III EPA ecoregions at opposite ends of the State (Figure 2A): the Willamette Valley (Figure 2B) and the Northern Basin and Range (called the North Basin from here on out) (Figure 2C) (Omernik and Griffith 2014). The Willamette Valley is bounded by the Coast Range to the west, the Cascade mountains mountains to the east and north, and the Calapooia mountains to the south. The Northern Basin and Range ecoregion covers the southeastern portion of the state and, in Oregon, is bordered on the west by the Cascades mountains and foothills, and on the north by the Blue Mountains. Although the the two selected ecoregions contain similarly classified ecosystems

(Vogelmann et al. 1998), at 480 kilometers apart, their varying geo-climatic settings create specific differences in temporal-ecohydrological behavior. Broadly, the North Basin can be characterized as a water-limited ecoregion, where water availability is typically the primary limiting resource in determining hydrology and vegetation patterns (Fernandez-Illescas and Rodriguez-Iturbe 2003) (Figure 1). Conversely, the Willamette Valley sits in an energy-limited setting where solar irradiation (sunlight) limits wetland ecological dynamics (Gallucci 1973).

To further specify our study sites, we chose wetland habitat areas in both ecoregions from the National Wildlife Refuge System (NWRS) (Figure 2B,C). NWRS listed wetlands were chosen specifically because of the NWRS federal directive to maintain biological integrity, diversity, and environmental health of habitats protected under the system's authority. This policy uses historic conditions ("those prior to substantial human related changes to the landscape") as the standard condition and goal for the integrity and environmental health directive. Oregon has lost over 98% of its wetland ecosystems in the past century with losses continuing (Fickas et al. 2015) and finding ecologically consistent and low anthropogenic disturbance wetland habitats can be difficult. However, the NWRS Improvement Act's focus on ecosystem integrity makes NWRS sites ideal locations as reference systems (Andel and Aronson 2012) when exploring intra-annual wetland dynamics at different categorical resolutions. In the Willamette Valley we chose the Willamette

Valley National Wildlife Complex, and in the North Basin, we chose the Malheur National Wildlife Refuge.

Willamette Valley National Wildlife Complex

A system of three NWRs managed by the U.S. Fish and Wildlife Service was established in the mid-Willamette Valley the 1960s: Ankeny, Baskett Slough, and William L. Finley National Wildlife Refuges (Figure 2B). Spread across the Willamette Valley, these refuges are a combined total of 4450 ha. These refuges contain some of the most ecologically significant blocks of native habitat in the Willamette Valley, including large tracts of undisturbed or restored wetlands and one if the last remaining intact wet prairie wetlands in the valley. The Refuge is hosts five species of plant listed as endangered or threatened under to U.S. Endangered Species Act (USDI 2013), all of which utilize wetland habitat: Golden paintbrush (Castilleja levisecta), Bradshaw's desert parsley (Lomatium bradshawii), Willamette daisy (Erigeron decumbens), Kincaid's lupine (Lupinus sulphureus), and Nelson's checker-mallow (Sidalcea nelsoniana). In addition to endangered and threatened vegetation species, these refuges are also home to several federally listed wildlife and fish species such as Fender's blue butterfly (Icaricia icarioides fenderi) and Oregon chub (Oregonichthys crameri). The refuges additionally provide large tracts of suitable habitat for the streaked horned lark (Eremophila alpestris strigata), an avian species consistently listed as a candidate for the federal listing (Stinson 2005).

The NWRs in the Willamette Valley do not contain large lake habitat systems the like the Malheur National Wildlife Refuge. To match the wetland habitat categorical breadth from reference wetlands in the North Basin and the greater Willamette Valley, we augment the wildlife refuges in the Willamette Valley with another protected wetland managed by the the Oregon Department of Fish and Wildlife (ODFW), the Fern Ridge Wildlife Area (FRWA) (Figure 2B). The FRWA was established in 1956 and is management area that includes a large lake feature and surrounding wetland habitat. As with its Willamette Valley NWR counterparts, the FRWA supports a variety of endangered and endemic flora a fauna. The Willamette Valley National Wildlife Complex combined with the Fern Ridge Wildlife Area brings the Willamette Valley study sites to a total of 10,000 ha.

The Willamette Valley's climate is greatly influenced by the Pacific Ocean, which regulates temperature as marine air masses move from west to east across the Pacific Northwest. The climate in the Valley is generally mild throughout the year and clear of extreme temperatures, with cool, wet winters and warm, dry summers. The Valley has a prevalent winter rainfall climate with precipitation largely varying inversely with temperature; cooler months of the year are the wettest and the warm, summer months are the driest (Taylor and Bartlette 1993). Winters in the Valley are likely to be cloudy. Average cloud cover through the coldest months is greater than 80 percent, with a mean of roughly 26 cloudy days in January. Conversely, in the summer months, sunshine is more abundant with mean cloud cover less than 40

percent and greater than 50 percent of days in July are cloud-free (Taylor and Bartlette 1993). Specifically, average mean monthly temperatures at the refuges ranged from 4°C in January to 19°C in August. Roughly 50% of all annual precipitation in the refuges falls from December through February and varies from 102 to 155 centimeters each year. On average, the MNWR receives measurable precipitation 267 days per year (USFWS 2011). Rainfall is the predominant form of precipitation in the region; annual snowfall only averages 15 centimeters per year (Figure 1B).

Malheur National Wildlife Refuge

One of the first NWRs, the Malheur National Wildlife Refuge (MNWR) was established in 1908 by President Theodore Roosevelt as a preserve and breeding ground for native birds. The MNWR is located within the Harney Basin watershed in southeastern Oregon, roughly 48 kilometers south of the city of Burns, Oregon and is comprised of two large lakes, the Malheur and Mud and the Donner und Blitzen River (Figure 2). This part of the State is sparsely populated, arid with cold winters, and defined by wide open spaces. The MNWR is only a small portion of the North Basin's comprehensive area, but represents immense ecological importance as a source of wildlife habitat within the region. The MNWR is a crucial stop along the Pacific Flyway (Smith et al. 1989) and supports resting, breeding, and nesting habitat for hundreds of migratory birds and other wildlife, including species highlighted as

top priority in national bird conservation plans (USFWS 2013). In addition to supporting critical habitat to migratory birds, the MNWR also supports four federally listed or under consideration under the U.S. Endangered Species Act: Malheur wire-lettuce (Stephanomeria malheurensis), Great Basin Columbia spotted frog (Rana luteiventris), Yellow-billed cuckoo (Coccyzus americanus), and the Greater sage-grouse (Centrocercus urophasianus) (USFWS 2013).

The MNWR is situated in the open spaces of the Harney Basin in southeastern Oregon on the northern edge of the Great Basin (Figure 2). The Harney basin is a hydrographically closed catchment and is situated within the High Lava Plains and characterized as alluvial lowlands and surrounding volcanic rock uplands (USFWS 2013). The Refuge centers on three shallow playa lakes (shallow depressional recharge wetlands), the Malheur, Mud, and Harney. These lakes are within the lowest portion of the Harney Basin and collect their life-producing hydrology from the surrounding higher-relief topography. A drought year can yield very dry conditions with lakes reduced to a small percentage of their previous size. WIth very low topographic relief, a small change in water levels can result in several hectares of flooding. Years with anomalously high precipitation can drive water levels beyond refuge boundaries and double or triple the size of the marsh (USFWS 2013).

The mean annual temperature for the refuge is 8°C (USFWS 2013). July is the warmest month with a mean monthly maximum of 29°C and January is the coldest month with a mean monthly minimum of -8°C. Mean monthly minimum

temperatures are below 0°C from November through April with an average of 182 days of the year with temperatures below freezing. Temperatures only rise above 32°C for 18 days a year on average (USFWS 2013). Mean annual precipitation for MNWR is 28 centimeters with the majority (24 cm) falling from October to June. July through September is very dry with the exception of August in some years with thunderstorm activity (USFWS 2013).

Wetland habitat in MNWR is dependent on the annual availability of water resources, mainly from the Blitzen River. The Blitzen River begins on Steens Mountain and flows north through the Blitzen Valley and into Malheur Lake, joined by other tributaries as it flows northward. Except years of very high precipitation, the Blizten River provides the only water supporting the MNWR. The Blitzen River has an array of physical conditions including a deep, wide channel, limited riparian vegetation, bare banks, and minimal habitat complexity (USFWS 2013).

The Blizten River receives most of its volume from Steens Mountain as snowmelt and by the time it drains into refuge wetlands, it has drained an area of 197,000 hectares. Snowmelt discharge into the river begins in early March and reaches a peak in May. The average May volume is 10.5 cubic meters, representing 25 percent of the total annual runoff. Flows tend to decline sharply in June with minimum levels in August or september, averaging a discharge of 1.2 cubic meters for the month.

Water saturation level fluctuations in the wetlands are characteristic of closed basins and can observe high inter-annual variability.

Wetlands Reference Data

Currently, the NWI uses a hierarchical classification taxonomy of Cowardin et al. (1979) to delineate and characterize individual wetlands. Nationwide, the NWI has been found to be variable in its accuracy with low error of commission but high error of omission (Stolt and Baker 1995; Wright and Gallant 2007). Although the NWI is unsuccessful in its goal to map all wetlands, because of its low error of commission, it can be used as baseline wetland distribution for regional-scale classification and identification (Nielsen et al. 2008).

Oregon's NWI dataset is considered public record and can be accessed directly from the USFWS. The color-infrared photos used for the latest Oregon NWI map were collected between 1990 and 1994 and delineation maps were generated in 1995. The structure of the NWI classification is hierarchical, advancing from *Systems* and *Subsystems* at the broadest levels to *Classes*, *Subclasses*, and *Dominance Types*. Additionally, *Modifiers* for water regime, water chemistry, and soil are applied to *Classes* and *Subclasses* (Cowardin et al. 1979, FGDC 2013). Within the taxonomy, *System* refers to a group of wetlands that have a similar influence from hydrologic, geomorphologic, chemical, or biological drivers and are divided into more specific categories called *Subsystems*. The five *Systems* include Marine, Estuarine, Riverine, Lacustrine, and Palustrine. While Oregon contains wetlands from all five *Systems*, we

investigate only Lacustrine and Palustrine wetlands in our study (**Table 1**). Neither the Willamette Valley ecoregion nor the North Basin ecoregion contain Marine or Estuarine wetlands and Riverine wetlands contain many, if not a majority of, delineated polygons that are less than one Landsat pixel wide (30 meters) and therefore heavily subject to edge effects (Zhang et al. 2016). It should be noted, however, that Riverine wetlands only represent areas within a channel and do not include floodplain wetland habitats associated with a specific river or stream, which are part of the Palustrine *System*.

Inland, freshwater Lacustrine wetlands include permanently flooded lakes and reservoirs and intermittent lakes with extensive areas of deep water. Lacustrine wetlands are geographically limited by upland habitat or by Palustrine wetlands dominated by trees, shrubs, and persistent emergents. In locations where a river enters a lake, the extension of the Lacustrine shoreline forms the Riverine-Lacustrine boundary. The Lacustrine *System* contains two *Classes*: Limnetic and Littoral, and six *Subclasses*: Rock Bottom, Unconsolidated Bottom, Aquatic Bed, Rocky Shore, Unconsolidated Shore, and Non-Persistent Emergent.

The Palustrine *System* was developed to group vegetated wetlands such as marshes, swamps, bogs, and fens. Palustrine habitats also include small, shallow, permanent or intermittent water bodies often called ponds. Palustrine wetlands can be found shoreward of lakes and river channels, on river floodplains, in isolated catchments, or on slopes. They can also occur as island patches in lakes or rivers. In

the NWI taxonomy, the Palustrine *System* contains no *Classes* and eight *Subclasses*: Rock Bottom, Unconsolidated Bottom, Aquatic Bed, Unconsolidated Shore, Moss-Lichen Wetland, Emergent Wetland, Scrub-Shrub Wetland, and Forested Wetland.

To conceptually simplify the understanding of wetland types, the NWI also contains a category of "*Generalized Wetland Habitat Type*", from here on out referred to as *'Type*', which aggregates *Subclasses* into broader categories. Lacustrine wetlands contain one generalized habitat, Lakes, while Palustrine wetlands contain Ponds, Emergent, Forested, and Scrub Shrub (**Table 2**).

NWI wetland *Modifiers* are used to further characterize wetland dynamics within the classification hierarchy. *Water Regime Modifiers*, from here on out referred to as '*Hydroperiods*', describe hydrologic characteristics such as timing of intra- and inter- annual surface inundation and groundwater fluctuations. Nontidal *Hydroperiods* are defined in relation to the growing season which begins with green-up and bud-break of native plants in the spring and ends with plant dieback and leaf-drop in the fall. NWI *Hydroperiods* investigated in this study are described in **Table 3**.

To explore the utility of STFs for wetland classification at different categorical resolutions, we test our model on the separability of wetland *System*, *Type*, and *Hydroperiod*. As formal NWI wetland classification terms could be confused with informal wetland language (i.e. the word 'type'), we remain consistent

in capitalizing and italicizing NWI categorical terms (e.g. *Type*), and refer to individual features within each category as 'habitats' and capitalize their label (i.e. Lacustrine).

Oregon NWI polygons used as reference data were selected based on their spatial intersection with the study site boundaries. To augment the quality of the reference dataset, NWI polygons were additionally filtered based on size. Small polygons can be subject to edge effect, therefore polygons less than 5 pixels were eliminated. Three separate reference datasets were derived based on categorical resolution: *Systems* polygons, *Types* polygons, and *Hydroperiod* polygons. Due to the hierarchical nature of the NWI classification scheme, these data overlap. For example, Palustrine wetlands also contain wetland habitats from different *Types* and *Hydroperiods*.

Classification Inputs

Landsat Data

We used Google Earth Engine (GEE) (Gorelick et al. 2017) to access all available Landsat Thematic Mapper (TM) Surface Reflectance Tier 1 pixel-level data for the period January 1 1995 through December 31 1995. Landsat Tier 1 data are atmospherically corrected using LEDAPS (Masek et al. 2006), processed at Level-1 Precision Terrain (L1TP), and georegistered consistently and within <=12 m RMSE. Pixels were masked for cloud, shadow and snow using CFMASK (Foga et al. 2017) and further masked by the reference dataset polygon boundaries. The Tasseled Cap

(TC) Transformation spectral vegetation index (Crist et al. 1985) was then applied to every unmasked pixel for all available dates.

Remote sensing of wetland ecosystems has utilized a variety of spectral vegetation indices for classification and change detection. Most recent remote sensing wetland studies have taken advantage of the Tasseled Cap (TC) indices (Fickas et al. 2015, Pasquarella et al. 2016, Kayastha et al. 2012, Baker et al. 2006, Baker et al. 2007, Wright and Gallant 2007). In our study, we rely on TC as our main spectral feature when transforming over time and do not investigate the applicability of individual Landsat bands in wetland classification. The TC transformation of the six Landsat reflectance bands results in three vegetation indices known as brightness (TCB), greenness (TCG), and wetness (TCW) (Crist et al. 1985). We recognize that other indices and individual bands could be used to differentiate among wetland *Systems*, *Types*, and *Hydroperiods*, however, it was not feasible to explore every possible spectral combination for this study. Further, because TC is calculated directly as a straightforward transformation of spectral bands, it allows consistent spatial, temporal, and spectral comparisons in monitoring seasonal, intra-and inter-annual, and long-term variations of landscape biophysical parameters. TC indices add more data dimensionality than single SVIs, such as NDVI, which is especially important in spatially and temporally heterogeneous ecosystems such as wetlands. In addition to TCG's link to landscape vegetation dynamics, the combination of the TCB and TCW indices is correlated with soil moisture content,

giving additional insight to distinction between wetland and upland vegetation (Fickas et al. 2015).

Spectral-Temporal Features

To coincide with the date of acquisition of the NWI reference data, annual primary STFs were derived from our processed Landsat pixels from the year 1995. The first five derived STFs include the 1995 annual 1) maximum (max), 2) minimum (min), 3) median (med), 4) mean, and 5) range (difference between maximum and minimum), for our three spectral features, TCB, TCG, and TCW, individually. In addition to the primary reflectance STFs, their respective day of year (DOY) was also derived; these are also considered primary STFs. This includes DOY of the annual 1) max, 2) min, 3) med, and 4) range (range of days between the DOY of annual max and min) of TCB, TCG, and TCW. Together, the primary STFs add 27 features to the classification model.

Climate-Temporal Features

To supply spatial climate datasets that are realistic representations of the major forcing factors that affect spatial climate patterns, Daly et al. 2008 developed the Parameter-elevation Relationships on Independent Slopes Model (PRISM). Currently, the PRISM Climate Group houses two types of datasets: 1) long-term climate averages and 2) climate time-series. Long-term average datasets calculate a climate–elevation regression for an 800m digital elevation model (DEM) pixel using location, elevation, coastal proximity, topographic facet orientation, vertical

atmospheric layer, topographic position, and orographic power of the landscape as feature inputs (Daly et al. 2008). Conversely, the time-series datasets are modeled with climatologically-aided interpolation (CAI). In CAI, the long-term average datasets act as the predictor grids, instead of a DEM. Broadly, CAI is based on the assumption that the best first guess of the spatial pattern of climatic conditions for a given month or day is the long-term average pattern. PRISM long-term average datasets exist from 1971 - present and time-series datasets are available on a daily or monthly temporal resolution from 1985 - present.

To create what we term 'climate-temporal features' (CTFs) as model inputs, we accessed the PRISM Daily Spatial Climate Dataset (AN81d) from GEE (Gorelick et al. 2017) from January 1, 1995 to December 31, 1995, which includes 365 days of measurements for four climate features, including daily 1) maximum temperature (tMax), 2) minimum temperature (tMin), 3) mean temperature (tMean), and 4) total precipitation (ppt). From the 365 daily measurements available, we abstracted five CTFs for each of the four climate features: 1) max, 2) min, 3) med, 4) mean, and 5) range (**Table 6**). To match the spatial resolution of our Landsat STFs, data were resampled from 800 m pixels to 30 m pixels using the nearest neighbor approach. Together, these CTFs add 20 features to the classification model.

Ancillary Datasets

Digital Elevation Model

Since wetlands are more likely occur in relatively-depressional terrain surfaces, knowledge of topography is key in determining the existence of wetlands in a given area. For this reason, we used a 30m DEM, labeled as Elevation, derived from the Shuttle Radar Topography Mission (SRTM), flown in February 2000 (Farr et al. 2007) (**Table 7**).

Global Surface Water

To investigate the applicability and accuracy of the Pekel et al. 2016 Global Surface Water data-set, we utilized GSW features as their own feature-set and combined with other feature-sets as model inputs for our wetland classification models. Using GEE (Gorelick et al. 2017), we collected 1) GSW Occurrence, 2) GSW Recurrence), and 3) GSW Seasonality (Table **7**). GSW Occurrence and Recurrence are both abstracted from a 32 year time series and GSW Seasonality is calculated for each year, but the only available dataset is for the year 2014-2015. Consequently, we used the 2014-15 GSW Seasonality data-set to determine if this type of spatio-temporal feature was applicable and relevant to wetlands classified at an earlier date. Given they are derived from Landsat data, GSW features have a corresponding 30 m pixel resolution (Pekel et al. 2016). Combined with Elevation, GSW features create four additional model input features.

Wetland Classification

A series of classifications were used to systematically compare the utility of STFs, CTFs, and ancillary data for discriminating among two wetland *Systems*, four wetland *Types*, and 10 wetland *Hydroperiods*. A Random Forest (RF) classifier (Breiman, 2001) was used to assign wetland *System*, *Type*, and *Hydroperiod* labels to pixels based on the given combination of individual feature inputs, termed 'feature-sets' (Table 8). The RF family of classifiers have become increasingly common in remote sensing applications due to their flexible, non-parametric nature and ability to limit overfitting (Rodríguez-Galiano 2012, Gómez et al., 2016), and have been shown to outmatch a number of other classifiers across a variety of datasets (Fernández-Delgado et al., 2014).

We employed a Python implementation of the RF classifier (Pasquarella et al. 2018, Pedregosa et al., 2011), building ensembles of 500 trees (Belgiu and Drăguț 2016). For each feature-set (Table 8), we employed a winner-takes-all hard classification output, where each pixel was assigned to a single RF class for the purposes of assessing agreement and feature importance. To create a continuous data-set in which to test individual feature values against the likelihood of a given pixel classified as a specific wetland habitat, RF probabilities were also built and output for the 'All Features' feature-set classification for individual wetland habitats within *System*, *Type*, and *Hydroperiod* categories.

Agreement Assessment

Agreement between RF results and the NWI wetland *System*, *Type*, and *Hydroperiod* reference dataset acted as our estimate of model feature performance. For each classification, training data were selected and a three-fold cross-validation (CV) methodology was used where two-thirds of the reference polygons were used for training and one-third allocated for testing. Considering the autocorrelation of pixels derived from the same polygon in the reference dataset, folds were randomly assigned and determined based on polygon ID, guaranteeing that all pixels from a given polygon were placed in the same fold (Friedl et al., 2000, Pasquarella et al. 2018). Given agreement scores can vary considerably based on the metric used, we characterized classification result quality using three metrics, (1) out-of-bag (OOB) agreement, (2) overall agreement, and (3) area-weighted (adjusted) agreement.

Numerous remote sensing classification studies have employed OOB scores as a measure of classification agreement or accuracy (e.g. Rodriguez-Galiano et al., 2012; DeVries et al., 2016). When reference training data is composed of an independent pixel-level sample, OOB scores can provide reasonable estimates of error with reduced supplementary analytical requirements (Genuer et al. 2010). However, in many, if not most, reference datasets, including the NWI polygon layer used here, training data are delineated at the polygon scale, yielding inherent spatial autocorrelation at the pixel-level. In this study, the OOB agreement scores are calculated within each fold and may include both training and testing pixels from the

same polygon. Therefore, the OOB estimates of agreement are included here to examine the effect of autocorrelation on agreement scores. For overall agreement, each location (e.g. pixel) equally contributes to the final calculation of agreement, while in the case of area-weighted agreement, the input of each location is inversely proportional to the total number of locations in that class, such that each habitat (rather than each pixel) contributes uniformly to the final measure of agreement. Consequently, area-weighted agreement better represents wetland classification performance for both rare and common classes, and as the number of wetland locations labeled correctly in each class increases, area-weighted agreement will trend towards overall agreement.

To compare the configuration and significance of agreement between the NWI reference data and the predicted classification for wetland *System*, *Type*, and *Hydroperiod*, confusion matrices were built to calculate producer and user agreement scores for each feature-set . Accuracy percentages (the inverse of error percentages) were subsequently built from confusion matrices.

Feature Importance Assessment and Correlation

While differences in agreement across feature-sets help to explore how different feature combinations can accurately predict wetland categories, more information is needed to examine which individual features *within* feature-sets are most important for classification of wetland *System*, *Type*, and *Hydroperiod* across different climate gradients. When running the RF classification using the ‘All

Features' feature-set, feature importance scores were calculated using the Gini index (Pal et al. 2005) and reported as additional model outputs. Greater Gini index scores correlate with features that are systematically used more frequently and used higher up in the splits of individual RF decision trees (Strobl et al. 2007). An advantage of using the TC index as our primary spectral feature set, as opposed to individual Landsat spectral bands, is a weaker correlation among the three bands (TCB, TCG, and TCW) compared to stronger correlation within individual Landsat spectral bands containing overlapping information. The weaker the correlation among the features, the higher the Gini feature importance score. Individual feature importances were calculated as percentages of the ratio of individual Gini score to the entire wetland category (i.e. *Type*) Gini score sum.

Feature importance scores demonstrate which features were most valuable in discriminating wetland habitats across an entire wetland category, however, they do not clarify how feature values correspond to individual wetland habitats. To explore this explore this issue, we ran a per-pixel Kendall Tau (KT) correlation test (Kendall 1938) with fuzzy classification probabilities of individual wetland habitats within wetland categories against individual feature values. KT was chosen because it is a strong, nonparametric measure of the strength and direction of association that exists between two variables measured on a continuous scale. Especially within wetland *Systems*, binary wetland habitat probabilities were not normally distributed, making other common regression and correlation tests, such as Pearson's correlation

coefficient, inapplicable (Ahlgren et al. 2003). High, positive KT values indicate a strong correlation between high wetland habitat classification probability and high feature values. Low, negative KT values suggest a strong correlation between high wetland habitat probabilities and low feature values. KT scores were calculated for each wetland habitat in each wetland category and for all classification features.

Results

Feature-set Accuracy Agreement

Feature-set agreement assessments exhibited a wide range of variability across both ecoregions and wetland categories (**Figure 3,4**). The OOB agreement score for each classification is consistently higher than the overall agreement score and exhibits a much smaller range of variability than overall and area-adjusted measures of agreement. The comparison between overall accuracy and OOB accuracy serves as an indicator of spatial-autocorrelation in the classification of wetland *Systems* and the difference between overall accuracy and area-adjusted accuracies yields insight into model performance with more frequent versus rarer wetland *Systems.*

Willamette Valley Wetland Systems

Compared to all Willamette Valley wetland categories, feature-set classifications run to distinguish between Lacustrine and Palustrine *System* wetlands contained the highest of all three accuracies scores across the entire range of feature-sets, within individual sets, and for all sets combined (**Figure 3A**). ‘STFs’ and

'DOY STFs' classification runs contained similar, high scores across all three accuracies types. After 'All-Features', accuracies were highest in the 'All-STFs + GSW' classification run and displayed the smallest difference between OOB accuracy and overall and area-adjusted accuracies, suggesting a minimization of spatial autocorrelation for that feature-set. Both the 'CTFs' and 'GSW' classifications contained relatively high overall accuracies without containing any STF features, correctly distinguishing between Palustrine and Lacustrine wetlands 71.6% and 93.9% of the time, respectively. Adding elevation to the 'All STFs' feature-set improved accuracies scores marginally.

The OOB accuracy scores compared to overall accuracy for wetland *Systems* classification were higher, but not substantially so (**Figure 3B)**. This suggests that for distinguishing between two wetland *Systems*, spatial-autocorrelation does not play a large role in affecting classification performance. Similarly, area-adjusted accuracy scores were generally between 30-40% lower than overall accuracies, indicating that the rarity of wetland *System* had an impact on classification performance, but only dipped below 50.0% for one feature-set, 'CTFs' at 47.5%.

Producer and user accuracy matrices help to explore which *Systems* were most problematic in overall accuracies (**Figures 5,6, Table 9**). Palustrine wetlands had a high user accuracy of 96%, with reference Palustrine pixels only being incorrectly identified as Lacustrine 4% of the time. Lacustrine wetlands had a lower producer accuracy (and higher error of omission) of 81%, meaning reference Lacustrine pixels

were misidentified as Palustrine wetlands 19% of the time. However, Palustrine wetlands had a lower user accuracy of 83%, indicating that 17% of pixels labeled as Palustrine were actually Lacustrine. That's compared to Lacustrine wetlands, which had a user accuracy of 96%, indicating that only 4% of labeled Lacustrine pixels were actually Palustrine.

Willamette Valley Wetland Types

Going from two classification categories in Willamette Valley *Systems*, to four categories in wetland *Type* classification, *Type* consistently contained lower scores across all three accuracies compared to *System* (**Figure 3B**). The 'STFs' classification outperformed 'DOY STFs' in overall accuracy by 6.7% (81.4% compared to 74.7%) and when combined into 'All STFs', improved overall accuracy by less than 1.0%. Unlike the wetland *Systems* classification, the 'CTFs' feature-set correctly predicted wetland *Types* less than 50% of the time, with an overall accuracy of 44.5%. The 'GSW' feature-set, on the other hand, performed relatively well without any STF feature input, with an overall accuracy of 66.4%, but still nearly 30% less accurate than when distinguishing between wetland *Systems*. When both GSW and Elevation features were added to the 'All STFs' feature-set, overall accuracy improved by less than 1.0%, to 82.7% and 81.96% respectively. The final wetland *Type* classification of the 'All Features' feature-set was less accurate than wetland *System* classification, but still performed well with an overall accuracy of 80.4%.

When comparing OOB and area-adjusted accuracy to overall accuracy, variability between the three was higher in classifying wetland *Types* compared to *Systems* (**Figure 3A, B**). The 'DOY STFs' feature-set, for example, had OOB, overall, and area-adjusted accuracy scores of 90.8%, 74.7%, and 25.3% respectively. This suggests that classification using DOY features to distinguish between wetland *Types* is not only subject to spatial-autocorrelation, but also shows a high discrepancy in performance between more frequently occuring *Types* versus rare *Types*. Using the three accuracy scores as an indicator, spatial-autocorrelation and underperformance in rare Types occurs within each feature-set, including the 'All Features' set.

Wetland *Types* had lower producer accuracies for individual categories compared to wetland *Systems* (**Figure 5, Table 9**). Lake, Forested, and Emergent wetlands all had relatively high producer accuracies at 85%, 83%, and 73% respectively. Pond wetlands were more problematic. Reference Pond wetland pixels were only identified correctly 4% of the time, with the most (67%) misclassified as Emergent wetlands 17% misclassified as Forested wetlands, and 12% misclassified as Lake wetlands. Other notable (>10%) misclassifications came from reference Lake wetlands misclassified as Ponds 14% of the time, reference Forested wetlands identified as Emergent 17% of the time, and reference Emergent wetlands labeled as Forested wetlands 17% of the time.

User accuracies saw similar issues for Pond wetlands with only 17% of predicted Pond wetlands actually being Pond (**Figure 6, Table 10**). The majority

(38%) of labeled Pond wetlands were actually Emergent, 26% were Lake wetlands, and 19% were Forested. Other notable (>10%) mislabels include 23% of predicted Forested wetlands actually being Emergent, and 23% and 10% of labeled Emergent wetlands actually being Lake and Forested wetlands respectively.

Willamette Valley Wetland Hydroperiods

Transitioning from two and four categories in wetland *Systems* and *Types*, to six categories in wetland *Hydroperiods*, overall accuracy of the final *Hydroperiods* classification using the 'All Features' feature-set was reduced, but still relatively high at 79.6% (**Figure 3C**). Across all feature-sets, overall accuracy was reduced between roughly 5-10% compared to *Types*, and between 20-30% compared to *Systems*. Both the 'STFs' and 'DOY STFs' feature-sets had overall accuracies greater than 65%, with the 'STFs' feature-set performing better at 74.0% compared to 66.9%. When the two feature-sets were combined into 'All STFs', overall accuracy rose to 76.7%. Like wetland *Types* classification, the 'CTFs' feature-set correctly predicted wetland *Types* less than 50% of the time, with an overall accuracy of 44.1%. The 'GSW' feature-set performed even worse, with a very low overall accuracy score of 12.3%. Adding the 'GSW' and 'Elevation' feature-sets individually to 'All STFs' both improved the score by roughly 4.0%, bringing it up to 78.0% and 78.10% respectively. As noted, although wetland *Hydroperiod* contained 200% more wetland categories than *Systems* and 50% more categories than *Types*, overall accuracy for the 'All Features'

feature-set was lower than the other two groups, at 80% overall accuracy, it was still within 1% of Types and 13% of *Systems*.

When comparing OOB to overall accuracy, variability between the two was similar in classifying wetland *Hydroperiods* compared to *Types* and higher when compared to *Systems* (**Figure 3B, C**), yielding the indication that classification using DOY features to distinguish between wetland *Hydroperiods* is also subject to spatial-autocorrelation. Differences between overall accuracy and area-adjusted accuracy were smaller in classifying wetland *Hydroperiods* compared to *Types* and similar compared to *Systems*, again suggesting a difference in performance between more frequently occuring *Hydroperiods* versus rare *Hydroperiods* . Further, because accuracies of some individual feature-sets were much lower in *Hydroperiod* classification, area-adjusted accuracies were also very low. For example, in the 'GSW' feature-set classification, area-adjusted accuracy barely breaks zero accuracy at 1.1%, indicating the GSW features perform very poorly for rarer *Hydroperiods*.

While the 'All Features' classification had relatively high overall accuracy, individual *Hydroperiod* categories were imbalanced in their accuracies, as indicated by the adjusted accuracy and further by examining the producer and user accuracy matrices (**Figure 5C, 6C, Table 11**). *Hydroperiods* 1 and 3 had the highest producer accuracies of 63% and 92% respectively and when Temporarily Flooded was misclassified, it was labeled as Seasonally Flooded the majority of the time (37%). Hydroperiods 2, 4, 5, and 6, all had producer accuracies below 50%, meaning

reference wetland pixels were misidentified more often as the wrong type of *Hydroperiod* than the correct *Hydroperiod*. When misclassified, these reference *Hydroperiod* pixels were majority (all 70% or greater) identified as Seasonally Flooded.

Compared to producer accuracies, user accuracies were higher and more balanced than producer accuracies for wetland *Hydroperiods* (**Figure 5C, 6C, Table 11**). Only *Hydroperiods* 4 and 5 had user accuracies lower than 70%, but they were substantially low at 2.2% and 1.1% respectively. This means that less than 3% of classified *Hydroperiods* 4 and 5 actually represent those *Hydroperiods*. The majority (93%) of pixels labeled *Semipermanently Flooded* actually represented Seasonally Flooded, as did the majority (75%) of pixels labeled *Permanently Flooded*.

North Basin Wetland Systems

In comparison to all North Basin wetland categories, feature-set classifications run to distinguish between Lacustrine and Palustrine *System* wetlands contained the highest of all three accuracies scores across the entire range of feature-sets, within individual sets, and for all sets combined (**Figure 4A**). 'STFs' and 'DOY STFs' classification runs contained similar, high scores (82.7% and 81.0%) but combining the two together into the 'All STF' feature set improved overall accuracy by less than 1%. After the 'All-Features' top overall accuracy score of 84.5%, overall accuracies were highest and very similar in the 'GSW', 'All-STFs + GSW', and 'All-STFs +

Elevation' classification runs. Without any additional spectral input, the 'CTFs' feature-set had a relatively high overall accuracy of 79.9%.

The OOB accuracy scores were roughly 5-15% higher compared to overall accuracy for the wetland *Systems* classification (**Figure 4A, B**). This suggests that for distinguishing between the two North Basin wetland *Systems*, spatial-autocorrelation does not play a large role in affecting classification performance. Additionally, area-adjusted accuracy scores were generally between 5-10% lower than overall accuracies, indicating that the rarity of wetland *System* had a relatively small impact on classification performance, with adjusted accuracies never dipping below 70%.

Producer accuracy was high for both Palustrine and Lacustrine wetlands at 88% and 83% respectively, indicating that wetland *System* classification performed well in correctly classifying reference wetland pixels, only misclassifying the two wetland *System* pixels 12% and 17% of the time (**Figure 7A, Table 12**). User accuracy performed similarly with scores at 83% for Palustrine wetlands and 88% for Lacustrine wetlands, meaning wetland *System* pixels were only labeled incorrectly 17% of the time for Palustrine wetland pixels and 12% for Lacustrine pixels (**Figure 8A, Table 12**).

North Basin Wetland Types

Going from two classification categories in North Basin *Systems*, to four categories in wetland *Type* classification, *Type* consistently contained lower scores across all three accuracies compared to *System* (**Figure 4A, B**). The 'STFs'

classification outperformed 'DOY STFs' in overall accuracy (79.2% compared to 65.0%) and when combined into 'All STFs', the two feature-sets together actually decreased overall accuracy. Unlike the wetland *Systems* classification, the 'CTFs' feature-set correctly predicted wetland *Types* less than 50% of the time, with an overall accuracy of 43.1%. The 'GSW' feature-set also underperformed in wetland *Types* compared to *Systems*. Without any STF feature input, GSW features had an overall accuracy of 34.3%, still over 50% less accurate than when distinguishing between wetland *Systems*. When both GSW and Elevation features were added to the 'All STFs' feature-set, overall accuracy decreased slightly in both feature-sets. Interestingly, the 'All Features' feature-set was less accurate than the 'STFs', 'All STFs', 'All STFs + Elevation', and 'All STFs + GSW'. This indicates that, when combined, these feature-sets may have informational redundancies that leads to poorer model performance.

When comparing OOB and area-adjusted accuracy to overall accuracy, variability between the three was higher in classifying wetland *Types* compared to *Systems* (**Figure 4A, B**). The 'CTFs' feature-set, for example, had OOB, overall, and area-adjusted accuracy scores of 71.1%, 43.1%, and 8.4% respectively. This suggests that classification using CTF features to distinguish between North Basin wetland *Types* is not only subject to spatial-autocorrelation, but also shows a high discrepancy in performance between more frequently occuring *Types* versus rare *Types*. Using the comparison of three accuracy scores as an indicator, spatial-autocorrelation and

underperformance in rare *Types* occurs within each feature-set, but is lowest in 'STFs'.

Wetland *Types* had lower producer accuracies for individual categories compared to wetland *Systems* (**Figure 7B**). Lake and Emergent wetlands both had relatively high producer accuracies at 83% and 81% respectively. Pond and Forested wetlands, however, had more issues with accuracy. Reference Pond wetland pixels were only identified correctly 18% of the time, with the most (58%) misclassified as Emergent wetlands and 24% misclassified as Lake wetlands. Other notable (>10%) misclassifications came from reference Lake wetlands classified as Emergent 15% of the time, Forested wetlands misclassified as Emergent 27% of the time and Pond wetlands 11% of the time, and Emergent wetlands classified as Lake wetlands 13% of the time.

Similar to producer accuracy, user accuracy and error of omission varied among wetland *Types* (**Figure 8B, Table 13**). As with producer error, Lake and Emergent wetlands both had relatively high user accuracies at 87% and 77%, but Pond and Forested wetlands were only labeled correctly 20% and 11% of the time, respectively. For both Pond and Forested wetlands, the majority (59% and 66%, respectively) of labeled Pond wetlands were actually Emergent wetlands, while 21% of labeled Pond pixels and 23% of Forested pixels were actually Lake wetlands. Other notable (>10%) misclassifications came from 11% of labeled Lake wetlands actually being Emergent and 17% of labeled Emergent wetlands actually being Lake.

North Basin Wetland Hydroperiods

Transitioning from two and four categories in wetland *Systems* and *Types*, to six categories in North Basin wetland *Hydroperiods*, overall accuracy of all *Hydroperiods* classifications was significantly reduced, with overall accuracy never reaching above 37% (**Figure 4C**). Across all feature-sets, overall accuracy was reduced between roughly 30-40% compared to *Types*, and between 45-60% compared to *Systems*. The 'STFs', 'DOY STFs', 'All STFs', 'All STFs + Elevation', and 'All STFs + GSW' feature-sets had low overall accuracy percentages in the mid-to-low 30s. Like wetland *Types* classification, the 'CTFs' and 'GSW' feature-sets poorly predicted wetland *Hydroperiods* with overall accuracies of 18.1% and 19.1%. After the 'CTFs' and 'GSW' feature-sets, the 'All Features' set had the lowest overall accuracy.

The most substantial variability in the North Basin *Hydroperiods* classifications comes from the large divergence between OOB, overall, and adjusted accuracies (**Figure 4C**). OOB accuracies are significantly higher than overall accuracies. The 'All Features', 'All STFs', 'All STFs + Elevation', and 'All STFs + GSW' feature-sets all have OOB accuracy percentages in the low to mid 90s. That, for example, yields a nearly 65% difference between OOB and overall in the 'All Features' feature-set, indicating high influence of spatial-autocorrelation on the model. Area-adjusted accuracies are also low for wetland *Hydroperiods*, but the difference between overall and adjusted accuracies are not as great compared to

OOB. However, both 'CTFs' and 'GSW' feature-sets have area-adjusted accuracies below 1%, indicating nearly zero confidence in mapping rare-type *Hydroperiods* with these feature-sets. Generally, area-adjusted accuracy scores were generally between 15-20% lower than overall accuracies, indicating that the rarity of wetland *System* had a noticeable impact on classification performance.

Overall accuracy in *Hydroperiod* classification was at 30.0% and this is reflected in low producer and user accuracies (**Figure 7C, 8C, Table 14**). No *Hydroperiods* had producer accuracies above 40%, meaning error of commission was at least 60% for all *Hydroperiods*. With this low producer accuracy, reference wetland pixels were misidentified more often than not, across all *Hydroperiods*. *Temporarily Flooded* was most commonly misclassified as *Seasonally Flooded* 58% of the time, followed by *Semipermanently Flooded*, 19% of the time. Seasonally Saturated was misclassified as Seasonally Flooded 62% of the time and Temporarily Flooded 12% of the time. Seasonally Flooded reference pixels were misclassified as Semipermanently Flooded 52% of the time and Temporarily Flooded 17% of the time. Semipermanently Flooded wetlands were misclassified as Seasonally Flooded 48% of the time, whereas Permanently Flooded wetlands most commonly misclassified as Artificially Flooded 51% of the time and Seasonally Flooded 11% of the time. Artificially Flooded was misclassified 90% of the time as Semipermanently Flooded.

User accuracies across all Hydroperiods were comparably low compared to producer accuracies (**Figure 7C, 8C**). Similar to *Hydroperiod* producer accuracies, user accuracies never rose above 45%, meaning error of omission was at least 55% across all *Hydroperiods*. The majority, 62% of labeled Temporarily Flooded wetlands were actually Seasonally Flooded, and 13% were truly Semipermanently Flooded. Nearly all, 86%, of pixels labeled Seasonally Saturated were actually Temporarily Flooded, whereas labeled Seasonally Flooded pixels had no majority (>50%) mislabeled *Hydroperiod*, and were actually Semipermanently Flooded 29% of the time and Temporarily Flooded 25% of the time. Similarly, labeled Semipermanently Flooded pixels were actually Seasonally Flooded 49% of the time and Artificially Flooded 31% of the time. Labeled Permanently Flooded wetlands had the lowest user accuracy of 2.7% and were actually Artificially Flooded 70% of the time and Seasonally Flooded 22% of the time. Lastly, pixels labeled Artificially Flooded wetlands were actually Semipermanently Flooded 60% of the time and Seasonally Flooded 16% of the time.

Feature Importance

Willamette Valley System Feature Importances

When the classifier was trained using the 'All Features' feature-set to discriminate between Willamette Valley Lacustrine and Palustrine wetland *Systems*, Tasseled Cap Greenness STFs and the Global Surface Water features comprised the top six most important features (**Figure 9A**). Max TCG had the highest overall

importance (0.16), followed by Med TCG (0.13), GSW Occurrence (0.11), GSW Seasonality (0.09), Mean TCG (0.08), and GSW Recurrence (0.08).

Feature importance scores only points to feature importance for the entire classification, not individual categories within the *Systems*. Due to the binary nature of wetland *Systems*, KT scores of feature importances were positive and negative reciprocals of each other for Palustrine and Lacustrine classes. For example, the most positive KT score for Lacustrine wetlands, the GSW Recurrence feature (0.89), was the reciprocal, most negative, KT score for Palustrine wetlands (-0.89) (Figure 11). The result indicates that Lacustrine wetlands are strongly and significantly correlated with high GSW Recurrence values and Palustrine wetlands are strongly and significantly correlated with low GSW Recurrence values. For vegetated Palustrine wetlands, of the top five features that have the highest positive correlations with the *Class*, four include a Tasseled Cap Greenness STF. This includes Max TCG (0.75), Mean TCG (0.74), Med TCG (0.74), and Min TCG (0.72). Range of TCG (0.69) comes in sixth after Max TCB (0.70). Lacustrine wetlands followed a similar pattern. Of the top five features that have the highest positive correlations with the Lacustrine *Class*, the first three are GSW features, followed by two Tasseled Cap Wetness STFs. This includes GSW Recurrence (0.89), GSW Seasonality (0.88), GSW Occurrence (0.80), Mean TCW (0.73), and Med TCW (0.73). Not far behind, Min TCW (0.72) and Max TCW (0.69) were sixth and seventh. As noted, the top positive features for each *System* correspond to the top negative features for the other.

Willamette Valley Wetland Types Feature Importance and Correlation

Similar to wetland *Systems*, when the classifier was trained using the 'All Features' feature-set to discriminate between Willamette Valley Lake, Pond, Forested and Emergent wetland *Types*, Tasseled Cap Greenness and Wetness STFs and the Global Surface Water features comprised the top six most important features (**Figure 9B**) . GSW Occurrence had the highest overall importance (0.15), followed by GSW Seasonality (0.14), Mean TCG (0.11), GSW Recurrence (0.08), Med TCW (0.06), and Med, Min and Max TCG (0.06).

Given that Lake *Type* wetlands, are comprised entirely of Lacustrine *System* wetlands, their top KT correlation scores for individual features are similar in composition (Figure 12). Lake wetlands are most strongly correlated with high GSW feature values and Tasseled Cap Wetness STF values. The top positively correlated features are GSW Seasonality and Recurrence (0.88), followed by GSW Occurrence (0.80), Mean TCW (0.73), Med TCW (0.73), Min TCW (0.72), and Max TCW (0.69). Lake wetlands were most strongly, negatively correlated with Tasseled Cap Greenness STFs. The strongest negative KT correlation score for Lake probabilities was Max TCG (-0.75), followed by Med and Mean TCG (-0.74), and Min TCG (-0.72).

Pond wetlands did not have any feature correlation, positive or negative, with a KT score above 0.20, but of its feature correlations, Tasseled Cap Brightness STFs were most-relatively-strongly, positively correlated. Max, Mean, and Med TCB and Min TCG all tied for the top positive correlations with KT scores of 0.14, followed by Med ppt, Mean TCG, Med TCG, and Min TCB, all with scores of 0.13. Pond wetland probabilities were most strongly, negatively correlated with GSW features and Tasseled Cap Wetness STFs. Pond probabilities were most strongly, negatively correlated with GSW Recurrence (-0.20), GSW Seasonality (-0.19), GSW Occurrence (-0.18), and Med, Mean, and Max TCW (-0.15).

High Forested wetland probabilities were strongly and positively correlated with the suite of Tasseled Cap Greenness STFs. Max, Mean, and Med TCG STFs all had the top positive KT correlation value of 0.61, followed by Range of TCG (0.58), and Min TCG (0.57). After Greenness, the suite of Tasseled Cap Brightness STFs makeup the the next 5 positively correlated KT values. Similar to Pond wetlands, Forested wetland probabilities were most strongly, negatively correlated with GSW Recurrence (-0.68), GSW Seasonality (-0.67), GSW Occurrence (-0.6), and Max TCW (-0.54), Mean TCW (-0.48), and Mean TCW (-0.46).

High Emergent wetland probabilities were strongly and positively correlated with STFs of Tasseled Cap Brightness, Greenness, and Wetness. Range of TCW had the strongest positive correlation value of 0.57, followed by Max TCB (0.51), Range of TCB (0.50), Mean TCB (0.48), and Min TCG (0.47). Similar to the other two

wetland *Types* (Pond and Forested) that fall into the Palustrine *Class*, Emergent wetlands were most strongly, negatively correlated with GSW features and Tasseled Cap Wetness STFs. Emergent probabilities were most strongly, negatively correlated with GSW Seasonality (-0.64), followed by Min TCW (-0.61), GSW Recurrence (-0.60), and Mean TCW (-0.56).

Willamette Valley Wetland Hydroperiod Feature Importance and Correlation

As will both Willamette Valley *Systems* and *Types*, when the classifier was trained using the 'All Features' feature-set to discriminate between Willamette Valley Temporarily Flooded, Seasonally Saturated, Seasonally Flooded, Semipermanently Flooded, Permanently Flooded, and Artificially Flooded *Hydroperiods*, the features with the top importances values were a mix of GSW features, Tasseled Cap Greenness STFs, and Tasseled Cap Wetness STFs (**Figure 9C**). GSW Occurrence had the highest overall importance (0.16), followed by GSW Seasonality (0.11), Max and Mean TCG (0.10), Med TCW (0.09), and Min TCG (0.08).

Probabilities for individual *Hydroperiods* had a wide range of variability for strong positive and negative correlations with individual features (Figure 13). The features with the highest positive correlation values with Temporarily Flooded probabilities include Max TCG (0.49), Range of TCG (0.49), Med ppt (0.48), Mean TCG (0.44), Med TCB (0.43), and Min TCG (0.43). Temporarily Flooded was

similarly strongly negatively correlated with GSW Recurrence (-0.54), Seasonality (-0.52), and Occurrence (-0.47), Mean tMean (-0.45), and Med TCW (-0.44).

Seasonally Saturated probabilities had similar reciprocal correlation values to Temporarily Flooded, with high probabilities positively correlated to GSW Occurrence (0.59), Seasonality (0.52), and Recurrence (0.5), DOY Min TCG (0.47), and Min TCW (0.43). Likewise, probabilities were positively correlated with Max TCG (-0.5), Med TCB (-0.47), Mean TCB (-0.45), and Range of TCG (-0.43).

The rest of the *Hydroperiods* all had considerably weaker positive correlation values compared to Temporarily Flooded and Seasonally Saturated. Seasonally Flooded was most positively correlated with Elevation (0.33), DOY Max TCG (0.32), Range of tMax (0.27), and Min tMin (0.22). It had similarly strong negative correlation values, however, and was most negatively correlated with Max TCG (-0.50), Med TCB (-0.47), Mean TCB (-0.45), and Range of TCG (-0.43).

Semipermanently Flooded was weakly positively correlated with Min tMin (0.18) and DOY Max TCG (0.17) and weakly negatively correlated with DOY Min TCG (-0.16), GSW Seasonality (-0.13), GSW Recurrence (-0.13), and Med tMean (-0.13). With correlation values just at or above 0.10, Permanently Flooded was even more weakly correlated with Mean TCB (0.11), Med ppt (0.10), Max TCB (0.10), Med TCB (0.10), Min TCB (0.10), and Min TCG (0.10). Again, Permanently Flooded was weakly negatively correlated with GSW Recurrence (-0.14), Seasonality (-0.13), and Occurrence (-0.13), Med TCW (-0.11), Mean TCW (-0.11), Max TCW

(-0.11), and Min TCW (-0.10). Permanently Flooded was the only *Hydroperiod* that had its top correlation values correspond to CTFs. It was most positively correlated with Range tMin (0.13), Med tMax (0.13), Mean tMax (0.12), Max tMin (0.12), and min tMax (0.12). Permanently Flooded was most negatively correlated with GSW Recurrence (-0.14), Mean ppt (-0.14), Seasonality (-0.13), and Max TCW (-0.13).

North Basin Systems Feature Importances and Correlations

When the classifier was trained using the 'All Features' feature-set to discriminate between North Basin Lacustrine and Palustrine wetland *Systems*, GSW Occurrence was the top most important feature (0.13), with Med TCB (0.08) and Mean TCW (0.08) in second place (**Figure 10A**). These top three importance values are lower in magnitude compared to Willamette Valley *Systems* feature importances. In fourth place is Max TCW (0.07), followed by Min TCW (0.06) and Elevation (0.06).

As with the Willamette Valley ecoregion, within fuzzy classification probabilities for North Basin Palustrine and Lacustrine *Systems*, individual KT correlation values of feature importances were positive and negative reciprocals of each other (Figure 14). At the top, Palustrine wetlands were most strongly, positively correlated with high Elevation values and a KT value of 0.64. This was followed by Min TCG (0.60), Max and Mean TCG (0.59), and Med TCG (0.56). These strong, positive KT correlation values of the Palustrine *System* correspond to the strong, negative KT correlation values of the Lacustrine wetlands. The strong, positively

correlated features of the Lacustrine *System* include GSW Occurence (0.72), GSW Recurrence (0.69), Mean TCW (0.60), Med TCW (0.59), Min TCW (0.57), and Max TCW (0.51). The negative reciprocals of these values account for the features that Palustrine *System* probabilities are most strongly,negatively correlated with.

North Basin Types Feature Importances and Correlations

Classification of North Basin wetland *Types* had nearly identical top feature importances compared to North Basin *Systems*, but with lower feature importance values (**Figure 10B**). GSW Occurrence and Med TCB were the top most important feature (0.10), followed by Mean TCW (0.08) and Med TCW (0.07).

Like Willamette Valley Lake wetlands, this wetland *Type* in the North Basin consists of only Lacustrine *System* wetlands, and, consequently, their KT correlation scores for individual features are nearly identical. At the top is GSW Occurrence (0.72), followed by GSW Recurrence (0.69), Mean TCW (0.60), Med TCW (0.59), Min TCW (0.57), and Max TCW (0.51).

Pond *Type* wetlands had lower degrees of both positive and negative KT correlation values (Figure 15). Ponds were most strongly, positively correlated with Mean TCB (0.19), Med Brightness (0.18), Max TCB (0.13), Range of TCW (0.13), and DOY of Med TCB, TCG, and TCW (0.12). Pond were most strongly correlated to low values of Med TCW (-0.18), Min and Mean TCW (-0.17), GSW Seasonality (-0.15), and DOY of Min TCB (-0.14).

Forested *Type* wetlands had lower magnitude KT correlation values compared to Lake wetlands and Emergent wetlands, but higher values than Pond wetlands. At the top, Forested wetlands were most strongly correlated with high values of Elevation (0.22), Max tMean (0.17), Range of tMean (0.17), Mean TCG (0.17), Max TCG (0.16), and Med TCG (0.16). Forested wetlands were most strongly correlated with low values of GSW Occurrence and Recurrence (-0.19), and Max and Range in ppt (-0.12).

Like Lake wetlands, Emergent *Type* wetlands had high negative and positive correlation values with top features. Emergent wetland probabilities were most strongly correlated with high values of elevation (0.62), followed by Max, Mean, and Min TCG (0.59), Med TCG (0.56), and Med TCB (0.50). Similar to Forested wetlands, Emergent wetlands were most strongly, negatively correlated with GSW Occurrence (-0.70) and GSW Recurrence (-0.67). These features were followed by Mean TCW (-0.57), Med TCW (-0.56), Min TCW (-0.54), and Mac TCW (-0.49).

North Basin Hydroperiods Feature Importances and Correlations

As with the classification runs using 'All Features' to distinguish between North Basin *Systems* and *Types*, North Basin Hydroperiods had GSW Occurrence, Med TCB and Mean TCW as the top three most important feature, but with lower feature importance values of 0.08, 0.06, and 0.04 (**Figure 10C**). Med TCG, Mean TCG, Min TCW, and Max TCW were next, all with feature importance values of 0.04.

Probabilities for individual *Hydroperiods* had a wide range of variability for strong positive and negative correlations with individual features' high and low values (Figure 16). Temporarily Flooded was most strongly positively associated with DOY Med TCB, TCG, and TCW (0.37), followed by Mean TCB (0.36), Med TCB (0.34), Min TCB (0.25), and Max TCB (0.20). This *Hydroperiod* was most strongly correlated with low values of Med TCW (-0.33), Mean TCW (-0.33), GSW Seasonality and Occurrence (-0.29), Min TCW (-0.28), and GSW Recurrence (-0.27).

Seasonally Saturated had the weakest correlation values, both positive and negative, of any North Basin *Hydroperiod*. Max tMin, Max tMean, 'Range of tMin, Range of tMean, Med tMean, Mean tMean, Min TCG, DOY of Max TCW, and Elevation all tied for the top, positive correlation value of 0.02. GSW Recurrence, Occurrence, Max TCW, Range of ppt, and Max ppt all tied for the strongest, negative correlation values of -0.02. Of the 51 features tested, 36 of them (71%) had absolute value KT correlation scores at or below 0.01.

Fuzzy classification probabilities of Seasonally Flooded wetlands were most strongly correlated with high values of DOY of Min TCG (0.41), DOY of Max TCB (0.36), Mean tMax (0.03), Range tMean (0.28), and Max and Mean tMean (0.27). This Hydroperiod was most strongly correlated with low values of Range of TCB (-0.29), DOY Med TCW, TCG, and TCB (-0.28), Max TCV (-0.28), and Mean ppt (-0.28).

Semipermanently Flooded had relatively high KT values was most strongly, positively correlated with high Tasseled Cap Greenness STF values. Med TCG (0.38), Mean TCG (0.37), and Max TCG (0.36) had the top correlation values with Semipermanently Flooded, followed by Range of TCW (0.32), and Min TCG (0.31). GSW Seasonality (-0.33), Occurrence (-0.32), and Recurrence (-0.30) were most strongly, negatively correlated with Semipermanently Flooded probabilities, followed by Min TCW (-0.27), and DOY of Min TCB (-0.22).

Similar to Seasonally Saturated wetlands, Permanently Flooded classification probabilities had very weak KT correlation values. At the top, DOY of Med TCB, TCG, and TCW had positive KT values of 0.09, followed by GSW Seasonality (0.08). Negative correlation scores were stronger, but still relatively weak, with low values of Med and Mean TCB (-0.1) and Min TCB and Max and Range of tMin most strongly correlated with high probabilities values of Permanently Flooded wetlands.

North Basin Artificially Flooded wetlands had the strongest positive and negative KT correlation values across this ecoregion's Hydroperiod classification probabilities. High probabilities were most strongly correlated with high values of GSW Occurrence (0.43) and Recurrence (0.41), Mean ppt (0.36), Max TCW (0.36), and Range of DOY for TCB (0.35). High probabilities were most strongly correlated with low values of Med TCB (-0.44), DOY of min TCG (-0.40), DOY Max TCB (-0.36), and Mean TCB (-0.36).

Discussion

Accurate wetland mapping and monitoring is essential to the conservation of area and functionality of these valuable ecosystems. In the U.S., the NWI is over-classified for the level of detail and spatial, temporal, and spectral scale used to classify, delineate, and monitor wetlands. Using the NWI taxonomy, there are currently 7,500 unique classification codes available for interpreters (Cowardin 1979). While there has been a recognition by the USFWS to limit the number of classification codes and aim for quality over detail, there is still a disconnect between the ecological and hydrological classifications applied and the types of data used. This disconnect begins with the USFWS's working definition of a wetland (FGDC 2013):

"Wetlands are lands transitional between terrestrial and aquatic systems where the water table is usually at or near the surface or the land is covered by shallow water. For purposes of this classification wetlands must have one or more of the following three attributes (1) at least periodically, the land supports predominantly hydrophytes; (2) the substrate is predominantly undrained hydric soil; and (3) the substrate is nonsoil and is saturated with water or covered by shallow water at some time during the growing season of each year."

In the given definition, there is an explicit temporal element in two out of three attributes used to distinguish wetland from upland habitat. However, a single image can only capture conditions at one point, in one day, during one year and will lend no insight into ecological, hydrological, or climatic conditions the rest of the year and may confound classifications if conditions happen to be anomalous on the acquisition date.

In spite of wetland habitats being intrinsically linked to temporal phenomena, global and local wetland classification and monitoring remains largely devoid of robust, long-term, intra-annual temporal analysis of hydrology or other wetland functions. Wetlands are key ecosystems across the planet and we argue that to fully comprehend significant patterns of global wetland degradation and loss (Gibbs 2000), wetland phenological dynamics must be understood to place habitat change in the context of fundamental ecosystems drivers. In this study, we used spectral-temporal features as a way to capture intra-annual variability in Oregon wetlands to classify habitats across climate gradients and categorical resolutions. Across climate gradients and wetland categories, we then compared classification accuracies over feature-sets , feature importances, and correlations among features and wetland habitat classification probabilities.

Wetland Systems

At the coarsest categorical resolution in our study, Palustrine and Lacustrine wetlands broadly represented vegetated and unvegetated wetlands respectively. By

measure of overall accuracy, classification performance for distinguishing between these two habitats was higher in the Willamette Valley compared to the North Basin by roughly 10%, suggesting it may be easier to make a binary delineation between vegetated and unvegetated wetland habitats in the energy-limited ecoregion. Water availability is not a limiting factor in the Willamette Valley and Lacustrine wetlands, in particular, may see more continuous saturation throughout the year, making them easier to differentiate between wetlands that have less saturation and more vegetative cover.

Although the Willamette Valley had higher accuracies overall, the climate-temporal feature-set had a higher overall accuracy score for North Basin wetlands compared to the Willamette Valley. This suggests that annual climate features may more easily predict whether a wetland is vegetated or unvegetated in the water-limited ecoregion. In the Willamette Valley, because temperatures remain relatively mild throughout the year and below freezing temperatures are observed less than 25 percent of the calendar year, temperature alone is not a limiting factor in vegetation phenologies. In contrast, roughly half of the year in the North Basin (from November to April) observes temperatures below freezing, severely limiting vegetative growth, even if sunlight (energy) is abundant. In addition to vegetation, snowpack melt, a primary input for North Basin wetland water budgets, is also directly related to ambient temperature. The timing of snowpack melt will determine when, where, and which vegetation species propagate and senesce within the wetland

habitat. Additionally, soil temperature regulates the rate of chemical reactions (described above), which significantly slows at temperatures below 5°C. Because the refuge is so cold, these reactions will have a narrow window in spring and summer and will be dependent on ambient temperature. The timing of these reactions will create a specific climate-temporal pattern of vegetation species based on temperature of soil. In addition to temperature, precipitation is also a limiting factor for North Basin wetland phenologies. Snowpack melt is typically released from April through June. Precipitation in this region, a direct driver of snowpack accumulation, will influence duration of saturation and water table depth into the dry season, influencing when and where different species are established (with topography as additional driver). The stronger, climate-driven vegetation phenological pattern may explain why climate features can better classify North Basin vegetated and non-vegetated wetlands without any other features as inputs.

Based on producer accuracy scores, in both the Willamette Valley and the North Basin, it was easier to correctly predict Palustrine wetlands compared to Lacustrine wetlands, but classification performance in the Willamette Valley was better in predicting Palustrine wetlands compared to the North Basin, but worse for predicting Lacustrine wetlands compared to the North Basin. These results were unanticipated. Lacustrine wetlands are, generally, ecologically 'simpler' compared to Palustrine wetlands, and we predicted that they would be easier for our RF classification to predict on the landscape. We believe our hypothesis may have been

rejected because many NWI classified Lacustrine wetlands are in a status of ecological ambiguity and exist as a mix of Palustrine and Lacustrine, making them harder to definitively differentiate between vegetated and non-vegetated wetlands, especially in a water-limited ecoregion. In contrast to producer accuracy, user accuracy for both the Willamette Valley and North Basin was higher for Lacustrine wetlands compared to Palustrine and the Willamette Valley had lower error of commission for Lacustrine wetlands. Given Lacustrine wetlands had lower error of commission, this indicates that when wetland pixels were labeled Lacustrine, they did were labeled accurately more often than Palustrine wetlands. Comparing user and producer accuracies, for both ecoregions, more reference Palustrine wetlands were correctly classified as Palustrine but fewer predicted Lacustrine wetlands were confused with reference Palustrine wetlands in classification.

Feature importances in distinguishing between vegetated and non-vegetated wetlands were divergent between the Willamette Valley and the North Basin. In the Willamette Valley, a mix of features that represent vegetation cover (such as TCG) and surface water cover (such as the GSW features) were most important in classifying Lacustrine and Palustrine wetlands. This result is logical given that Lacustrine wetlands are surface water features and Palustrine wetlands contain vegetation cover. In contrast, classification North Basin Lacustrine and Palustrine wetlands was most dependent on features that represent surface water, such as GSW Occurrence and TCW, exclusively. We theorize that features that represent vegetation

cover were not as important in the North Basin because it is a water-limited ecoregion. As noted above, water is the limiting factor in establishment of North Basin wetlands, especially Lacustrine wetlands, so saturation level, rather than vegetative cover, may be most important in determining between vegetated and non-vegetated wetlands. It is interesting to note that both the Willamette Valley and North Basin had GSW Occurrence as the top GSW feature within feature importances for classification. This indicated that the persistence of surface water, rather than seasonality or recurrence, may be most valuable in classifying between Palustrine and Lacustrine wetlands, regardless of climatic context.

Despite differences in the overall RF hard classification feature importances, Willamette Valley and North Basin Palustrine and Lacustrine wetland classification probabilities had very similar top feature compositions in respect to KT correlation scores. Palustrine wetlands in both ecoregions were most positively correlated with Tasseled Cap Greenness STFs and most negatively correlated with GSW features and Tasseled Cap Wetness STFs. Interestingly, high probabilities of Willamette Valley Palustrine wetlands were most closely correlated with high values of maximum greenness, meaning the absolute highest values of greenness are linked to Palustrine wetlands. Conversely, high probabilities of North Basin Palustrine wetlands were most closely correlated with high values of minimum greenness, which means something subtly different than being correlated with high values of maximum greenness. It indicates that North Basin Palustrine wetlands may require a specific

lower threshold of intra-annual vegetation cover in order to persist. It should also be noted that the top positive correlation with North Basin Palustrine wetland probabilities was with Elevation, suggesting that in the context of the landscape, Palustrine wetlands are positioned in higher elevations than Lacustrine wetlands. In both the Willamette Valley and North Basin, Lacustrine wetland probabilities were most strongly, positively correlated with GSW features, and wetness features, although the Willamette Valley had stronger KT scores. This, once again, suggests that Lacustrine wetlands are more distinct habitat features compared to Palustrine wetlands, in the Willamette Valley.

Wetland Types

At a finer categorical scale than wetland *Systems*, wetland *Types* represent more ecologically specific wetland habitats and ecosystem variables. By measure of overall accuracies, classification performance was weaker in both Willamette Valley and North Basin wetland *Types*; this is expected as the RF classifier has more habitats to choose from and more specificity in feature values. For both ecoregions, classification accuracies decreased generally uniformly across all feature sets except for CTFs and GSW features, and North Basin accuracies decreased by a lower magnitude going to a finer categorical resolution compared to the Willamette Valley. For both ecoregions, this indicates that, on their own, climate features and measures of surface water dynamics cannot capture the ecological variability seen between Lakes, Ponds, Forested Wetlands, and Emergent Wetlands as well as they could for

Palustrine and Lacustrine wetlands. This may represent the divergence between categorical resolutions that are dependent on climate for intra-annual variability. While climate features still have a notable role, predicting wetland *Types* correctly nearly 50% of the time for both ecoregions without any other feature input, species composition may begin to play a larger driving function for wetland *Types*, as wetland Type habitats are no longer vegetated and non-vegetated like *Systems*, but, instead, represent a vegetation cover density gradient from Lakes (no vegetation) to Forested wetlands (dense, woody vegetation).

When comparing against *Systems*, in the North Basin GSW accuracies decreased by a greater magnitude compared to the Willamette Valley, suggesting that particularly for the water-limited ecoregion, surface water dynamics are poor measures of variability in finer wetland habitats. This is somewhat unexpected given that two out of four (50%) of the wetland *Types* are surface water wetlands. However, 75% of the wetland types have associated vegetation dynamics, perhaps demonstrating lower dependence on GSW features on their own, similar to the limitations noted for climate features.

Despite low accuracies when classifying wetlands on their own, GSW features had top feature importance scores for both ecoregions, indicating that when combined with other features, measures of surface water dynamics are valuable in distinguishing between Lakes, Ponds, Forested Wetlands, and Emergent Wetlands. Similar to wetland *Systems*, top features in classifying Willamette Valley wetland

Types were a mixture of surface water features (such as GSW features and TCW) and TCG and top features in North Basin wetland *Types* were almost all surface water features. One notable difference for the North Basin is the addition of Max TCG as a top five most important feature. While vegetation cover features did not play top roles in hard classification for North Basin *Systems*, the added categorical refinement of a vegetation gradient in wetland *Types* likely required a feature representative of vegetation. However, even at finer categorical resolution, surface water dynamic features were still the top features for both the energy-limited and water-limited ecoregions, further reinforcing the importance of hydrology in wetland ecosystem classification and characterization.

Lake *Type* wetlands are comprised entirely of Lacustrine *System* wetlands, and therefore had very similar positive and negative KT correlations for both ecoregions. Pond wetland classification probabilities had very low positive and negative KT correlations for both ecoregions. We contribute this to a higher level of categorical uncertainty of this wetland habitat in the NWI, defined as 'Wetlands with vegetative cover less than 30 percent and lack of large stable surfaces for plant and animal attachment'. Ecologically, we theorize that Pond wetlands may exist in a categorical space of a mixture of Emergent and Lake wetlands and, therefore, do not have high correlations with any particular feature because they do not have distinct ecological signatures. This is confirmed with high error of omission and commission for Ponds. The top three positive feature correlations with Pond wetland probabilities

are TCB STFs for both ecoregions. This is a confounding result and warrants further exploration. We theorize high Pond probability correlations with TCB could come from three different sources, or a mixture. First, surface aquatic vegetation, such as algae or cyanobacteria, reflects highly in TCB. Second, ponds may experience more areas of bare soil in the hot, dry months, devoid of both vegetation and water, which would cause them to reflect highly in TCB. Last, while we did include a snow and ice mask for our Landsat pixels, gaps could occur; because they are shallower than Lakes, Pond would be more vulnerable to surface water freeze in the winter months, which would also yield high TCB values. The last hypothesis would be more applicable in the North Basin, where freezing temperatures are common in winter. An additional unexpected result from Pond classification probability correlations is the strongly negative KT values for surface water features (GSW and TCW) for both the Willamette Valley and North Basin. Although there are a number of reasons this could be the case, we theorize that this result is from the RF classifier comparing between Lake habitat and Pond habitat, and placing pixels with higher GSW and TCW feature values in Lakes because they are deeper and, perhaps, more saturated.

The most interesting comparisons between ecoregions in wetland *Type* probability correlations comes from the transition into wetlands classified by their vegetation type. Willamette Valley Forested Wetland probabilities were most strongly correlated with high values of all five TCG STFs and low values of GSW features and TCW STFs. This result is intuitive as high TCG is very well established as an

indicator of forested ecosystems (Healey et al. 2005) and, although they are wetlands, surface water features and reflectance will not be as great compared to Ponds or Lakes, because the majority of wetland surface area is vegetated. Results for North Basin KT correlations in Forested Wetlands were much different. High probabilities of Forested Wetlands were correlated first with high values in elevation, suggesting they are positioned in areas of relatively higher elevation rather than in depressions, followed by high values of annual maximum of the mean daily temperature and annual range of the mean daily temperature. Generally, this means that in the North Basin, in areas that contain vegetated wetlands, the warmer it is on average during the year, the more likely it is to be Forested (compared to Emergent). Woody vegetation is better at surviving during periods of water stress (i.e. high temperature) compared to herbaceous vegetation (Griffin and Smith 2004) so it could be that in vegetated wetlands, habitats that are found in sites where it gets relatively warmer, wetlands are more likely to be Forested. High probabilities of North Basin Forested Wetlands were most strongly correlated with lower values of GSW Occurrence and Recurrence and annual max and range of daily total precipitation. The negative correlation with surface water features is likely explained by similar factors as Willamette Valley Forested wetlands, and precipitation by similar reciprocal factors as temperature.

High probabilities for Willamette Valley Emergent wetlands were correlated with high values of TCW, TCB, and TCG STFs and low values of GSW features and

TCW STFs. Herbaceous vegetation generally reflects higher in the TCB spectral domain, thus a mix of high TCG and high TCB values makes sense here. The interesting comparison is between correlations with high values of the range of TCW and low values of minimum, mean, median, and max TCW. Broadly, this indicates emergent wetlands are found in sites that have a wide range in wetness values, i.e. places where the maximum and minimum saturation values are far apart. Plainly, these are places where it gets relatively very wet and very dry within the year. However, with negative correlations with low minimum, mean, median, and max wetness values, it seems Willamette Valley Emergent wetlands have a threshold for *how* wet they get. We theorize that if a Willamette Valley emergent wetland gets too wet, it then becomes a Pond or Lake. High probabilities in North Basin Emergent Wetlands had the same strong, negative correlations as the Willamette Valley, but differing positive correlations. As with Forested Wetlands, Emergent Wetland probabilities were correlated first with high values in elevation, suggesting they are positioned in areas of relatively higher elevation rather than in depressions, followed by maximum, mean, min, and median TCG, indicating North Basin Emergent wetlands are linked to high vegetation cover.

Wetland Hydroperiods

One of the most important features in wetland characterization and classification is the wetland hydroperiod. At a finer categorical scale than both wetland *Systems* and wetland *Types*, wetland *Hydroperiods* represent a

eco-hydrologically specific wetland classification based on intra-annual variability. By measure of overall accuracies, classification performance was weaker in both Willamette Valley and North Basin wetland *Hydroperiods* compared to wetland *Types* and *Systems*. This is not surprising given that *Hydroperiods* are specifically classified based on intra-annual variability and require more complex contextual information beyond differences in vegetation density and type. While both ecoregions had lower accuracies in *Hydroperiods*, Willamette Valley *Hydroperiods* classification performance was not substantially lower than Type classification in most feature-sets, except for CTFs and GSW features. In contrast, North Basin Hydroperiod accuracies were reduced by more than half compared to wetland Types, with CTFs and GSW features barely registering accuracies above 15%. As with wetland *Types*, these results suggest that climate features and measures of surface water dynamics cannot capture the intra-annual hydrological and ecological variability needed to distinguish between different *Hydroperiods* on their own.

The sharp divergence between classification performance for Willamette Valley and North Basin *Hydroperiods* suggests there could be a meaningful difference between the intra-annual dynamics that our input features can capture for energy-limited wetland versus water-limited wetlands. NWI *Hydroperiod* classification is based around magnitude of inundation (saturated versus flooded) and the intra-annual duration of inundation (continuously, seasonally, temporarily, or permanently). We hypothesize that Willamette Valley wetlands may have a stronger

temporal-hydrological signal because water is not a limiting resource and, therefore, the differences between magnitude and duration of inundation are more distinct and distinguishable using our input features. Further, this could also point to the known and described limitation of NWI classification in which single date imagery or single date site visits cannot accurately characterize hydrological dynamics of the entire year, with this effect exaggerated in more hydrologically variable, water-limited ecosystems.

Individual feature importances were also much lower for North Basin Hydroperiod classification compared to the Willamette Valley. For both ecoregions, however, despite performing poorly as their own feature-set in classification, GSW features landed as the top most important features when combined with all 51 features in classification. GSW Occurrence, which could also be thought of as a proxy measure of long-term averages of inundation duration, ranked highest for both ecoregions. This suggests that, while the long-term measures of GSW features may not be able to accurately distinguish differences in wetland *Hydroperiods* on their own for individual years, they are very useful when combined with other features such as TCG and TCW STFs in the Willamette Valley and TCB, TCG, and TCW STFs in the North Basin and should be considered as feature inputs for future classification of wetland *Hydroperiods*.

Individual feature correlations with *Hydroperiod* habitat classification probabilities were the most diverse between any wetland category. For the sake of

brevity, we will not discuss feature correlations for each Hydroperiod between and within each ecoregion (which would result in nearly 20 individual comparisons). Instead, we highlight first analyze one *Hydroperiod* in depth and then highlight other interesting aspects of the other five. For Willamette Valley Temporarily Flooded wetland classification probabilities, i.e. wetlands that have high inundation for low duration, Max TCG and the annual median of daily precipitation were the most strongly, positively features. Ecologically, Max TCG represents the highest vegetation signal throughout the year so it makes sense that wetlands with high greenness would be associated with hydroperiods of low inundation duration because lower duration inundation and high inundation magnitude will yield an increased hydrological input through flooding and then more opportunity for vegetation to grow by receding quickly. The annual median of daily precipitation as a strong, positive correlation with Willamette Valley classification probabilities is also logical; areas with annually high daily intermediate values are more likely to have flooding. GSW features were most strongly, negatively correlated with GSW features and annual mean temperature of the daily mean. Given that GSW features can be conceptually linked to duration and recurrence of inundation, it makes sense that wetlands that have low inundation duration are correlated with low GSW values, especially seasonality. Classification probability correlation with low values of average temperature is an intriguing result that could have a variety of hydro-ecological

explanations. For example, Low temperatures could facilitate a free-thaw cycle that creates flooded wetlands for a short period of time.

Feature correlations for North Basin Temporarily Flooded wetland classification probabilities differed considerably compared to the Willamette Valley. The DOY of median TCB, TCG, and TCW were the most strongly, positively correlated with classification probabilities in this ecoregion. This suggests that time is an essential component for characterizing low duration, high magnitude inundation for this water-limited ecoregion. Broadly, if the median of TC reflectance values occur later in the year, the more likely it is to be a Temporarily Flooded wetland in the North Basin. This suggests that for the North Basin, this Hydroperiod wetland is most likely to have its extrema, specifically inundation and vegetation growth earlier in the year, which could be linked to the habitat's dependence on hydrologic input availability, such as runoff. North Basin Temporarily Flooded wetland classification probabilities were most strongly, negatively correlated with high values of TCW STFs and GSW features suggesting that high magnitude inundation wetlands were not characterized well by common measures of wetness. We hypothesize that in the North Basin, water is a limited resource so Temporarily Flooded wetlands are inundated for periods shorter than systems where water is not a limited resource. Therefore, it is possible that satellite imagery could more easily miss TCW extrema due to date of acquisition mismatch or obscruction by clouds.

Important differences in feature correlations with individual Hydroperiod wetlands between the two ecoregions exist for the other five habitats as well and they do not, generally, appear to follow a pattern in relation to each other. However, within-ecoregion patterns appear to exist. For the Willamette Valley, three out of four "Flooded" Hydroperiods have strong negative correlations with GSW features and four out of four have strong positive correlations with climate features. This indicates that flooded wetlands may be more spatially ephemeral and not characterized well by surface water dynamics are more dependent on local climate conditions. Saturated wetlands in the Willamette Valley do not have a similar distinguishable pattern. In the North Basin, three out of four "Flooded" Hydroperiods have strong positive or negative correlations with DOY STFs, suggesting that persistence of flooded wetlands is connected to timing of eco-hydrological dynamics.

In the Willamette Valley Seasonally Saturated wetlands are strongly positively correlated with GSW features, while Continuously Saturated wetlands are strongly, negatively correlated. In contrast, in the north basin both "Saturated" wetlands are strongly negatively correlated with GSW features. High GSW features values indicate wetlands that occur, recur and occur for many months, and it could be that "Seasonally Saturated" wetlands have relatively stable inter-annual persistence and contain more temporal-autocorrelation year to year.

Future Use Of Landsat STFs In Wetland Ecosystems

In our study, we chose to explore the usability of specific primary spectral-temporal, climate-temporal, and ancillary features for wetland *classification* in areas of known wetland and did not investigate model performance or feature importance to wetland *detection*. In wetland classification, the model had specific wetland habitats to choose from for each wetland category and each pixel was assumed to have a base condition as a wetland. In wetland detection, pixel state is unknown at the beginning of the model run and upland systems need to be included as possible classification categories. Wetland detection with Landsat imagery presents an even more challenging task but is the next critical step in remote sensing of wetland ecosystems.

The presence of a distinct hydroperiod may serve as the first step in differentiating wetlands from uplands. Accurate classification of wetland hydroperiods has been a subject of multiple remote sensing studies in recent years. However, these studies tend to be based on wetlands that are in arid landscapes (Halabisky et al. 2016, Dvorett et al. 2015), individual wetland sites (Díaz-Delgado et al. 2016), or a fusion of multisource imagery such as Landsat, MODIS, and SAR (Townsend et al. 2001). Here, we demonstrate that NWI Hydroperiods can be classified in both energy-and water-limited ecosystems for areas of known wetland presence and believe the transition to hydroperiod detection using spectral-temporal

features will be complementary. Once a binary presence of a hydroperiod is established, wetland classification can follow.

In addition to wetland detection and classification, we also believe there is utility in improving upon the categorical NWI hierarchical taxonomy, especially for hydroperiods. Hydroperiod definitions are moderately esoteric, overlapping, and not necessarily ecologically relevant. One solution lies in unsupervised classification. Our results demonstrate that primary STFs are able to capture the intra-annual variability needed to characterize different wetland categories and habitats. Allowing STFs and other relevant features to separate and 'cluster' hydroperiods into separate habitats based purely on statistical measures may yield more hydro-ecologically relevant Hydroperiod definitions.

After annual classification or detection of intra-annual wetland dynamics, the next step is applying the classification across time. Due to the inter-annually ephemeral nature of wetland habitats, we believe fuzzy classification, i.e. utilizing classification probabilities rather than hard classification, will be most useful and yield more stable insight into long term wetland dynamics. Wetlands are transient and transitional and may naturally migrate between two wetland habitats from year to year, however, monitoring probabilities generates more consistent, continuous, information about wetland behavior over time. Further, specific features identified here were strongly correlated with different wetland habitats. Researchers or managers interested in studying habitat functioning or area over time can also monitor

features as proxies for relevant biophysical parameters in the ecosystem. Lastly, the inclusion of climate data that also predicts values into the future, such as the NASA earth Exchange Global Daily Downscaled Projections (NEX-GDDP) (Ahmadalipour et al. 2016) could be utilized to predict wetland behavior into the future for the purposes of planning, management, and conservation.

Conclusions

- Through systematic exploration and quantification of feature-set accuracies and wetland classification performance, we found that STFs-only feature-sets consistently produced high overall accuracies and were able to accurately delineate wetland habitats across climate gradients and wetland categorical resolutions even further when combined with other features. Additionally, accuracies decreased with increasing categorical resolution in both energy-and water-limited ecosystems.
- Evaluation of individual feature importance for distinguishing between different wetland habitats showed that different features are more important for different climate gradients and categorical resolutions. However, GSW Occurrence was consistently valuable for both ecoregions across all categorical resolutions, exemplifying the value of utilizing the GSW dataset for wetland classification.

- Although not all types of features were found to be important in overall classification, in quantifying correlations between individual features and individual wetland habitat classification probabilities, we found that all feature types -- primary reflectance STFs, DOY STFs, CTFs, GSW features, and Elevation -- had strong positive and negative correlations with individual habitats. This indicates the importance of using the various features as inputs for wetland classification.
- Future studies should focus on using the feature-sets described here for wetland detection and apply the model through time for long term trend analysis.

CHAPTER 2 FIGURES

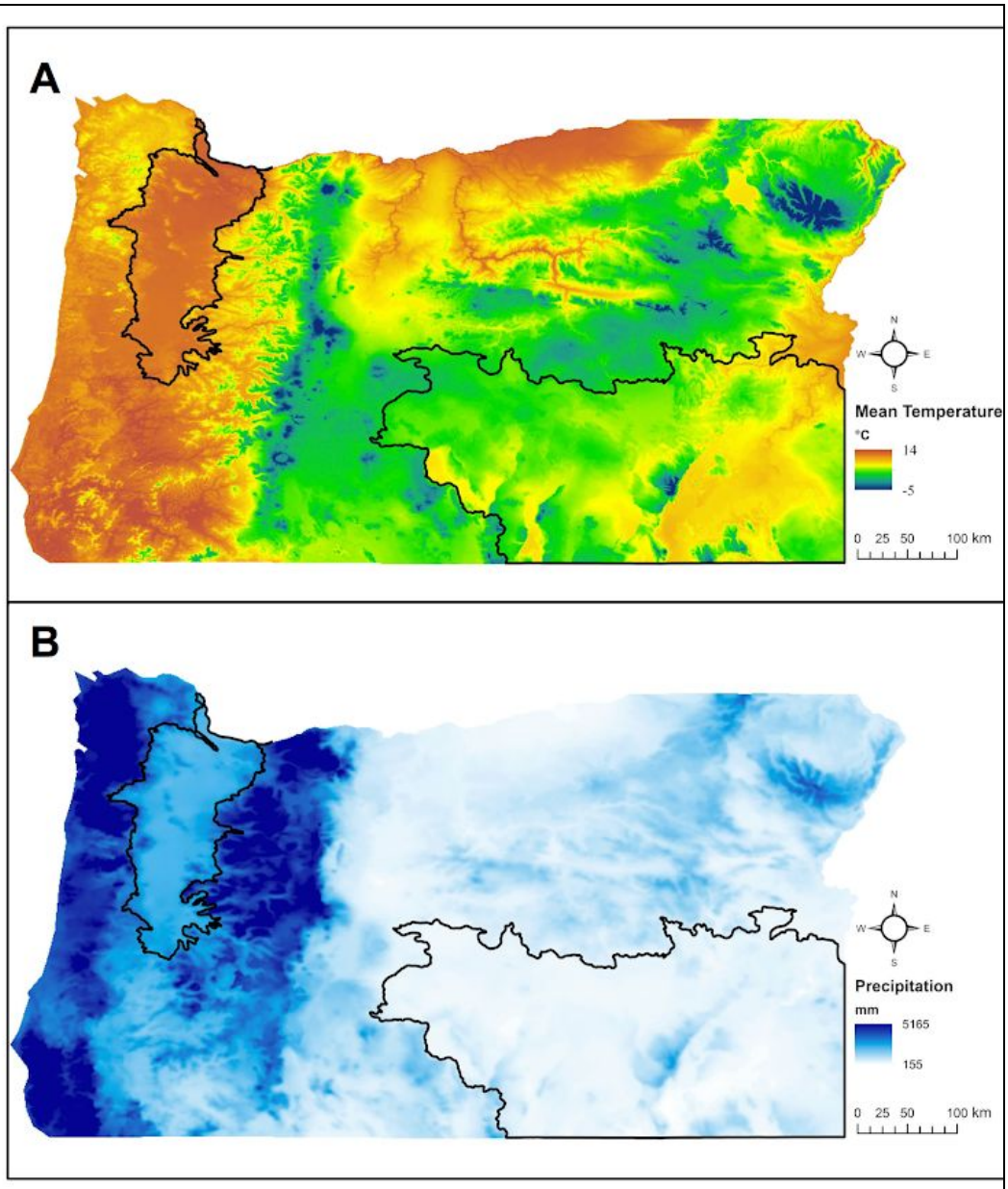

Figure 2.1: 30-year average of mean annual temperature (A) and mean annual precipitation (B) for the state of Oregon. Willamette Valley (left) and Northern Basin and Range (right) EPA Level III Ecosystems are outlined in black.

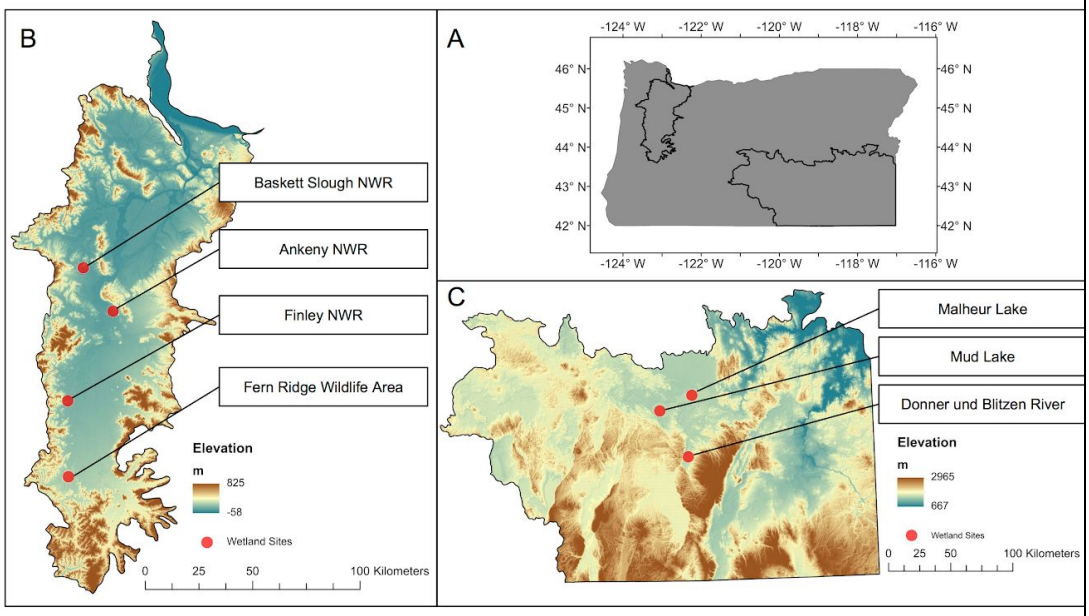

Figure 2.2: State of Oregon with EPA Level III Ecoregion study areas outlined in black (A) . Individual wetland study sites in the Willamette Valley Ecoregion are indicated with red dots (B); the Willamette Valley ranges in elevation from 825 m to -58 m. Wetland study sites in the Northern Basin and Range Malheur NWR are indicated with red dots (B); higher than the Willamette Valley, the Northern Basin and Range ranges in elevation from 2965 m to 687 m.

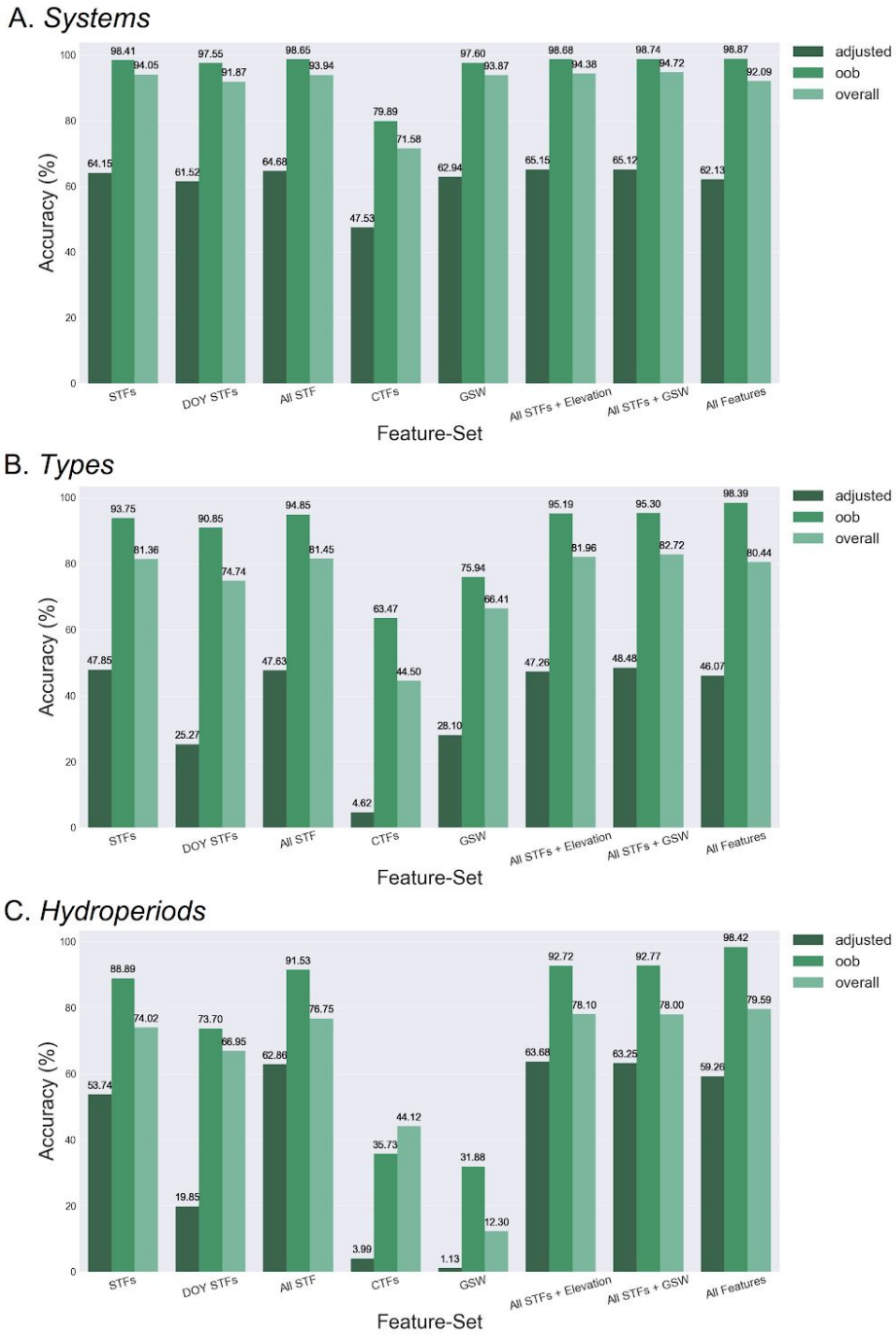

Figure 2.3: Distribution of three pixel-scale agreement scores (Out-of-Bag [oob] from Random Forest and independently assessed overall and area-weighted [adjusted] agreements), measured as percentage correct relative to reference labels, for each feature-set in classification of Willamette Valley wetland Systems (A), Types (B), and Hydroperiods (C).

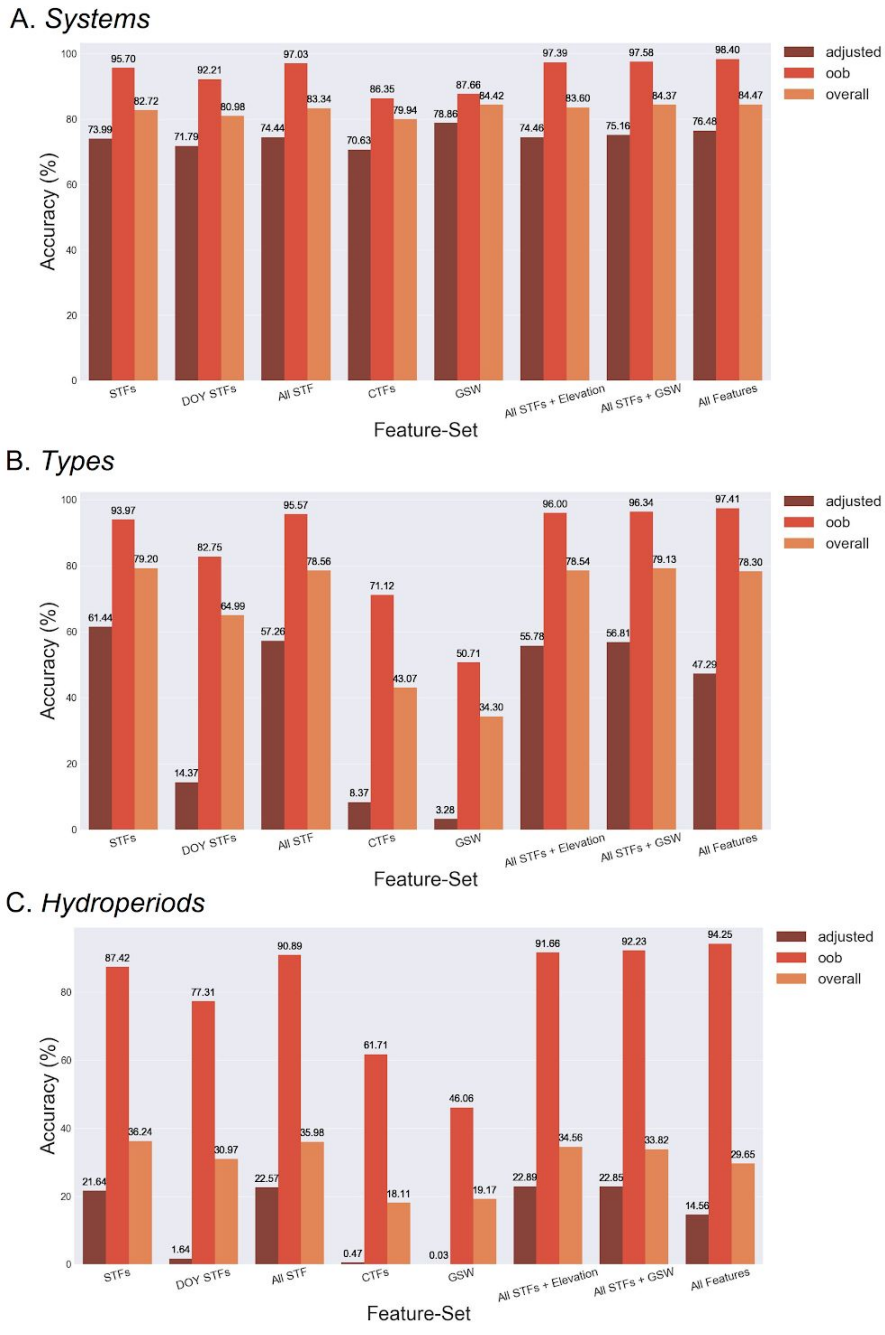

Figure 2.4: Distribution of three pixel-scale agreement scores (Out-of-Bag [oob] from Random Forest and independently assessed overall and area-weighted [adjusted] agreements), measured as percentage correct relative to reference labels, for each feature-set in classification of North Basin wetland Systems (A), Types (B), and Hydroperiods (C).

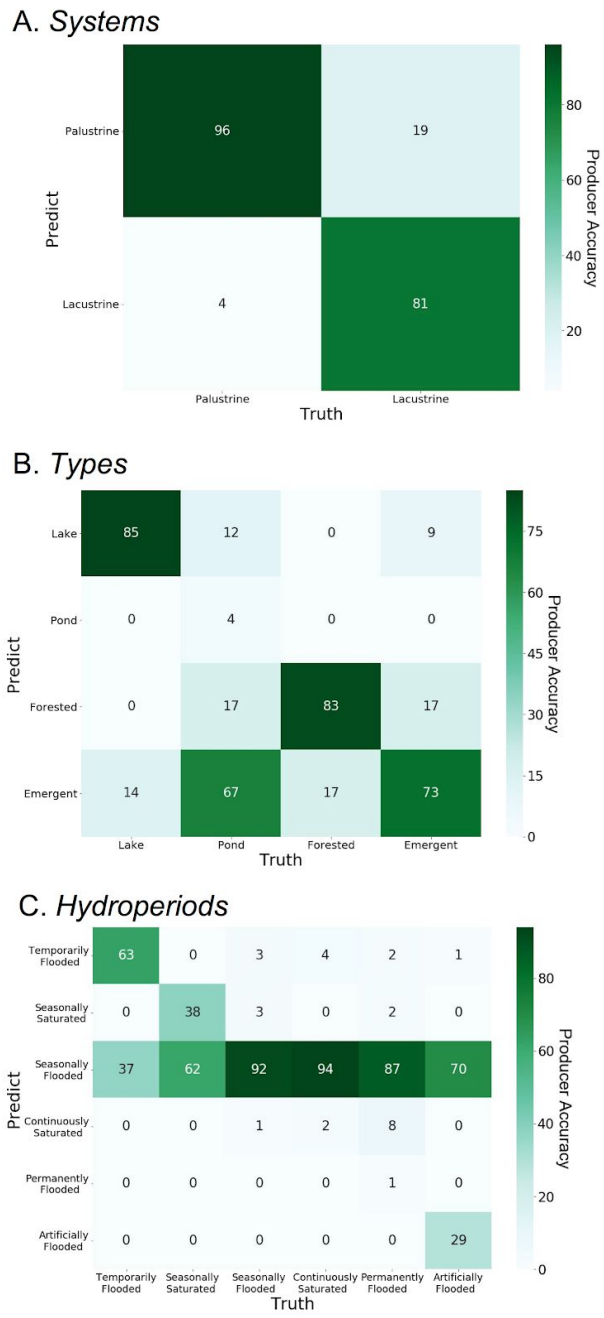

Figure 2.5: Habitat level producer accuracy for 'All Features' feature-set. Confusion matrices are shown as heat maps, with darker colors corresponding to higher scores for each habitat in classification of Willamette Valley wetland Systems (A), Types (B), and Hydroperiods (C).

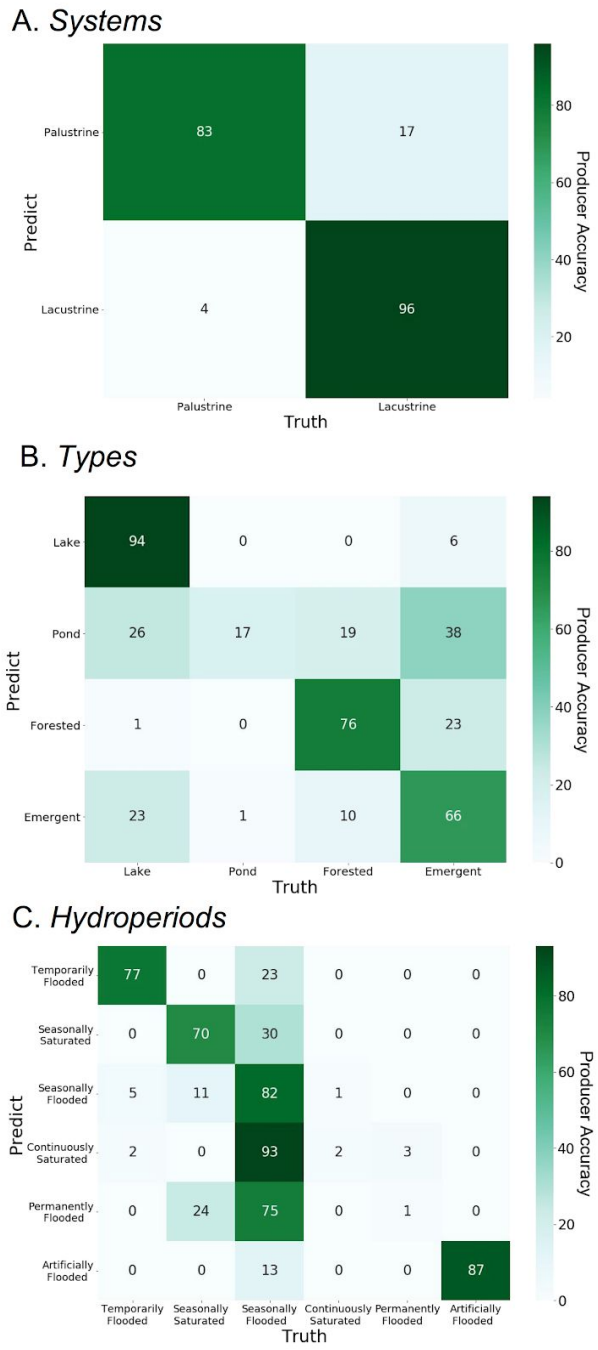

Figure 2.6: Habitat level user accuracy for 'All Features' feature-set. Confusion matrices are shown as heat maps, with darker colors corresponding to higher scores for each habitat in classification of Willamette Valley wetland Systems (A), Types (B), and Hydroperiods (C).

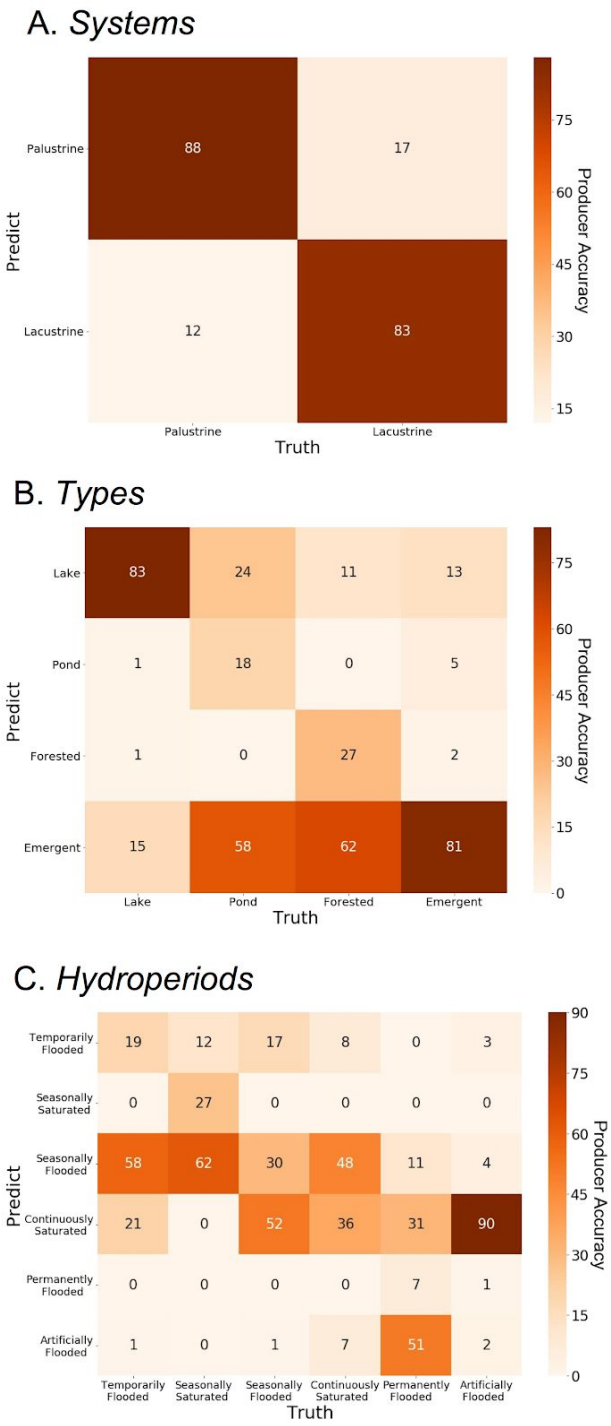

Figure 2.7: Habitat level producer accuracy for 'All Features' feature-set. Confusion matrices are shown as heat maps, with darker colors corresponding to higher scores for each habitat in classification of North Basin wetland Systems (A), Types (B), and Hydroperiods (C).

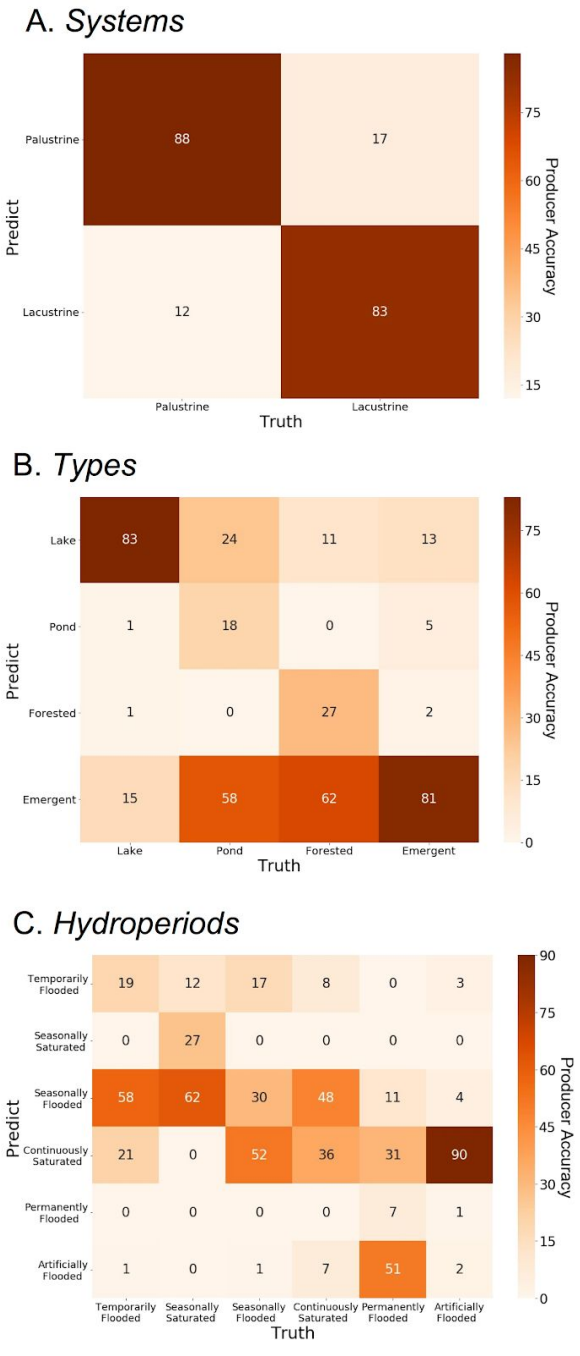

Figure 2.8: Habitat level user accuracy for 'All Features' feature-set. Confusion matrices are shown as heat maps, with darker colors corresponding to higher scores for each habitat in classification of North Basin wetland Systems (A), Types (B), and Hydroperiods (C).

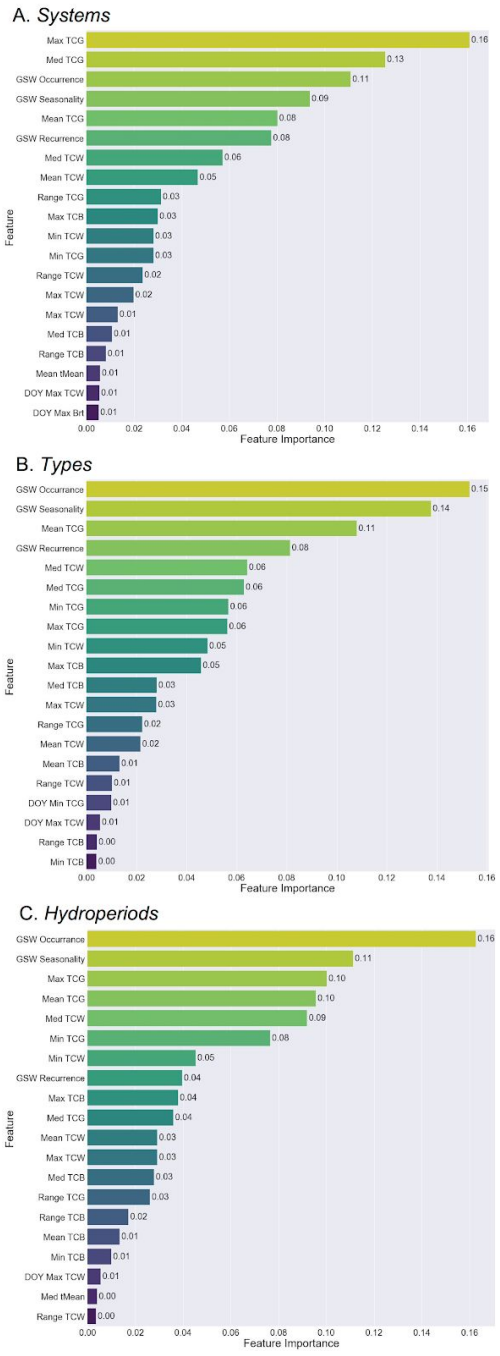

Figure 2.9: Feature importances for discriminating among Willamette Valley wetland Systems (A), Types (B), and Hydroperiods (C). Higher feature importances suggest higher placement across trees and thus greater discriminatory power.

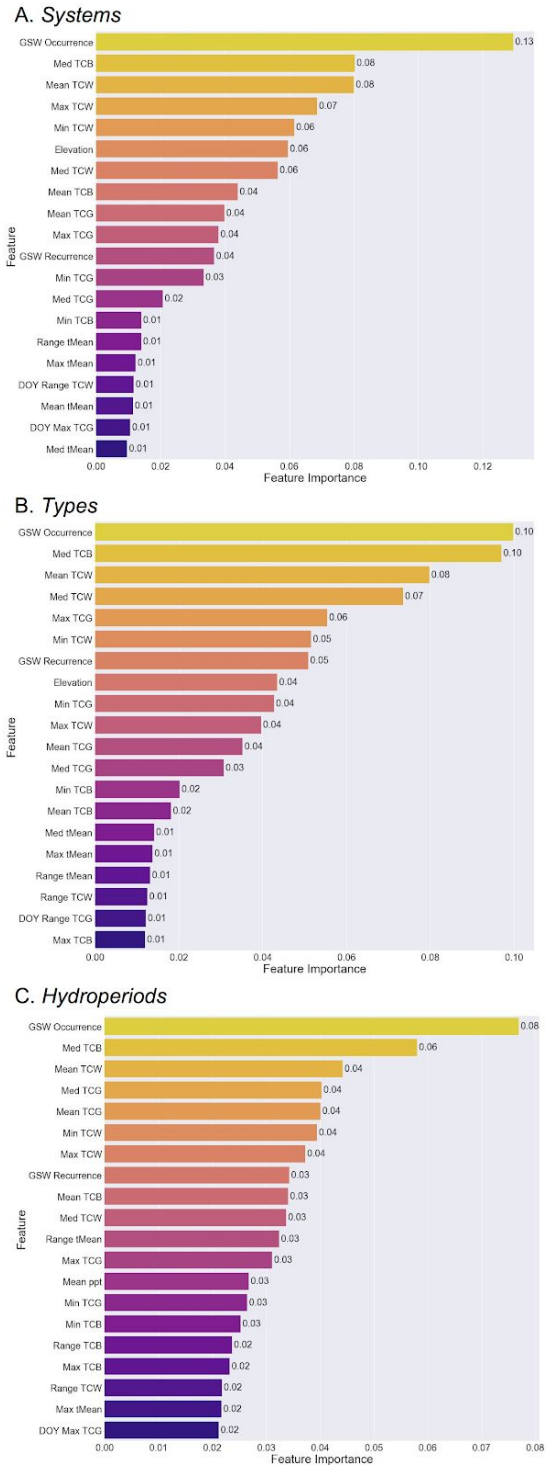

Figure 2.10: Feature importances for discriminating among North Basin wetland

Systems (A), Types (B), and Hydroperiods (C). Higher feature importances suggest higher placement across trees and thus greater discriminatory power.

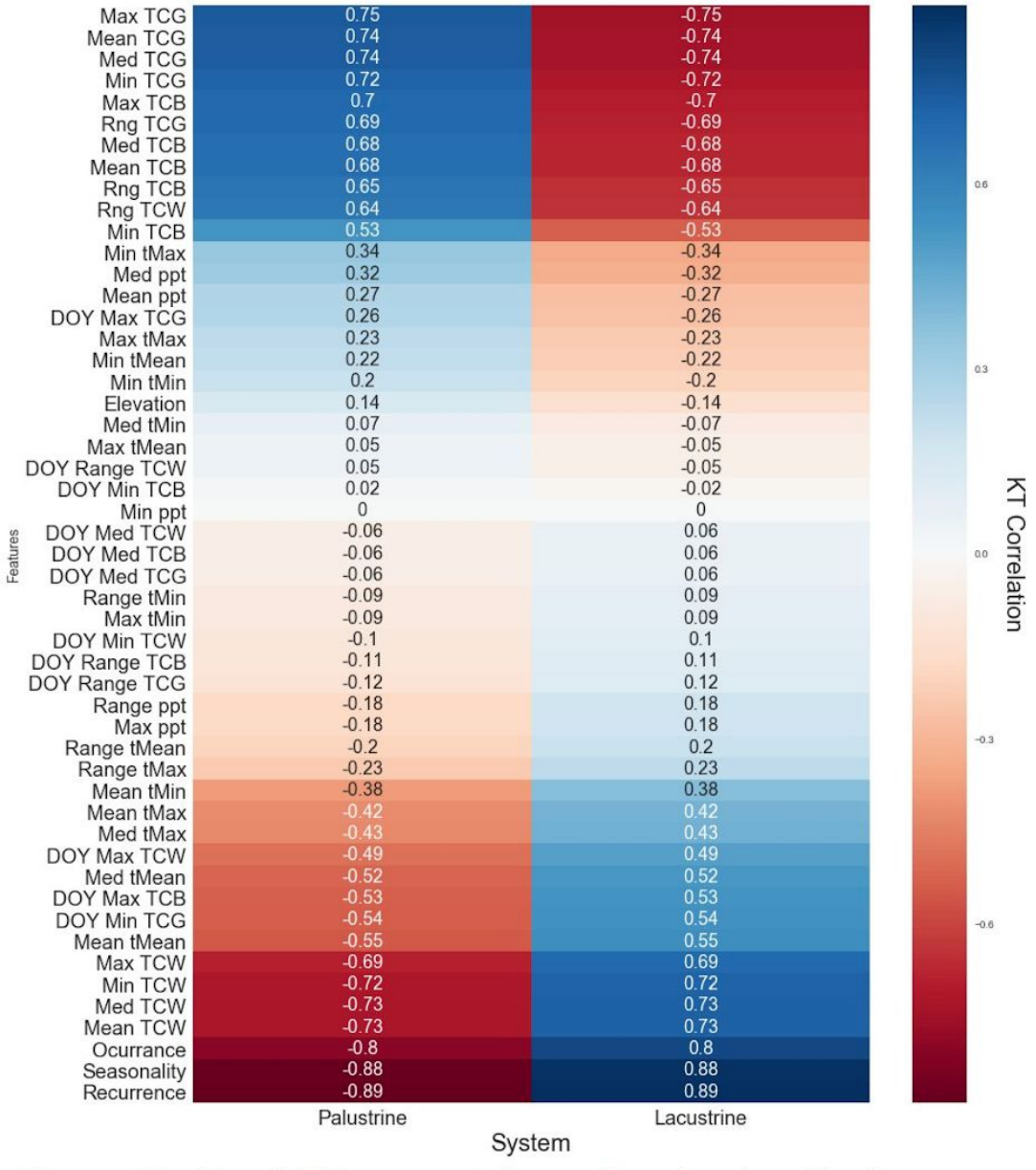

Figure 2.11: Kendall Tau correlation scores for classification features and System classification probabilities.

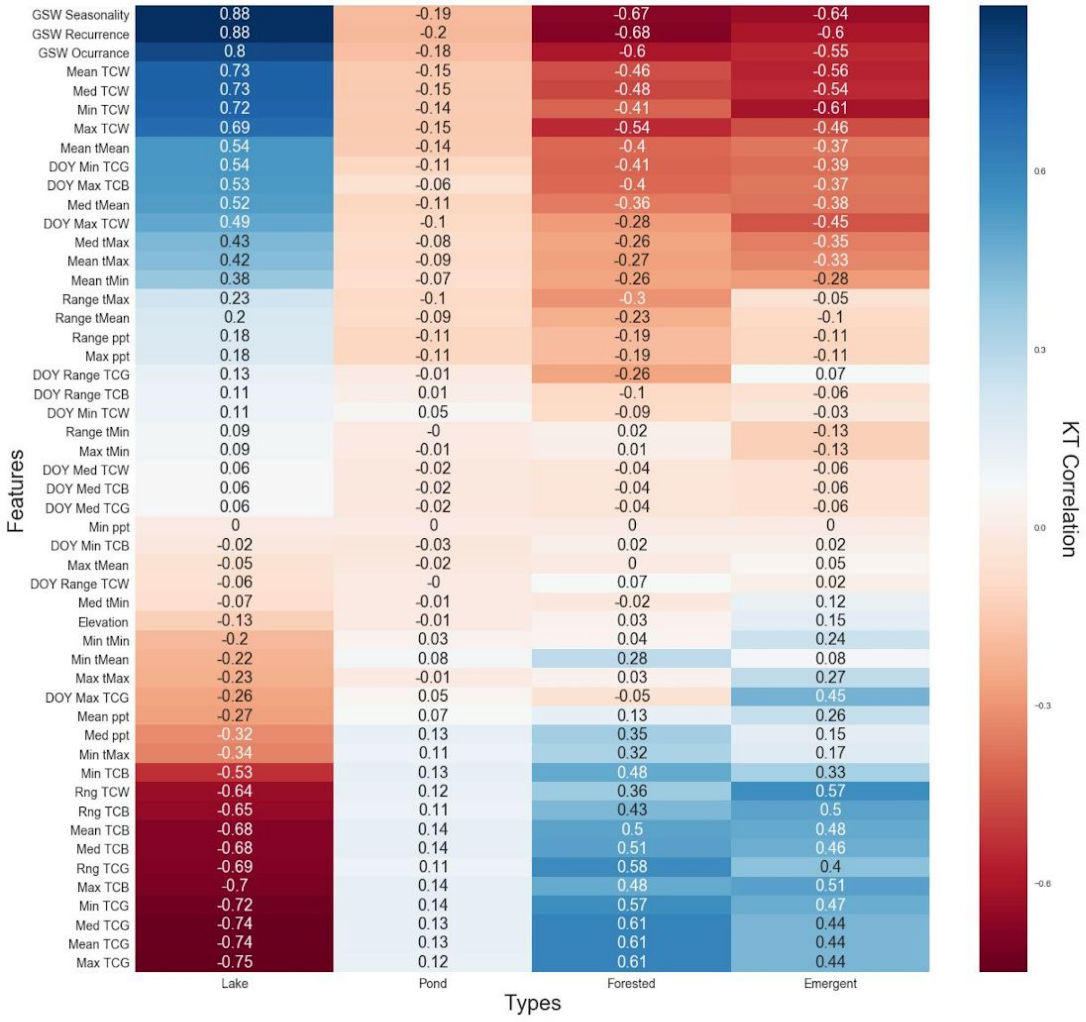

Figure 2.12: Kendall Tau correlation scores for classification features and Type classification probabilities.

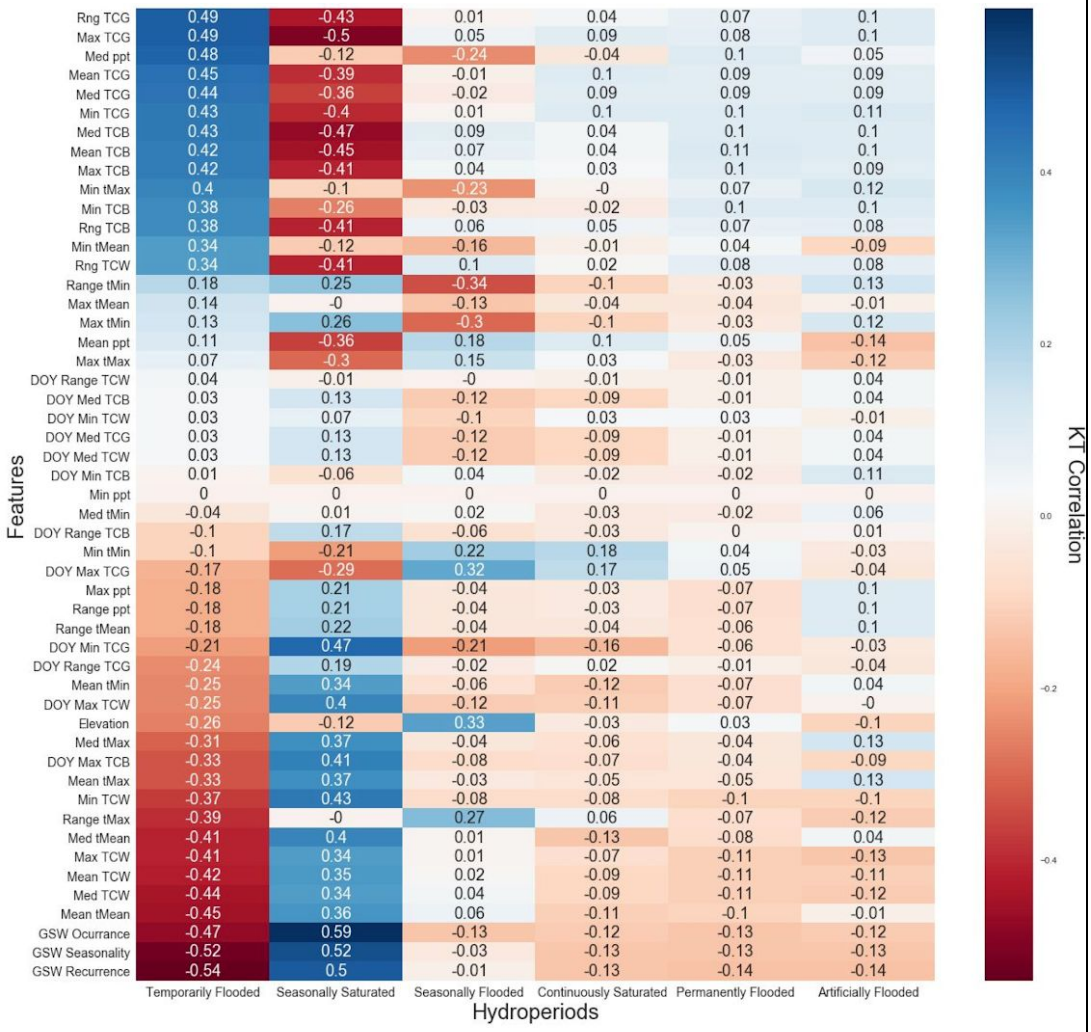

Figure 2.13: Kendall Tau correlation values for classification features and Willamette Valley Hydroperiod classification probabilities.

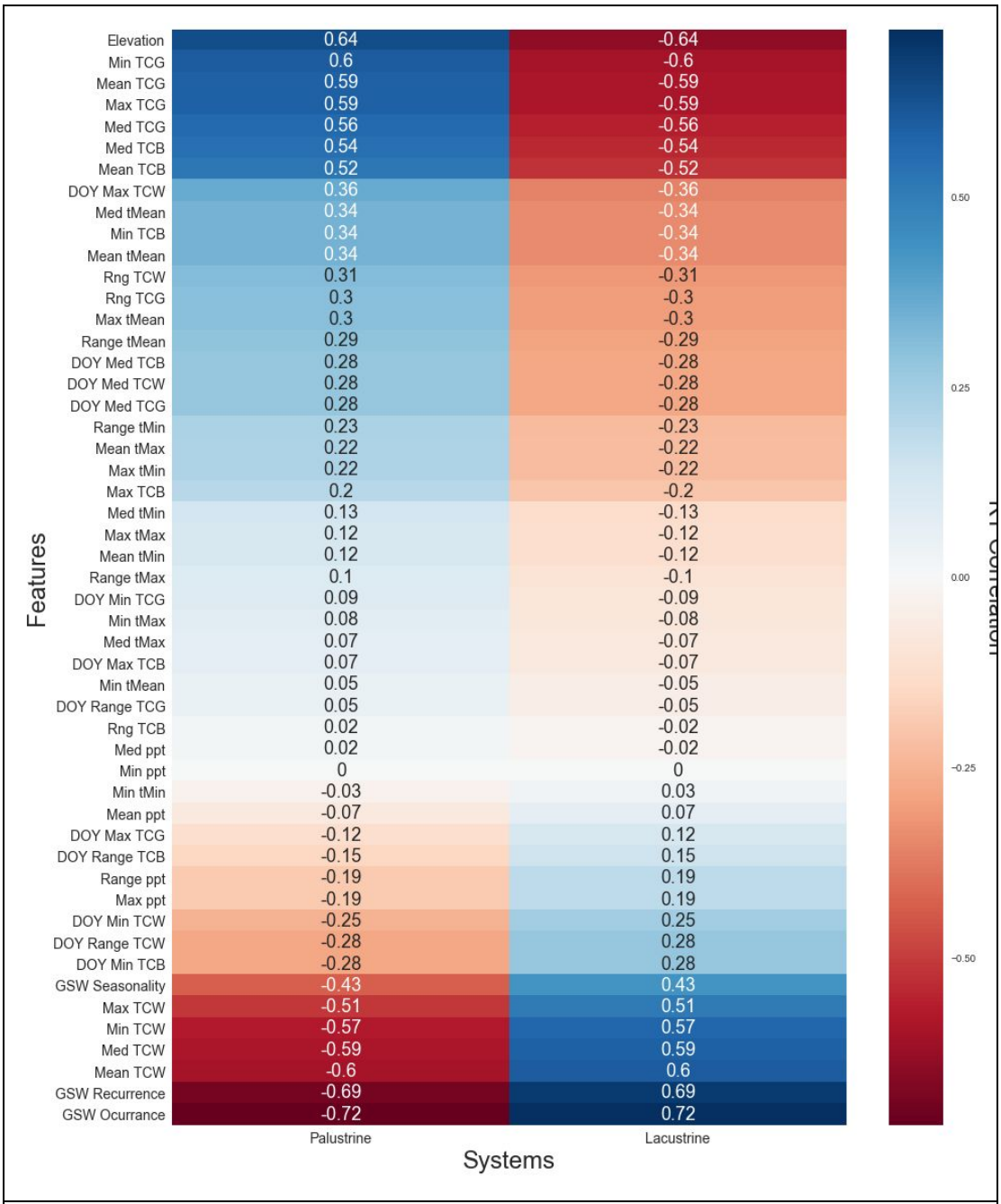

Figure 2.14: Kendall Tau correlation values for classification features and North Basin System classification probabilities.

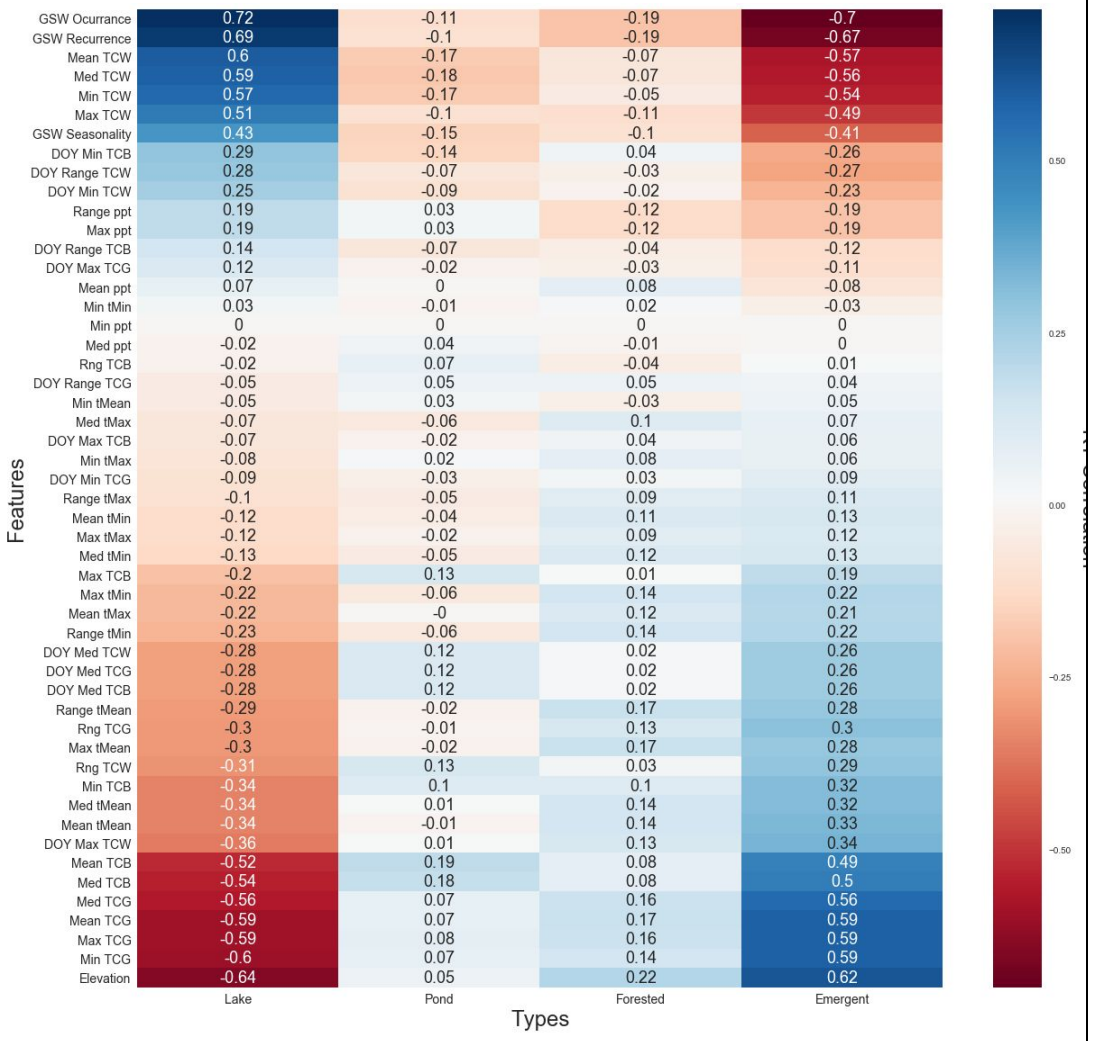

Figure 2.15: Kendall Tau correlation values for classification features and North Basin Type classification probabilities.

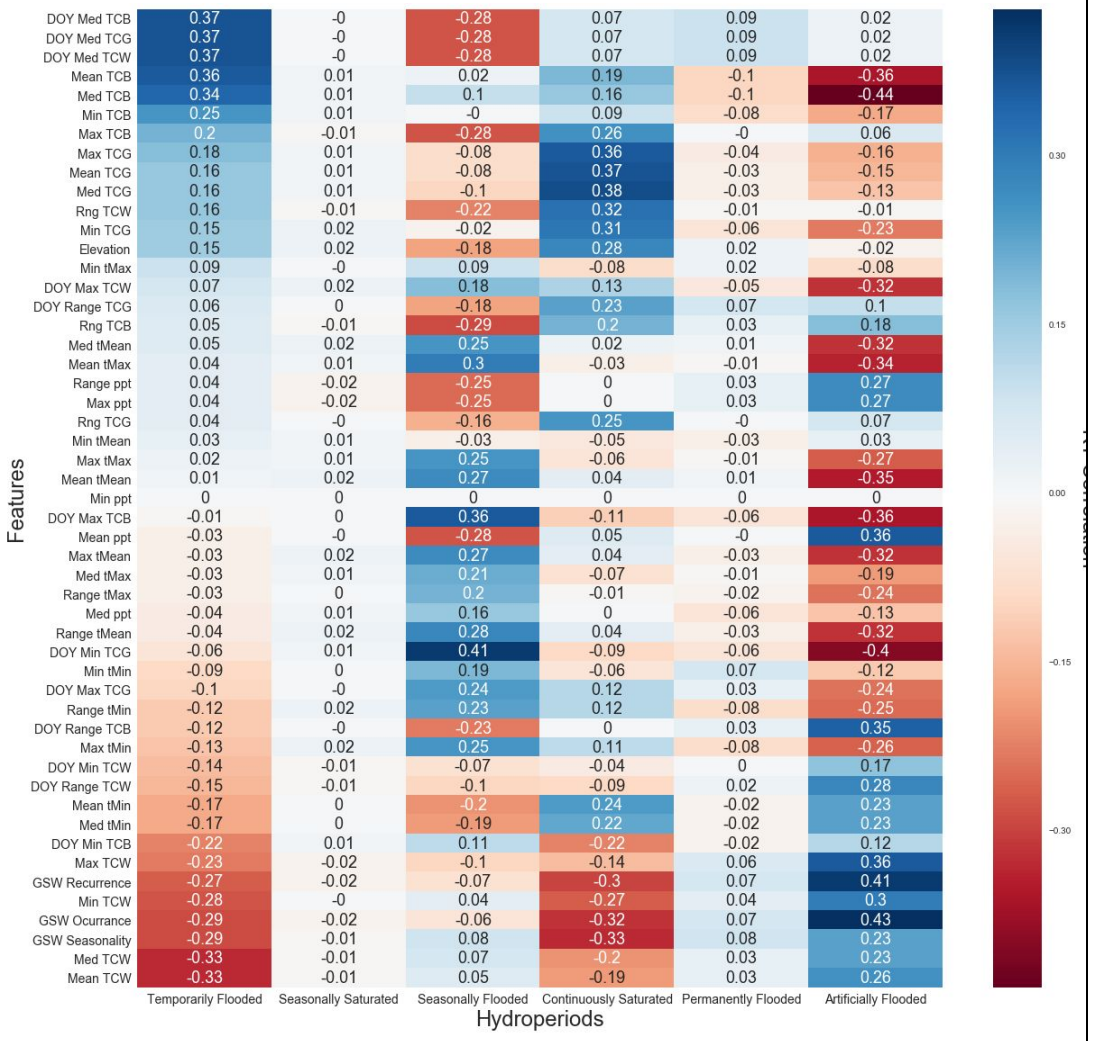

Figure 2.16: Kendall Tau correlation values for classification features and North Basin Hydroperiod classification probabilities.

CHAPTER 2 TABLES

Wetland System Habitat	Description
Palustrine	Vegetated wetlands traditionally called by such names as marsh, swamp, bog, fen, and prairie. Also includes small, shallow, permanent or intermittent water bodies. May be situated shoreward of lakes and river channels, on river floodplains, or in isolated catchments. They may also occur as islands in lakes or rivers.
Lacustrine	Permanently flooded lakes and reservoirs, and intermittent lakes. Typically, there are extensive areas of deep water and there is considerable wave action. Islands of Palustrine wetlands may lie within the boundaries of the Lacustrine System.

Table 2.1: NWI descriptions of System level wetland habitats (Cowardin et al. 1979; FGDC 2013)

Wetland Type Habitat	**Description**
Lake	All Lacustrine *System* wetlands.
Pond	Palustrine *System*, includes subclass 'Unconsolidated Bottom'. Wetlands with vegetative cover less than 30 percent and lack of large stable surfaces for plant and animal attachment.
Forested	Palustrine *System*; includes subclasses 'Scrub Shrub' and 'Forested'. Wetlands where woody plants are the dominant vegetative life for. Wetlands possess an overstory of trees, an understory of young trees or shrubs, and an herbaceous layer.
Emergent	Palustrine *System*; includes subclass 'Emergent'. Wetlands where erect, rooted, herbaceous hydrophytes are the tallest life form with at least 30% areal coverage. Vegetation is present for most of the growing season in most years.

Table 2.2: NWI descriptions of *Type* level wetland habitats (Cowardin et al. 1979; FGDC 2013)

Wetland Hydroperiod Habitat	**Description**
Temporarily Flooded	Surface water is present for brief periods (from a few days to a few weeks) during the growing season, but the water table usually lies well below the ground surface for the most of the season.
Seasonally Saturated	The substrate is saturated at or near the surface for extended periods during the growing season, but unsaturated conditions prevail by the end of the season in most years. Surface water is typically absent, but may occur for a few days after heavy rain and upland runoff.
Seasonally Flooded	Surface water is present for extended periods (generally for more than a month) during the growing season, but is absent by the end of the season in most years. When surface water is absent, the depth to substrate saturation may vary considerably among sites and among years.
Continuously Saturated	The substrate is saturated at or near the surface throughout the year in all, or most, years. Widespread surface inundation is rare, but water may be present in shallow depressions that intersect the groundwater table.
Permanently Flooded	Water covers the substrate throughout the year in all years.
Artificially Flooded	The amount and duration of flooding are controlled by means of pumps or siphons in combination with dikes, berms, or dams.

Table 2.3: NWI descriptions of *Hydroperiod* level wetland habitats (Cowardin et al. 1979; FGDC 2013)

Feature	**Label**	**Equation**
TCB Maximum	TCB Max	max(*TCB*)
TCG Maximum	TCG Max	max(*TCG*)
TCW Maximum	TCW Max	max(*TCW*)
TCB Minimum	TCB Min	min(*TCB*)
TCG Minimum	TCG Min	min(*TCG*)
TCW Minimum	TCW Min	min(*TCW*)
Range of TCB	Range of TCB	|max(*TCB*) - min(*TCB*)|
Range of TCG	Range of TCG	|max(*TCG*) - min(*TCG*)|
Range of TCW	Range of TCW	|max(*TCW*) - min(*TCW*)|
TCB Median	TCB Med	$\tilde{x}(TCB)$
TCG Median	TCG Med	$\tilde{x}(TCG)$
TCW Median	TCW Med	$\tilde{x}(TCW)$
TCB Mean	TCB Mean	$\bar{x}(TCB)$
TCG Mean	TCG Mean	$\bar{x}(TCB)$
TCW Mean	TCW Mean	$\bar{x}(TCW)$

Table 2.4: Reflectance spectral-temporal features calculated for Tasseled Cap Brightness (TCB), Greenness (TCG), and Wetness (TCW). Features are calculated for all available images for the year 1995.

Feature	**Label**	**Equation**
DOY TCB Maximum	TCB Max	DOY max(*TCB*)
DOY TCG Maximum	TCG Max	DOY max(*TCG*)
DOY TCW Maximum	TCW Max	DOY max(*TCW*)
DOY TCB Minimum	TCB Min	DOY min(*TCB*)
DOY TCG Minimum	TCG Min	DOY min(*TCG*)
DOY TCW Minimum	TCW Min	DOY min(*TCW*)
DOY Range of TCB	Range of TCB	DOY |max(*TCB*) - min(*TCB*)|
DOY Range of TCG	Range of TCG	|DOY max(*TCG*) - DOY min(*TCG*)|
DOY Range of TCW	Range of TCW	DOY |max(*TCW*) - min(*TCW*)|
DOY TCB Median	TCB Med	DOY $\tilde{x}$(*TCB*)
DOY TCG Median	TCG Med	DOY $\tilde{x}$(*TCG*)
DOY TCW Median	TCW Med	DOY $\tilde{x}$(*TCW*)

Table 2.5: Day of year (DOY) spectral-temporal features calculated for Tasseled Cap Brightness (TCB), Greenness (TCG), and Wetness (TCW) reflectance STFs (Table 4). Features are extracted from all available images for the year 1995.

Feature	**Label**	**Equation**
Maximum of the Daily Maximum Temperature	Max tMax	max(*tMax)*
Minimum of the Daily Maximum Temperature	Min tMax	min(*tMax)*
Range of the Daily Maximum Temperature	Range of tMax	|max(*tMax*) - min(*tMax*)|
Median of the Daily Maximum Temperature	Med tMax	$\tilde{x}$(*tMax)*
Mean of the Daily Maximum Temperature	Mean tMax	$\bar{x}$max(*tMax)*
Maximum of the Daily Minimum Temperature	Max tMin	max(*tMin)*
Minimum of the Daily Minimum Temperature	Min tMin	min(*tMin)*
Range of the Daily Maximum Temperature	Range of tMin	|max(*tMin*) - min(*tMin*)|
Median of the Daily Minimum	Med tMin	$\tilde{x}$(*tMax)*

Temperature		
Mean of the Daily Minimum Temperature	Mean tMin	$\bar{x}$max(*tMax)*
Maximum of the Daily Median Temperature	Max tMed	max(*tMed)*
Minimum of the Daily Median Temperature	Min tMed	min(*tMed)*
Range of the Daily Median Temperature	Range of tMed	|max(*tMed*) - min(*tMed*)|
Median of the Daily Median Temperature	Med tMed	$\tilde{x}$(*tMed)*
Mean of the Daily Median Temperature	Mean tMed	$\bar{x}$max(*tMed)*
Maximum of the Daily Mean Temperature	Max tMean	max(*tMean)*
Minimum of the Daily Mean Temperature	Min tMean	min(*tMean)*
Range of the Daily Mean Temperature	Range of tMean	|max(*tMean*) - min(*tMean*)|
Median of the Daily Mean Temperature	Med tMean	$\tilde{x}$(*tMean)*

Mean of the Daily Mean Temperature	Mean tMean	$\bar{x}$max(*tMean)*
Maximum of the Daily Total Precipitation	Max ppt	max(*ppt)*
Minimum of the Daily Total Precipitation	Min ppt	min(*ppt)*
Range of the Daily Total Precipitation	Range of ppt	|max(*ppt*) - min(*ppt*)|
Median of the Daily Total Precipitation	Med ppt	$\tilde{x}$(*ppt)*
Mean of the Daily Total Precipitation	Mean ppt	$\bar{x}$max(*ppt)*

Table 2.6: Per-pixel climate-temporal features calculated for daily Max, Min, Med, and Mean temperature, and Max, Min, Med, and Mean ppt. Features are extracted from 365 days of PRISM climate model data from 1995.

Feature	**Label**	**Description**
Global Surface Water Occurrence	GSW Occurrence	The frequency with which water is present.
Global Surface Water Recurrence	GSW Recurrence	The frequency with which water returns from year to year.
Global Surface Water Seasonality	GSW Seasonality	Number of months water is present.
Digital Elevation Model	Elevation	Elevation

Table 2.7: Ancillary data features. GSW Occurrence and Recurrence are calculated for the time period 1984 - 2015 and GSW Seasonality is calculated for the period 2014-2015. Elevation is derived from the The Shuttle Radar Topography Mission in February 2000.

Feature-Set	**Features**
STFs	All reflectance STFs
DOY STFs	All DOY STFs
All STFs	Reflectance STFs and DOY STFs
CTFs	CTFs
GSW	GSW features
All STFs + Elevation	Reflectance STFs, DOY STFs, and Elevation
All STFs + GSW	Reflectance STFs, DOY STFs, and GSW features
All Features	Reflectance STFs, DOY STFs, CTFs, GSW features, and Elevation

Table 2.8: Feature-set names and the features that are contained within each group

	Truth			
Predicted	**Palustrine**	**Lacustrine**	**Total**	**Error of Commission (%)**
Palustrine	27399	5757	33156	17.4
Lacustrine	995	24070	25065	4.0
Total	28394	29827	58221	
Error of Omission (%)	3.5	19.3		

Table 2.9: Pixel-scale confusion matrix for Willamette Valley Wetland Systems. Values correspond to number of pixels correctly or incorrectly labeled based on agreement between reference data (truth) and classified pixels (predicted).

	Truth					
Predicted	**Lake**	**Pond**	**Forested**	**Emergent**	**Total**	**Error of Commission (%)**
Lake	25432	30	48	1569	27079	6.1
Pond	15	10	11	22	58	82.8
Forested	88	40	9398	2887	12413	24.3
Emergent	4292	161	1877	12341	18671	33.9
Total	29827	241	11334	16819	58221	
Error of Omission (%)	14.7	95.85	17.1	26.6		

Table 2.10: Pixel-scale confusion matrix for Willamette Valley Wetland Types. Values correspond to number of pixels correctly or incorrectly labeled based on agreement between reference data (truth) and classified pixels (predicted).

	Truth							
Predicted	**Temporarily Flooded**	**Seasonally Saturated**	**Seasonally Flooded**	**Continuously Saturated**	**Permanently Flooded**	**Artificially Flooded**	**Total**	**Error of Commission (%)**
Temporarily Flooded	4220	7	1259	21	4	1	5512	23.4
Seasonally Saturated	0	3340	1444	0	3	0	4787	30.2
Seasonally	2511	5386	38639	530	152	109	47327	18.4

Flooded								
Continuously Saturated	7	0	417	10	14	0	448	97.8
Permanently Flooded	0	23	71	0	1	0	95	98.9
Artificially Flooded	0	0	7	0	0	45	52	13.5
Total	6738	8756	41837	561	174	155	58221	
Error of Omission (%)	37.4	61.8	7.6	98.2	99.4	71.0		

Table 2.11: Pixel-scale confusion matrix for Willamette Valley Wetland Hydroperiods. Values correspond to number of pixels correctly or incorrectly labeled based on agreement between reference data (truth) and classified pixels (predicted).

	Truth			
Predicted	**Palustrine**	**Lacustrine**	**Total**	**Error of Commission (%)**
Palustrine	276132	55846	331978	16.86
Lacustrine	37124	276604	313728	11.83
Total	313256	332450	645706	
Error of Omission (%)	11.8	16.8		

Table 2.12: Pixel-scale confusion matrix for North Basin Wetland Systems. Values correspond to number of pixels correctly or incorrectly labeled based on agreement between reference data (truth) and classified pixels (predicted).

	Truth					
Predicted	**Lake**	**Pond**	**Forested**	**Emergent**	**Total**	**Error of Commission (%)**
Lake	275170	5881	370	35696	317117	13.2

Pond	4775	4559	1	13244	22579	79.8
Forested	1830	14	890	5278	8012	88.9
Emergent	50675	14517	2094	230712	297998	22.6
Total	332450	24971	3355	284930	645706	
Error of Omission (%)	17.2	81.7	73.5	19.0		

Table 2.13: Pixel-scale confusion matrix for North Basin Wetland Types. Values correspond to number of pixels correctly or incorrectly labeled based on agreement between reference data (truth) and classified pixels (predicted).

	Truth							
Predicted	**Temporarily Flooded**	**Seasonally Saturated**	**Seasonally Flooded**	**Continuously Saturated**	**Permanently Flooded**	**Artificially Flooded**	**Total**	**Error of Commission (%)**
Temporarily Flooded	6599	0	9469	3971	0	2528	22567	70.8
Seasonally Saturated	44	5	0	0	0	0	49	89.8
Seasonally Flooded	24871	2	29374	13761	51	2737	70796	58.5
Continuously Saturated	7604	0	21578	18516	0	1368	49066	62.3
Permanently Flooded	0	0	0	103	0	0	103	100.0
Artificially Flooded	721	0	872	3716	145	582	6036	90.35785288
Total	39839	7	61293	40067	196	7215	148617	
Error of Omission (%)	83.4	28.6	52.1	53.8	100.0	91.9		

Table 2.14: Pixel-scale confusion matrix for North Basin Wetland Hydroperiods. Values correspond to number of pixels correctly or incorrectly labeled based on agreement between reference data (truth) and classified pixels (predicted).

CHAPTER 3

APPLYING ANNUAL LANDSAT SPECTRAL-TEMPORAL FEATURES TO MONITOR INTRA-AND INTER-ANNUAL WETLAND ECOSYSTEM DYNAMICS FROM FROM 1985 - 2017

Introduction

Globally, wetlands cover between 5 and 10% of the land surface but are decreasing in area and functionality at accelerating rates as a result of land use change and water resource expansion for agricultural, urban and industrial development (Tockner et al., 2008, Fickas et al. 2015). A probable impact of climate change will be increasing rates of wetland decline across the planet, as wetland ecosystems are specifically vulnerable to changes in quantity and quality of water supply (Burket and Kusler, 2000; Dawson et al.,2003; Kingsford, 2011). As it progresses, climate change will, broadly, modify precipitation and evapotranspiration rates and yield changes in runoff and groundwater levels (House et al. 2016). The essential roles of these drivers in controlling wetland vegetation (Baldwin et al., 2001, animals (Ausden et al., 2001; McMenamin et al., 2008) and biogeochemical cycling (Grimm et al., 2003) means that climate change is likely to have major impacts on global wetlands, species dependent on these habitats, and the various ecosystem services which they provide. However, the effects of climate and other anthropogenic change in wetlands are unlikely to be uniform across climate zones and ecohydrological contexts (Arnell and Reynard,1996; Radojevic et al., 2010).

Wetland Hydrology and Phenology

Hydrology is regarded as an essential determinant characteristics of establishment and persistence of wetlands and wetland processes (Zhang et al. 2012, Todd et al. 2010). Wetland hydrology starts at the interaction between climate and landscape geomorphology . With all other metrics held constant, wetlands are more likely to persist in cool wet climates than hot or dry climates. Cooler climates are less subject to evapotranspirative water loss and wetter climates experience greater precipitation, often in surplus (Mitsch and Gosselink 2015). Geomorphology of the system, catchment, and greater landscape also frame wetland habitat persistence. Areas of high relief and steep terrain are less likely to house wetlands than locations with gentle slopes and depressions. Further, wetlands in isolated catchments will have distinct differences in hydrologic behavior than ecosystems with connectivity to streams or tidal inundation. Considered together in the context of hydrology climate and geomorphology constitute a wetland system's hydrogeomorphology.

The hydrogeomorphology of a wetland ecosystem drives and influences the inflow and outflow of water into the system, creating a wetland water budget. A freshwater wetland's water budget can be seen as (Mitsch and Gosselink 2015):

$$V/t = Pn + Si + Gi - ET - SO - GO$$

where

V= volume of water storage in wetlands

V/t = change in volume of water storage in wetlands per unit time, t

Pn = net precipitation

Si = surface inflows, including stream flooding

Gi = groundwater inflows

ET = evapotranspiration

SO = surface outflows

GO = groundwater outflows

In addition to hydrogeomorphology, the temporal hydrologic signature of a wetland further characterizes and distinguishes wetland behavior. The seasonal pattern of a wetland's water budget can be defined as a hydroperiod (Euliss et al. 1999) (also referred to as a water regime). A hydroperiod describes the temporal rise and fall pattern of a wetland ecosystem's surface and subsurface water through temporal specification of the wetland's water budget. A wetland hydroperiod is not the same each year and can fluctuate annually, seasonally, daily, or unpredictably with climate and antecedent conditions (Brooks 2004).

A wetland's hydroperiod is significantly related to its vegetation community variation (Toogood and Joyce 2009) and is a key physical factor underlying ecosystem conditions at a given time (Katz et al. 2009). Specifically, wetland hydrology drives chemical and physical processes in wetlands creating biotic feedbacks. First, hydrology acts as a limiter or stimulus to vegetative species richness by selecting water-tolerant species (hydrophytes) and excluding flood-intolerant species. The hydroperiod, therefore, influences the spatio-temporal competitive

interactions among species (Keddy & Reznicek 1986). Hydroperiods that include sustained flooding for extended durations tend to be associated with lower species richness and primary productivity, whereas species richness and primary productivity tends to be higher in wetlands with pulsing hydrology and hydroperiods with greater complexity (Odum et al. 1995). The temporal pattern of hydrology, therefore has a direct affect on wetland phenology.

Phenology can be characterized as the timing of recurrent biological events, the causes of their timing with regard to biotic and abiotic forces, and the interrelation among phases of the same or different species (Lieth 1974). From organisms to ecosystems, plant species are highly calibrated to the temporal patterns of their surrounding environment (Cleland et al. 2007). Phenology varies widely over geographic scales and climate zones and significant variability in phenological features is seen as a result of interannual variability in climate and weather (Richardson et al. 2013).

Vegetation phenologies (as opposed to animal phenologies) are largely characterized through phenoclimatic measures (metrics of temperature that assimilate over important temporal stages for plant growth and development) and phenophases (period of development such as bud burst, flowering, or senescence). In many upland terrestrial ecosystems, such as deciduous hardwood forests, phenological processes and drivers are well studied with predictable annual cycles. For example, air temperature is the most important factor in regulating budburst and leaf-out in

temperate and boreal woody plants (Linkosalo et al. 2006; Polgar and Primack 2011) with photoperiod also understood to play a role (Ghelardini et al. 2014). However, given that wetlands are more transitional and spatially and temporally complex ecosystems, phenology cycles may not be as predictable and hydrology is likely to play a much larger role.

In addition to vegetation phenologies, wetland hydroperiods also drive geochemical patterns essential for wetland habitats. Soils that are subject to long periods of saturation are referred to as hydric soils and inundation or prolonged saturation creates chemical shifts in the soil environment. When oxygen is restricted below the soil surface, changes in the chemical composition of soil minerals and carbon will occur as both physical and biological processes . In reaction to restricted oxygen levels, there are changes in the activity of soil microbes that use oxygen as the terminal electron acceptor in the process of oxidation of organic molecules. Oxygen that is available in the soil is depleted through microbial metabolism. Once oxygen levels are drained, biological activity is restricted to microbial communities that have the capacity to use elemental minerals other than oxygen as electron receptors in metabolism. Through this process, the oxidized forms of the soil minerals are reduced.

In wetland ecosystems, the reduction-oxidation (redox) potential of soils is a key indicator of physically and/or biologically driven chemical reactions such as oxygen demand, decomposition, geochemical equilibria, and potential plant stress

(Thomas et al. 2009). Soil redox potential is controlled by soil temperature, water levels, soil carbon, and nutrient supply (Thomas et al. 2009; Pezeshki and DeLaune). Soil temperature regulates the rate of chemical reactions, which significantly slows at temperatures below 5°C (Megonigal and Faulkner 1996). Water level is also directly linked to redox potential. As water saturation levels decrease, redox potential increases linearly or exponentially, depending on wetland type (Niedermeier and Robinson 2007; Thomas et al. 2009). Water depth and temperature vary temporally and spatially and through multiple scales. Relative to wetland phenological metrics, the seasonal variation in water depth and temperature will result in temporal variability and therefore unique phenologies among different wetland ecosystems. From a phenological perspective, wetland vegetation phenophases are driven by both the more traditional phenoclimatic measures such as temperature, but also by timing of wetland hydrology. Hydrophytic species have a range of flood tolerances and will, therefore, be distributed temporally (both intra-and inter-annually) and spatially based on hydrologic drivers at the local, regional, and landscape scale.

Pacific Northwest

Monitoring the hydrologic change in global surface water dynamics has recently been recognized as a key necessity for monitoring important hydrological and ecological resources over time and observing the effects of climate and anthropogenic change on water resources. In the Pacific Northwest (PNW) of the United States, the various impacts of climate variations on hydrology have been well

studied (Hamlet and Lettenmaier, 1999; Payne et al., 2004; Luce and Holden, 2009; Lee et al., 2009; Elsner et al., 2010; Hamlet et al., 2010; Luce et al., 2013; Safeeq et al., 2014, Vano et al. 2015). The PNW is a topographically complex region with a unique relationship to climate, weather, and hydrology. In this region, most precipitation occurs in the fall and winter, and complex topography, such as the Cascade mountain range, allows precipitated snow to accumulate in winter, melt in spring and summer (Vano et al. 2015), and serve as a natural reservoir that slowly releases water throughout the dry season providing sustained streamflow critical for water-dependent ecosystems, such as wetlands.

For locations where water is not a limiting resource in the PNW, such as the Willamette Valley Ecoregion, runoff, precipitation, and groundwater all supply key hydrologic inputs to wetland ecosystems. In contrast, in water-limited regions, such as the Northern Basin and Range Ecoregion, surface streamflow released from seasonal snowpack is the main source of hydrologic input and essential to wetland persistence and function. While the Willamette Valley has more hydrologic inputs to buffer against change in individual variables compared to the Northern Basin and Range, both ecoregions are subject to climate variability through changes in temperature and precipitation patterns but may vary in their ecohydrological response . To begin to understand where, when, and how wetland habitats are changing over time, it is essential to implement wetland ecosystem classification and monitoring that captures both intra-and inter-annual variability across broad scales of space and time.

The U.S. monitors its national wetlands with the National Wetland Inventory, a mapping and monitoring program run by the U.S. Fish and Wildlife Service that utilizes digital delineation of single-date aerial photography, remote sensing data, field work, and other ancillary feature class maps to classify wetlands. However, the NWI is implemented at the State level and some maps are over three decades old. In other ecosystems, such as forests, remote sensing has emerged as the key technology for detailed mapping of land surface processes across a range of spatial scales. Specifically, with the free and open Landsat archive, intra-and inter-annual land cover classification of large geographic areas over multiple decades is now achievable (Hermosilla et al. 2018). In the study presented here, we use all available Landsat imagery from 1985 - 2017 to explore how Pacific Northwest wetland ecosystems are changing over time in different climate zones and at varying categorical resolutions. Additionally, we investigate the long term changes in abstracted Landsat spectral-temporal features that are closely associated with different aspects of wetland hydro-ecological processes. Specifically our objectives are to:

1) Employ a new modeling framework for annual wetland classification that captures intra-annual variability with Landsat spectral-temporal and related features,

2) Test our model on areas of known wetland land use changes,

3) Quantify how the probability of occurrence of individual wetland habitats arechanging over time, and

3) Explore how trends in specific Landsat spectral-temporal features can be used as measures for wetland hydrological and ecological dynamics change over time.

Methods

Study Area

Across its geographic boundaries, the Pacific Northwest has a wide gradient in temperature (Chapter 2, Figure 1A) and precipitation (Chapter 2, Figure 1B), yielding a fitting geographical context in which to explore how wetlands are changing over time and in divergent climate zones. The State of Oregon, specifically, contains a varied and distinct climatic gradient, and hosts a diversity of wetland habitat that is critical to sustaining important waterfowl populations in the Pacific Flyway migratory path as well as rare, threatened, and endangered species.

The most influential geographic feature of Oregon climate is the Pacific Ocean, which lines the entire state on the western border. Air masses move west to east off of the coast and have traveled extensively over the Pacific before making landfall. Subsequently, annual minimum and maximum temperatures are highly moderated, especially in the western portion of the state with temperature extremes generally associated with continental air masses. Journeys across the Pacific allow air masses access to an unlimited supply of moisture, a feature that yields abundant precipitation in western Oregon and high elevations in eastern Oregon.

With close proximity to and paralleling the coastline, Oregon's Coast Range mountains run the full length of the State and range between 600 - 1700 meters. As marine air systems move east across the state, the Coast Range forces the air masses to rise. Fontal storm systems, often already precipitating, are pushed against the range, producing heavy rainfall through orographic lift and significantly reducing available moisture in the air (Smith et al. 2005). Moving eastward, air then moves into the Willamette Valley and subsequently ascends into the Cascade Mountains, which parallel the Coast Range roughly 120 km inland through the majority of the state. Similar to the path over the Coast Range, air masses are forced to rise over the Cascades and let go of moisture. However, precipitation potential of the air mass was reduced by the transition over the Coast Range and, therefore, rainfall on the western slopes of the Cascades (at similar elevations) is at 50-65% of Coast Range levels. On the easterly, leeward side of the Cascades, precipitation is even further reduced and begins to sharply diminish as it moves east across the North Basin and Range.

To capture the spatio-temporal climate gradient in Oregon when evaluating wetland change over time, we chose two Level III EPA ecoregions: the Willamette and the Northern Basin and Range (called the North Basin from here on out) (Chapter 2, Figure 2). Broadly, the North Basin can be characterized as a water-limited ecoregion, where water availability is typically the primary limiting resource in determining hydrology and vegetation patterns (Fernandez-Illescas and Rodriguez-Iturbe 2003). Conversely, the Willamette Valley sits in an energy-limited

setting where solar irradiation (sunlight) limits wetland ecological dynamics (Gallucci 1973).

Wetlands Reference Data

We used the Oregon NWI map from 1995 as reference data to train our classification model. Currently, the NWI uses a hierarchical classification taxonomy of Cowardin et al. (1979) to delineate and characterize individual wetlands. Generally, NWI maps have shown variability in accuracy with low errors of commission but relatively high errors of omission (Stolt and Baker 1995; Wright and Gallant 2007). With its lower errors of commission, the NWI can act as a reliable source for reference wetland spatial data (Nielsen et al. 2008).

Due to both natural and anthropogenic change, locating functionally consistent and low anthropogenic disturbance wetland ecosystems can be a challenge. To further ensure our wetlands reference data was as accurate as possible, we used NWI wetland locations in both ecoregions from the National Wildlife Refuge System (NWRS) (Chapter 2, Figure 2). NWRS policy uses historic conditions as the reference condition for maintaining wetland ecosystem functioning, yielding optimal reference sites for wetland classification and characterization (Andel and Aronson 2012). In the Willamette Valley we chose the Willamette Valley National Wildlife Complex and Fern Ridge Wildlife Area, and in the North Basin, we chose the Malheur National Wildlife Refuge.

To explore long-term trends in wetland ecosystems at different ecological resolutions, we ran our classification model on NWI wetland System, Type, and Hydroperiod wetlands separately. In this study, system-level wetlands include Palustrine (vegetated) and Lacustrine (non-vegetated) wetlands. At a finer ecosystem categorical resolution, Type-level wetlands include Lake, Pond, Forested, and Emergent wetlands. Lastly, wetlands in different Hydroperiods are distinguished by their saturation level and inundation duration (Chapter 2, Tables 1-3).

The NWI polygons used as reference data were selected based on their spatial intersection with the NWRS boundaries in both ecoregions. These polygons were further refined based on size. To reduce the impact of edge effect, polygons less than 5 pixels were eliminated. Although both study areas contain Riverine System wetlands (Cowardin et al. 1979), many, if not a majority of, Riverine polygons are less than one Landsat pixel wide (30 meters) and therefore more influenced by edge effects. We, consequently, did not include Riverine wetland polygons in our study. By NWI definition, Riverine wetlands only represent habitats within a channel and do not include floodplain wetland habitats associated with a specific river or stream, which are part of the Palustrine System.

Three separate reference datasets were derived based on ecological categorical resolution: Systems polygons, Types polygons, and Hydroperiod polygons. Due to the hierarchical nature of the NWI classification scheme, these data overlap. For

example, Palustrine wetlands also contain wetland habitats from different Types and Hydroperiods.

Classification Inputs

Landsat Data

All available Landsat Thematic Mapper (TM), Enhanced Thematic Mapper Plus (ETM+), and Operational Land Imager (OLI) Surface Reflectance Tier 1 pixel-level data was accessed from Google Earth Engine (GEE) (Gorelick et al. 2017) for the period January 1 1985 through December 31 2017. Landsat Tier 1 data are atmospherically corrected using LEDAPS (Masek et al. 2006), processed at Level-1 Precision Terrain (L1TP), and georegistered to a consistent standard. Pixels were masked for cloud, shadow and snow using CFMASK (Foga et al. 2017). The Tasseled Cap (TC) Transformation spectral vegetation index, which orthogonally converts the six Landsat reflectance bands results into three indices known as brightness (TCB), greenness (TCG), and wetness (TCW) (Crist et al. 1985), was then applied to every unmasked pixel for all available dates.

While some spectral indices, such as the normalized difference vegetation index (NDVI) are computationally and theoretically simpler, many recent remote sensing wetland studies have found the utility in the TC transformation. TC indices adds more data dimensionality than single vegetation indices, which is especially important in spatially and temporally heterogeneous ecosystems such as wetlands. Further, in addition to TC greenness's link to vegetation dynamics, the combination

of the brightness and wetness indices is correlated with soil moisture content, giving additional insight to distinction between wetland and upland vegetation (Fickas et al. 2016). Several studies have successfully demonstrated the power of TC indices in spatio-temporal wetland classification and change detection (Fickas et al. 2016, Pasquarella et al. 2016, Kayastha et al. 2012, Baker et al. 2006, Baker et al. 2007, Wright and Gallant 2007).

Spectral-Temporal Features

Annual, primary STFs (Pasquarella et al. 2018 in prep) were calculated from our processed Landsat pixels for each year (Julian date 0-365) from 1985 - 2017. The first five derived STFs include the annual 1) maximum (max), 2) minimum (min), 3) median (med), 4) mean, and 5) range (difference between maximum and minimum), for our three spectral features, TCB, TCG, and TCW, individually. In addition to the primary reflectance STFs, their respective day of year (DOY) was also extracted. These DOY STFs include DOY of the annual 1) max, 2) min, 3) med, and 4) range (range of days between the DOY of annual max and min) of TCB, TCG, and TCW. Together, the primary STFs add 27 features to the classification model (Chapter 2, Table 5).

Climate-Temporal Features

Given the importance of local and regional climate variability to the functionality and persistence of wetland habitats, we include spatio-temporal climate features to our wetland classification model. To utilize what we term

'climate-temporal features' (CTFs) as model inputs, we accessed the PRISM Daily Spatial Climate Dataset (AN81d) (Daly et al. 2008) from GEE (Gorelick et al. 2017) from January 1, 1985 to December 31, 2017, which includes 365 days of annual measurements for four climate features, including daily 1) maximum temperature (tMax), 2) minimum temperature (tMin), 3) mean temperature (tMean), and 4) total precipitation (ppt). From the daily measurements available, we abstracted five annual (Julian dates 0-365) CTFs for each of the four climate features: 1) max, 2) min, 3) med, 4) mean, and 5) range. To match the spatial resolution of our Landsat STFs, data were resampled from 800 m pixels to 30 m pixels using the nearest neighbor approach. Together, these CTFs add 20 features to the classification model (Chapter 2, Table 6).

Ancillary Datasets

Digital Elevation Model

Wetlands habitats are more likely be situated in relatively-depressional terrain surfaces. Therefore, we augmented our model inputs with a 30m DEM, labeled as Elevation, derived from the Shuttle Radar Topography Mission (SRTM), flown in February 2000 (Farr et al. 2007) (Chapter 2, Table 7).

Global Surface Water

To investigate the applicability and accuracy of the Pekel et al. 2016 Global Surface Water (GSW) data-set, we utilized GSW features model inputs for our wetland classification models. Using GEE (Gorelick et al. 2017), we collected 1)

GSW Occurrence, 2) GSW Recurrence), and 3) GSW Seasonality. GSW Occurrence and Recurrence are both abstracted from a 32 year time series from 1984 - 2015, overlapping our study period almost exactly. GSW Seasonality is calculated for each year, but the only available dataset is for the year 2014-2015. Consequently, we used the 2014-15 GSW Seasonality data-set to determine if this type of spatio-temporal feature was applicable and relevant to wetlands classified in other years. GSW features are derived from Landsat data and have a corresponding 30 m pixel resolution (Pekel et al. 2016). Combined with Elevation, GSW features create four additional ancillary model input features (Chapter 2, Table 7).

Wetland Classification

A Random Forest (RF) classifier (Breiman, 2001) was used to assign wetland System, Type, and Hydroperiod labels to pixels based on all model inputs. We used a Python implementation of the RF classifier (Pasquarella et al. 2018, Pedregosa et al., 2011), building ensembles of 500 trees (Belgiu and Drăguț 2016). Our model was first trained using input features from 1995 and 1995 NWI reference polygons from the NWRS wetland habitats. For model training, we employed a winner-takes-all hard classification output, where each pixel was assigned to a single RF class (i.e. wetland habitats within System, Type, or Hydroperiod). The trained RF classification model was then applied to all NWI wetland pixels within the entirety of each ecoregion for each year from 1985 - 2017 using the annual input features for each year.

For this study, we aimed to investigate how the probability of wetland habitat occurrence is changing over time. Therefore, when applying the trained model to all years, instead of a winner-takes-all hard classification, per-pixel RF classification probabilities were built and output for individual wetland habitats within *S*ystem, Type, and Hydroperiod categories. This output yields a per-pixel probability value for each wetland System (x2), Type (x4), and Hydroperiod (x6) for each year (x32) for a total of 384 values per pixel. This is a much more informationally-rich dataset compared to hard classification, and, perhaps more importantly, accounts for the ephemeral nature of wetland ecosystems, where a given wetland pixel may be a mix of multiple habitats for a specific year.

Accuracy agreement between the 1995 trained RF hard classification results and the 1995 NWI wetland *System*, *Type*, and *Hydroperiod* reference dataset acted as our estimate of model performance. Detailed accuracy agreement methods and results can be found in Chapter 2.

Time-series Change Detection

Annual NWI reference data does not exist for the state of Oregon so there is no readily available way to systematically and consistently compare model classification probability performance and accuracy agreement for each year. To qualitatively assess model performance, we selected three sites within our study area of known wetland land use change to explore if our model was able to accurately

detect the identified change and to see how specific STFs performed in change detection.

Linear transects of varying lengths and single pixel height were drawn to intersect areas of known wetland change. Hovmoller diagrams were then built for each transect using all years (1985-2017) of classification probabilities and STFs. For Landsat pixels, Hovmoller diagrams can be characterized as a type of heat-map where the x-axis is the left-to-right pixel position (or change in longitude at 30 m intervals for a transect that runs perfectly west-to-east), the y-axis is time in years (ascending from top to bottom), and the value of a given feature (such as classification probability or STF) is represented through a colormap. Hovmoller diagrams give an illustrative and qualitative view of large amounts of data in a meaningful and understandable figure. For our study, we built Hovmollers to display 4 dimensions of data (x, y, time, and feature value) in a single figure, allowing us to visually assess model and STF performance for annual wetland change.

Time-series Trend Analysis

To assess trends in probability changes of wetland Systems, Types, and Hydroperiods, we extracted pixel-level classification probability values for all wetland habitats in both ecoregions, as bounded by the NWI reference dataset. We then calculated the mean per-pixel classification probability for each wetland System, Type, and Hydroperiod for each year from 1985-2017. To test the strength and direction of trends in wetland habitats over time, we calculated the Kendall Tau (KT)

correlation test (Kendall 1938) for each mean time series. KT was chosen over traditional linear regression tests, such as Pearson's r, because it is a strong, nonparametric measure of the strength and direction of association that exists between two variables measured on a continuous scale. Further, KT tests for monotonic relationships of any kind, not just linear, yielding a buffer against natural inter-annual variability in wetland habitat occurrence. Similarly, to assess changes in spectral-temporal features related to wetland ecosystem occurrence and persistence over time, we extracted pixel-level STF values for all wetland habitats in both ecoregions and calculated the mean per-pixel STF value, as bounded by the NWI reference dataset. We then calculated KT values for each mean STF time series from 1985-2017.

Results

Time-series Change Detection

Willamette Valley Shift from Emergent to Pond Wetland

Hovmoller diagrams constructed for four different locations across our two ecoregion study sites show distinct trends in wetland habitat type classification probabilities and STFs over time as wetland habitats change. The first location is situated adjacent to the Main Stem Willamette River to the west and agricultural fields to the east (Figure 1). This wetland transect begins as a mixture of riparian Forested and Emergent Type wetland habitat and is then converted into a quarry pond

with some remaining vegetation in 1995. Hovmollers show the annual Max TCB, TCG, and TCW over time, and the annual classification probabilities of the four Types of wetland habitats (Figure 1). All 7 Hovmollers display a distinct feature change in 1995, indicating both the STFs and our wetland Type classification model were able to detect the change in wetland habitat Type. Individually, Max TCB and TCG both decrease as the wetland shifts from Emergent and Forested to Pond and maximum TCW increases. The probabilities of the transect being classified as Lake and Pond wetland habitat increases, and the probability of the transect being classified as Forested and Emergent decreases, although Forested probabilities decrease at a greater magnitude.

Willamette Valley Creation of Emergent/Pond Wetland

The second transect is situated within an agricultural field matrix east of the Main Stem Willamette River and displays a more complex wetland land use change (Figure 2). This transect starts out as an agricultural field and was then converted to a series of ponds and emergent wetlands in 2007 as part of a wetland restoration project. To maximize visual change, we display the annual minimum TCB and TCG and the annual median TCW. All three STFs show a clear change in 2007 and highlight the distinct lateral-spatial pattern of the restored wetland complex. In 2007 and forward, annual TCB and TCG generally increase in pixels of created Emergent wetland and decrease in pixels containing restored Pond wetlands. Interestingly, Hovmollers of wetland Type classification probabilities show a more spatially distinct

increase in probabilities of Lake wetland compared to Pond wetland classification probabilities which are high across the entire transect, rather than being constrained to the spatial outline of the actual pond wetland. Following restoration, probabilities in Forested wetland classification increase with the spatial pattern of vegetation surrounding individual ponds. Emergent wetland probabilities display spatial behavior similar to Ponds where there is a general increase across the entirety of the transect rather than a distinct spatial pattern that fits the restored wetland outline.

North Basin Transitional Lake and Emergent Wetland

To observe how our classification model behaved for wetlands that are variabile inter-annually, our third transect is in the North Basin within the Malheur Wildlife Refuge and contains a wetland that switches annually between an Emergent island wetland within a Lake wetland or an entirely Lake wetland depending on inundation levels (Figure 3). To maximize visual change, we display the annual mean TCB, TCG, and TCW over time. The STF Hovmollers show a distinct spatial-temporal pattern of the transitional wetland. The east and west margins of the wetland transect appear to be most variable, with mean TCB and TCG decreasing on the ends of the transects in years where TCW increases. Hovmollers of wetland classification probabilities are less distinct although they do follow the similar spatial-temporal pattern in the margins of the transect. In years where mean TCW is high, probabilities of wetland classification of Lake wetlands are also high, although probabilities for this wetland Type are relatively high across the whole transect

throughout the 32 years. Both Pond and Forested wetland classifications remain relatively low in the transect pixels throughout the time series, however, Forested wetland probabilities are highest in the middle of the transect, where high inundation levels would, spatially, reach last. Emergent wetland classification probabilities, like Lake wetlands, are relatively high throughout the time series, but also follow a similar spatial pattern as all other Hovmollers where their probabilities are highest in the middle of the transect, especially in years where mean TCW increases on the transect margins.

Time-series Trend Analysis

Wetland Habitat Probabilities

Long term trends in KT correlation values were not consistent across wetland categorical resolutions, climate gradients, or features (Table 1). In the Willamette Valley, we found that Palustrine wetlands are decreasing at a rate of -0.14, but are increasing at a rate of 0.16 in the North Basin. In contrast, Lacustrine wetlands are increasing at a rate of 0.15 in the Willamette Valley and decreasing by -0.16 in the North Basin. Lake wetlands are decreasing for both ecoregions, but by more than double the rate in the North Basin. Pond wetlands are decreasing in the Willamette Valley by a rate of -0.23 and increasing in the North Basin by 0.26. Forested wetlands are increasing in both ecoregions but weakly so in the Willamette Valley (0.09) and strongly in the North Basin (0.40). Emergent wetlands are on the rise for both

ecoregions at similar rates; 0.29 for the Willamette Valley and 0.24 for the North Basin.

Moving into Hydroperiods, Temporarily Flooded wetlands show a weak decrease in the Willamette Valley (-0.01) and a moderate rate of increase in the North Basin (0.17). Seasonally Saturated wetlands are increasing in the Willamette Valley (0.19) and remaining relatively stable in the North Basin. Seasonally Flooded wetlands are not changing in the North Basin and have a very weak rate of decline (-0.01) in the Willamette Valley. Continuously Saturated wetlands are weakly declining in both ecoregions at at similar rates: -0.09 in the Willamette Valley and -0.06 in the North Basin. Permanently Flooded wetlands are barely changing in the Willamette Valley (0.03) and stable (0.0) in the North Basin. Artificially Flooded wetlands appear to be increasing weakly in the Willamette Valley (0.03) and increasing in the North Basin (0.23).

From 1985 - 2017, trends in STFs had stronger rates of change than wetland classification probabilities in many instances. Collectively, Max TCB, TCG, and TCW all had positive rates of change in both ecoregions although Max TCG and TCW both had a stronger rate of change in the Willamette Valley compared to the North Basin. Min TCB, TCG, and TCW all had negative rates of change in both ecoregions, except for min TCB in the North Basin, which had a positive rate of change. Range of TCB, TCG, and TCW had positive rates of change for both ecoregions, as did the Median TCB, TCG, and TCW, except for the Median TCW in

the North Basin which had a relatively strong rate of decline at -0.43. Mean TCB, TCG, and TCW was more varied between the ecoregions. The Mean TCB decreased by -0.08 in the Willamette Valley, but increased substantially more (0.49) in the North Basin. Mean TCG increased in the Willamette Valley by 0.41 and 0.25 in the North Basin. Mean TCW also increased in the Willamette Valley but decreased by nearly double in the North Basin.

In the 32 year time series, DOY STFs had variable rates of change between ecosystems and across STFs. The DOY of the annual maximum TCB increased positively, but weakly in both ecoregions. DOY of Max TCG decreased weakly in the Willamette Valley but increased by 0.13 in the North Basin. DOY of Max TCW did not change in the Willamette Valley and increased weakly in the North Basin. DOY of Min STFs had stronger rates of change than Max. In the North Basin, the DOY of Min TCB decreased more than three times the rate (-0.34) compared to the Willamette Valley (-0.10). DOY of Min TCG decreased at similar rates in both ecoregions both DOY of min TCW decreased at over double the rate (-0.32) in the North Basin compared to the Willamette Valley (-0.13). The number of days between the Max and the Min STFs, the Range of DOY, increased for TCB, TCG, and TCW in both ecosystems except for the TCW in the Willamette Valley which decreased weakly at -0.04. DOY of the median TCB, TCG, and TCW all decreased at a similar rate around -0.20.

Discussion

Wetlands are highly vulnerable to climate change due to the primary importance of the hydrological regime in controlling their ecological characteristics (e.g. Baker et al., 2009). To comprehend significant patterns of global wetland degradation and loss, wetland hydro-temporal and phenological dynamics must be understood to place habitat change in the context of fundamental ecosystems drivers. Both land cover classification and land cover change are key information needs when monitoring wetland ecosystems, highlighting status and trends, and providing key model features for carbon budgets, habitat, biodiversity, and resource management projects (Hermosilla et al. 2018).

In the traditional remote sensing supervised classification, results are given in a one-pixel-one-class method and class mixture cannot be taken into consideration in determining a specific pixel's class appointment (Wang 1990). Given that wetlands are naturally intra-and inter-annual ephemeral ecosystems with a higher degree of categorical ecosystem mixing than many other land use features, one-pixel-one-class (i.e. one-pixel-one-habitat here) significantly limits the ability to understand how naturally variable wetlands may be changing in a way that cannot be described by a single classification membership. An alternative to conventional hard classification is fuzzy classification, which allows partial land cover classification membership for each pixel and better represents cover type mixtures, ephemeral conditions. In this

study, we employed a fuzzy classification model for annual wetland classification that captured intra-annual variability with Landsat spectral-temporal features and quantified how wetland habitat classification probabilities, rather than hard classifications are changing over time. To yield further insight into why wetland habitat occurrence probabilities may be changing, we also explored trends in specific Landsat spectral-temporal features as measures of wetland hydrological and ecological dynamics change over time.

Wetland Land Use Change

To visually inspect the performance of our annual wetland fuzzy classification model, we built Hovmoller diagrams in areas of known wetland habitat change to inspect how STFs and classification probabilities behaved over time. We believe our results were promising. All three examples show clear change in STFs and wetland probabilities that correspond to the correct spatio-temporal patterns of wetland habitat change. As expected, results are clearer in more ecologically and categorically explicit contexts. For example, the distinct transition from Emergent/Forested riparian wetland to a Pond wetland resulted in more distinct feature changes compared to the creation of a mixed Emergent/Forested/Pond wetland in the second example.

The primary objective of this study was not to assess a wetland habitat model performance over time, rather we create and use our model to for the purpose of investigating how wetlands may be changing over time. An accurate model is

required for this objective, but we feel comfortable with the Hovmoller diagrams presented here, and many others that we did not include, provide an adequate measure of model performance capabilities. Additionally, we hope that researchers and managers may be able to employ our model with similar features in any region and for any time period. If users are constrained to the requirement of high-quality annual reference datasets to test model applicability in their study area, we believe this would be prohibitive. Hovmollers provide a way for model users to see where wetland classification time series probabilities perform well for their system and where the limitations lie.

Change in Wetland Habitat Over Time

In our study we did not quantify correlations with wetland habitat change and potential drivers of change such as climate metrics or land use features, like urban or agricultural expansion. However, we believe it is still valuable to have a qualitative discussion about potential drivers of change for different wetland habitat types in the different ecoregions. We utilize classification model time series, STF time series, and annual climate data time series for the two ecoregions collected from the NOAA National Centers for Environmental information (NOAA 2018) to explore how and why wetlands may be changing in the two different climate zones.

Willamette Valley

In the Willamette Valley, classification probabilities of vegetated Palustrine wetlands are decreasing and non-vegetated Lacustrine wetlands are increasing. This

result is in-line with what Fickas et al. 2015 found when exploring annual wetland loss, gain, and conversion in the Willamette River floodplain from 1972 - 2012. Similarly, Lake and Pond wetlands are increasing while Forested and Emergent wetlands are decreasing, with Emergent wetlands decreasing more rapidly than Forest. Fickas et al. 2015 attributed the majority of wetland change to agricultural and industrial expansion along the margins of Willamette River. However, we hypothesize that there is also likely a climate factor at play. In the Willamette Valley, average annual precipitation and temperature are both on the rise with precipitation increasing by 5.8 cm per decade and temperature warming by 0.11 °C per decade from 1985 -2017. The combination of increased precipitation mixed with increased temperatures could account for a gain of inundated wetlands and a loss of vegetated wetlands with biological and ecological elements that are sensitive to temperature.

We did not find any notable change in wetland Hydroperiods from 1985 - 2017 except for an increase in Seasonally Saturated wetlands. Seasonally saturated wetlands are 'saturated at or near the surface for extended periods during the growing season, but unsaturated conditions prevail by the end of the season in most years. Surface water is typically absent, but may occur for a few days after heavy rain and upland runoff' (Cowardin et al. 1979). Even though non-vegetated wetlands are increasing, the increase in this Hydroperiod may indicate that wetlands are trending towards lower intra-annual inundation and moderate duration.

Although vegetated wetlands are on the decline in the Willamette Valley, maximum annual TCG is increasing relatively substantially (along with both TCB and TCW) and the minimum of all three indices is decreasing. These results have two key ecological implications. First, an annual rise in max TCG suggests that wetland habitats that are able to persist as vegetated are experiencing ecological succession from Emergent hydrophytic vegetation to denser vegetation such as woody Forested or, vegetated wetlands are slowly transitioning into denser upland vegetation. Second, the increase in annual max TCB, TCG, and TCW and decrease in min TCB, TCG, and TCW (resulting in an increasing range for all three as well) indicates that intra-annual ecological conditions are tending towards extremes. Very high and very low TCB, TCG, and TCW values may correspond to increasing occurrence of very dry soil conditions and very wet or densely vegetated conditions.

The STFs that correspond to temporal and phenological conditions also changed across the time series. Of important note is a decrease in the day of year of minimum TCB, TCG, and TCW. If we consider TCB corresponding to bare soil, TCG as a proxy of vegetation cover, and TCW as a metric of inundation, this suggest that the driest soils, lowest vegetation density, and lowest inundation levels have a trend towards occurring earlier in the year. This trend is also seen in the day of year of median TCB, TCG, and TCW. Combined with results from our model classification and the other primary STFs, Willamette Valley wetlands appear to be

heading towards more non-vegetated wetlands, fewer vegetated wetlands, and extreme annual-conditions with the lower extrema occurring earlier in the year.

North Basin

In contrast to the Willamette Valley, North Basin classification probabilities of vegetated Palustrine wetlands are increasing and non-vegetated Lacustrine wetlands are decreasing, although at inversely similar rates as the Willamette Valley. Likewise, Lake and Pond wetlands are decreasing and Emergent and Forested wetlands are increasing, with Forested wetlands increasing nearly double the rate of Emergent wetlands. Outside of the Malheur NWR, long term wetland habitat change is not well studied in this ecoregion so it is hard to begin to explore primary and subsequent drivers of change. Wetlands in this ecoregion have recently been recognized by many conservation groups as focal habitats for restoration and conservation and one possible driver of change from over the three decades studied could be a natural resources management focus on converting un-vegetated wetlands to vegetated habitats. As with the Willamette Valley, we do not seek to make conclusive statements on drivers of change, so other potential anthropogenic factors should be explored. However, like the Willamette Valley, there is a compelling connection between climate change and wetland habitat change in this ecoregion. In the North Basin, average annual temperature is warming by 0.23 °C per decade and precipitation is decreasing by 0.25 cm per decade from 1985 - 2017. A partially inverse phenomenon of the Willamette Valley, the combination of decreased

precipitation mixed with increased temperatures could account for a loss of inundated wetlands that require sufficient hydrologic input for persistence and a gain of vegetated wetlands that are better adapted to extreme conditions compared to Willamette Valley wetlands.

Two Hydroperiods had notable increases in this ecoregion: Temporarily Flooded and Artificially Flooded wetlands. We hypothesize that these two wetlands may be very categorically similar to each other, especially considered in an annual context. This trend may suggest that due to increasing temperatures and decreasing precipitation, wetland hydroperiods are becoming 'flashier' with high inundation that does not last long, perhaps facilitated by natural resource managers.

Although inundated, un-vegetated wetlands are declining in the North Basin, max TCW is increasing, along with both TCG and TCB, and may be associated with the increased hydroperiod flashiness. As in the Willamette Valley, the increase in annual max TCB, TCG, and TCW and decrease in min TCG and TCW indicates that intra-annual ecological conditions in this ecoregion are also trending towards extremes. Min TCB was the exception here, which saw an increase in the study period. One possible explanation is an increase in vegetation cover through increase in vegetated wetlands, which limits soil brightness in the driest periods.

Some rates of change in STFs that correspond to temporal and phenological conditions were stronger in the North Basin compared to the Willamette Valley but also variable across features. Specifically, the day of year of max TCG is increased

but the day of year of minimum TCB, TCG, and TCW all decreased. Ecologically, this could indicate that there is trend toward vegetation reaching maximum growth earlier in the year and the driest soils, lowest vegetation density, and lowest inundation levels trending towards occurring earlier in the year. Combining these results with those from our model classification and the other primary STFs, Noth Basin wetlands seem to be trending towards more vegetated wetlands, fewer non-vegetated wetlands, and extreme annual-conditions with the lower extrema occurring earlier in the year, except for max TCW which occurring later in the year.

Ecohydrological Context and Consequences of Change

The distinct differences in habitat and climate trends in the Willamette Valley and North Basin are demonstrative of the importance of considering wetland trends in a climatic and ecohydrological context. Willamette Valley wetlands are already energy limited and are trending even further towards wetlands that are more heavily inundated from hydrologic inputs rather than higher functioning vegetated wetlands. North Basin wetlands are water-limited and a decrease in precipitation may be an emphasized driver for a loss of inundated wetlands that already relied on a limited water supply for persistence.

In the Willamette Valley, vegetated wetland habitats hold substantial ecological significance for many plant and wildlife species. Of the twenty species that

occur in the Willamette Valley that are listed under the federal Endangered Species Act and the 155 that are imperiled, wet prairies provide habitat for 31 for at least some portion of their lifecycle (Floberg et al. 2004). Wet prairies alone also provide critical reproductive habitat for 38 different wildlife species and an additional 54 breeding species (Primozichand Bastasch 2004). Annual decrease of these critically important wetland habitats could be problematic for the species that rely on them in any part of their lifecycle.

In the North Basin, an overall reduction in surface water may yield an increase in wetland salinity levels. Some local and migratory shorebirds that utilize North Basin wetlands in the Pacific Flyway depend on a mosaic of freshwater and saline wetlands to meet their needs at specific times of the year, especially during the breeding season. Because of the metabolic costs associated with feeding in higher salinity environments, this trend could yield higher mortality in shorebird chicks. Further compounding this issue, in wetland systems, shorebird species that require specific salinity levels and have a limited capacity to relocate to wetlands are more likely to be vulnerable to climate-induced changes in habitat and hydrology.

In addition to change in area and proportion of habitat types in both ecoregions, change in the timing hydrology and phenological features observed could also be problematic for flora and fauna dependent on key temporally-linked ecosystem dynamics. For example, both ecoregions host migratory waterfowl in their wetlands as part of the Pacific Flyway and different invertebrate species are important

food sources for migratory birds in these wetlands (Both et al. 2006). Changes in timing of wetland hydrology and soil dynamics could lead to changes in vegetation phenology, which are coupled with invertebrate phenologies. If invertebrate phenologies shift but avian migratory phenologies do not, there could be a substantial temporal mismatch in foodsource, which may lead to birds failing to breed and/or migrate at the time of maximal food abundance (Both et al. 2006).

We believe future studies should focus not only on annual wetland classification, but also wetland detection to explore if wetland habitats are changing in proportion to their upland counter parts. Additionally, this study utilized time series derived from classified pixels, which only exploits the temporal aspect of our model classification. Change in wetland spatial arrangement, fragmentation, and connectivity can all be derived from our model output and would be a very valuable data source for resource managers.

Conclusions

By evaluating wetland habitat change across climate gradients and categorical resolutions from 1985-2017 using Landsat spectral-temporal features, we found that:

- Through visual evaluation, our annual classification model built from Landsat spectral-temporal features, climate-temporal features, and ancillary datasets performs well in showing change in wetland habitat. Individual STFs also

display distinct changes in intra-annual wetland dynamics in the context of wetland land use change.

- Willamette Valley wetlands are trending toward more non-vegetated wetlands, fewer vegetated wetlands, and extreme annual-conditions with the lower extrema occurring earlier in the year. In addition to other drivers, this change may be attributed to increased precipitation and increased temperature.
- North Basin wetlands are trending towards more vegetated wetlands, fewer non-vegetated wetlands, and extreme annual-conditions with the lower extrema occurring earlier in the year, except for max TCW which is trending towards later annual occurrence.
- Change in both occurrence of wetland habitat type and timing of key hydrologic and phenological features and ecosystem drivers presents an issue for wetland-dependent flora and fauna.
- Future studies should attempt to detect wetlands across the entire landscape rather than just areas of known wetland habitat. Additionally, exploitation of the spatial domain in time series analysis would yield an even more informationally rich analysis of how, when, and where wetland ecosystems are changing.

CHAPTER 3 FIGURES

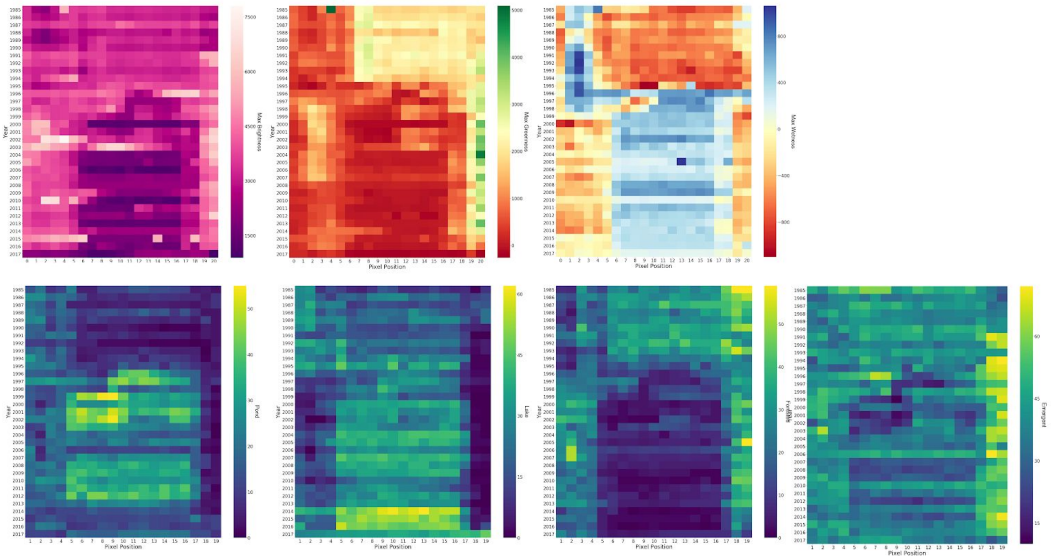

Figure 3.1: Hovmoller diagrams of STFs (top) and wetland classification probabilities (bottom) for a Willamette Valley wetland land use change from Emergent to Pond in 1995.

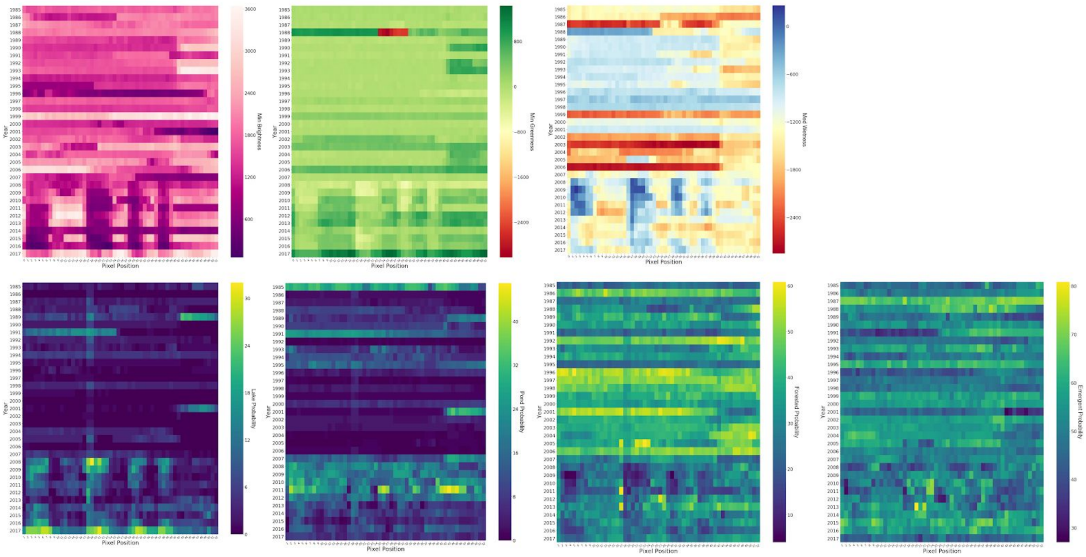

Figure 3.2: Hovmoller diagrams of STFs (top) and wetland classification probabilities (bottom) for a Willamette Valley wetland land use change from agriculture (no wetland) to a mosaic of Emergent and Pond in 2007.

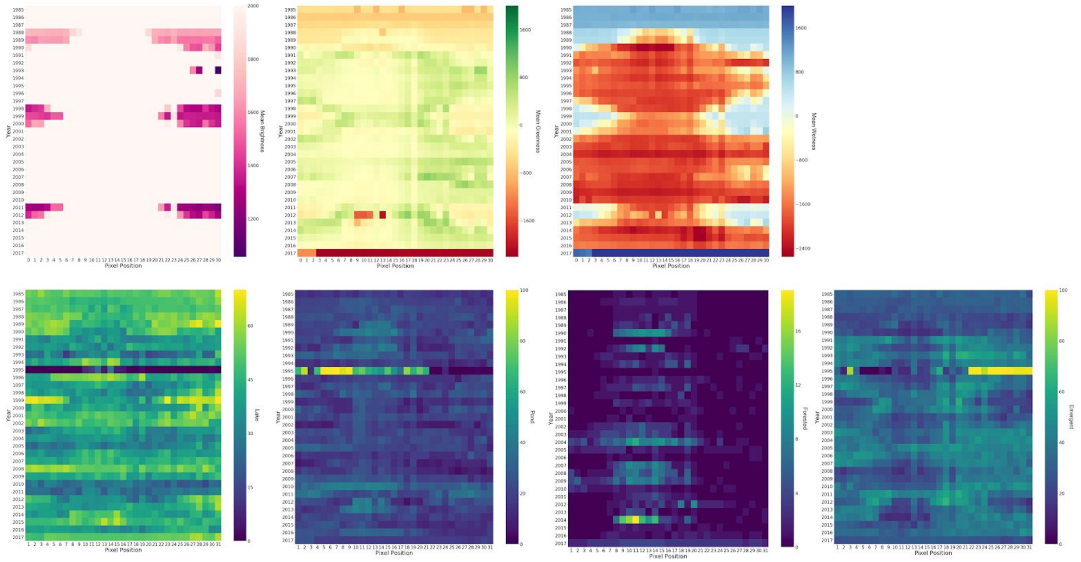

Figure 3.3: Hovmoller diagrams of STFs (top) and wetland classification probabilities (bottom) for a North Basin wetland inter-annually ephemeral land use change wetland between Lake and Emergent throughout the timeseries.

CHAPTER 3 TABLES

Habitat	Willamette Valley KT Correlation Value	North Basin KT Correlation Value
Palustrine	-0.14	0.16
Lacustrine	0.15	-0.16
Lake	-0.13	-0.32
Pond	-0.23	-0.26
Emergent	0.09	0.4
Forested	0.29	0.24
Temporarily Flooded	-0.01	0.17
Seasonally Saturated	0.19	0.00
Seasonally Flooded	-0.01	0.00
Continuously Saturated	-0.09	-0.06
Permanently Flooded	0.03	0.00
Artificially Flooded	0.01	0.23
Max TCB	0.31	0.34
Max TCG	0.5	0.39
Max TCW	0.34	0.16
Min TCB	-0.46	0.19
Min TCG	-0.24	-0.22
Min TCW	-0.23	-0.46
Rng TCB	0.38	0.32
Rng TCG	0.41	0.33
Rng TCW	0.33	0.27
Med TCB	0.08	0.62
Med TCG	0.46	0.37

Med TCW	0.18	-0.43
Mean TCB	-0.08	0.49
Mean TCG	0.41	0.25
Mean TCW	0.21	-0.37
DOY Max TCB	0.06	0.08
DOY Max TCG	-0.06	0.13
DOY Max TCW	0.00	0.05
DOY Min TCB	-0.1	-0.34
DOY Min TCG	-0.13	-0.12
DOY Min TCW	-0.13	-0.32
DOY Rng TCB	0.08	0.16
DOY Rng TCG	0.17	0.43
DOY Rng TCW	-0.04	0.21
DOY Med TCB	-0.2	-0.2
DOY Med TCG	-0.22	-0.2
DOY Med TCW	-0.25	-0.17

Table 3.1: Kendall Tau correlation values between time (years) and habitat fuzzy classification probabilities. This value is interpreted as rate of change.

REFERENCES

Chapter 1

1. Adams, J., O. Smith, M., E. Johnson, P., 1986. Spectral Mixture Modeling: A New Analysis of Rock and Soil Types at the Viking Lander 1 Site. J. Geophys. Res. 91.
2. Benz, U. C., Hofmann, P., Willhauck, G., Lingenfelder, I., & Heynen, M. (2004). Multi-resolution, object-oriented fuzzy analysis of remote sensing data for GIS-ready information. *ISPRS Journal of Photogrammetry and Remote Sensing*, 58(3-4), 239–258. http://doi.org/10.1016/j.isprsjprs.2003.10.002
3. Brooks, E.B., Wynne, R.H., Thomas, V.A., Blinn, C.E., & Coulston, J.W. (2014). On‐the‐Fly massively multitemporal change detection using statistical quality control charts and Landsat data. *IEEE Trans. Geosci. Remote Sens.* 52, 3316–3332. https://doi.org/10.1109/TGRS.2013.2272545
4. Bullock, E. L., Fagherazzi, S., Nardin, W., Vo-Luong, P., Nguyen, P., & Woodcock, C. E. (2017). Temporal patterns in species zonation in a mangrove forest in the Mekong Delta, Vietnam, using a time series of Landsat imagery. *Continental Shelf Research*, *147*, 144–154. http://doi.org/10.1016/j.csr.2017.07.007
5. Carr, J., & Miranda, F. D. (1998). The semivariogram in comparison to the

co-occurrence matrix for classification of image texture. I*EEE Transactions on Geoscience and Remote Sensing*, 36(6), 1945–1952. http://doi.org/10.1109/36.729366

6. Cohen, W. B., & Goward, S. N. (2004). Landsat's Role in Ecological Applications of Remote Sensing. *BioScience*, *54*(6), 535. http://doi.org/10.1641/0006-3568(2004)054[0535:lrieao]2.0.co;2
7. Cohen, W., Healey, S., Yang, Z., Stehman, S., Brewer, C., Brooks, E., et al. (2017). How Similar Are Forest Disturbance Maps Derived from Different Landsat Time Series Algorithms? Forests, 8(4), 98. http://doi.org/10.3390/f8040098
8. Cohen, W.B., Yang, Z., Stehman, S.V., Schroeder, T.A., Bell, D.M., Masek, J.G., Huang, C. & Meigs, G.W. (2016). Forest disturbance across the conterminous United States from 1985–2012: The emerging dominance of forest decline. *Forest Ecology and Management*, 360, 242–252. http://doi.org/10.1016/j.foreco.2015.10.042
9. Cohen, W. B., Yang, Z., Healey, S. P., Kennedy, R. E., & Gorelick, N. (2018). A LandTrendr multispectral ensemble for forest disturbance detection. *Remote Sensing of Environment*, *205*, 131–140. http://doi.org/10.1016/j.rse.2017.11.015
10. Collins, J. B. & Woodcock, C. E. (1994). Change detection using the Gramm-Schmidt transformation applied to mapping forest mortality. *Remote*

Sensing of Environment, 50(3), 267–279. http://doi.org/10.1016/0034-4257(94)90076-0

11. Collins, J. B. & Woodcock, C. E. (1996). An assessment of several linear change detection techniques for mapping forest mortality using multitemporal landsat TM data. *Remote Sensing of Environment*, 56(1), 66–77. http://doi.org/10.1016/0034-4257(95)00233-2
12. Coppin, P., Jonckheere, I., Nackaerts, K., Muys, B., & Lambin, E. (2004). Digital change detection methods in ecosystem monitoring: a review. *International Journal of Remote Sensing*, *25*(9), 1565–1596. http://doi.org/10.1080/0143116031000101675
13. Coulter, L.L., Stow, D.A., Tsai, Y.H., Ibanez, N., Shih, H.C., Kerr, A., Benza, M., Weeks, J.R., & Mensah, F. (2016). Classification and assessment of land cover and land use change in southern Ghana using dense stacks of Landsat 7 ETM imagery. *Remote Sensing of Environment*, 184, 396–409. http://doi.org/10.1016/j.rse.2016.07.016
14. Crist, E. P. (1985). A TM tasseled cap equivalent transformation for reflectance factor data. *Remote Sensing of Environment*, *17*(3), 301–306. https://doi.org/10.1016/0034-4257(85)90102-6
15. Defries, R., Hansen, M., & Townshend, J. (1995). Global discrimination of land cover types from metrics derived from AVHRR pathfinder data. *Remote Sensing of Environment*, 54(3), 209–222.

http://doi.org/10.1016/0034-4257(95)00142-5

16. Dey, V., Zhang, Y., & Zhong, M. (2010). A review on image segmentation techniques with remote sensing perspective. *Proceedings of the International Society for Photogrammetry and Remote Sensing Symposium (ISPRS10),* 37(7A), Austria, July 5–7, 2010.
17. Franklin, S., Wulder, M., Skakun, R., & Carroll, A. (2003). Mountain Pine Beetle Red-Attack Forest Damage Classification Using Stratified Landsat TM Data in British Columbia, Canada. *Photogrammetric Engineering & Remote Sensing*, 69(3), 283–288. http://doi.org/10.14358/pers.69.3.283
18. Gómez, C., White, J. C., & Wulder, M. A. (2016). Optical remotely sensed time series data for land cover classification: A review. ISPRS *Journal of Photogrammetry and Remote Sensing*, 116, 55–72. http://doi.org/10.1016/j.isprsjprs.2016.03.008
19. Gorelick, N., Hancher, M., Dixon, M., Ilyushchenko, S., Thau, D., & Moore, R. (2017). Google Earth Engine: Planetary-scale geospatial analysis for everyone. *Remote Sensing of Environment*, 202, 18–27. http://doi.org/10.1016/j.rse.2017.06.031
20. Guindon, B. (1997). Computer-based aerial image understanding: a review and assessment of its application to planimetric information extraction from very high resolution satellite images. *Canadian Journal of Remote Sensing*, 23(1), 38-47. http://doi.org/10.4095/218537

21. Halabisky, M., Moskal, L. M., Gillespie, A., & Hannam, M. (2016). Reconstructing semi-arid wetland surface water dynamics through spectral mixture analysis of a time series of Landsat satellite images (1984–2011). *Remote Sensing of Environment*, 177, 171–183. http://doi.org/10.1016/j.rse.2016.02.040

22. Hansen, M. C., & Loveland, T. R. (2012). A review of large area monitoring of land cover change using Landsat data. *Remote Sensing of Environment*, *122*, 66–74. http://doi.org/10.1016/j.rse.2011.08.024

23. Haralick, R. M., Shanmugam, K., & Dinstein, I. (1973). Textural Features for Image Classification. *IEEE Transactions on Systems, Man, and Cybernetics*, SMC-3(6), 610–621. http://doi.org/10.1109/tsmc.1973.4309314

24. He, D.-C., & Wang, L. Texture Unit, Texture Spectrum And Texture Analysis. *12th Canadian Symposium on Remote Sensing Geoscience and Remote Sensing Symposium*. http://doi.org/10.1109/igarss.1989.575836

25. Holden, C.E., Arevelo, P., Pasquarella, V., (2016). Yet Another Time Series Model (YATSM): v0.6.1. Zenodo. http://dx.doi.org/10.5281/zenodo.51336 .

26. Huang, C., Goward, S. N., Masek, J. G., Thomas, N., Zhu, Z., & Vogelmann, J. E. (2010). An automated approach for reconstructing recent forest disturbance history using dense Landsat time series stacks. *Remote Sensing of Environment*, 114(1), 183–198. http://doi.org/10.1016/j.rse.2009.08.017

27. Huete, A., Didan, K., Miura, T., Rodriguez, E., Gao, X., & Ferreira, L. (2002).

Overview of the radiometric and biophysical performance of the MODIS vegetation indices. *Remote Sensing of Environment*, *83*(1-2), 195–213. http://doi.org/10.1016/s0034-4257(02)00096-2

28. Hughes, M., Kaylor, S., & Hayes, D. (2017). Patch-Based Forest Change Detection from Landsat Time Series. *Forests*, 8(5), 166. http://doi.org/10.3390/f8050166
29. Jackson, R. (1983). Spectral indices in N-Space. *Remote Sensing of Environment.13:* 409-421. https://doi.org/10.1016/0034-4257(83)90010-X
30. Jin, S., Yang, L., Danielson, P., Homer, C., Fry, J., & Xian, G. (2013). A comprehensive change detection method for updating the National Land Cover Database to circa 2011. *Remote Sensing of Environment*, 132, 159–175. http://doi.org/10.1016/j.rse.2013.01.012
31. Jordan, C. F. (1969). Derivation of Leaf-Area Index from Quality of Light on the Forest Floor. *Ecology*, *50*(4), 663–666. http://doi.org/10.2307/1936256
32. Kauth, R. J., & Thomas, G. S. (1976). The tasselled cap--a graphic description of the spectral-temporal development of agricultural crops as seen by Landsat. *LARS Symposia*.
33. Kennedy, R.E., Andréfouët, S., Cohen, W.B., Gómez, C., Griffiths, P., Hais, M., Healey, S.P., Helmer, E.H., Hostert, P., Lyons, M.B., & Meigs, G.W. (2014). Bringing an ecological view of change to Landsat-based remote sensing. *Frontiers in Ecology and the Environment*, *12*(6), 339–346.

http://doi.org/10.1890/130066

34. Kennedy, R. E., Cohen, W. B., & Schroeder, T. A. (2007). Trajectory-based change detection for automated characterization of forest disturbance dynamics. *Remote Sensing of Environment*, 110(3), 370–386. http://doi.org/10.1016/j.rse.2007.03.010
35. Kennedy, R. E., Yang, Z., & Cohen, W. B. (2010). Detecting trends in forest disturbance and recovery using yearly Landsat time series: 1. LandTrendr — Temporal segmentation algorithms. *Remote Sensing of Environment*, 114(12), 2897–2910. http://doi.org/10.1016/j.rse.2010.07.008
36. Kennedy, R. E., Yang, Z., Cohen, W. B., Pfaff, E., Braaten, J., & Nelson, P. (2012). Spatial and temporal patterns of forest disturbance and regrowth within the area of the Northwest Forest Plan. *Remote Sensing of Environment*, 122, 117–133. http://doi.org/10.1016/j.rse.2011.09.024
37. Kriegler, F. J., Malila, W. A., Nalepka, R. F., & Richardson, W. (1969) Preprocessing transformations and their effects on multispectral recognition. *Proceedings of the Sixth International Symposium on Remote Sensing of Environment*, Ann Arbor, Michigan, US, 97–131.
38. Lewis, A., Oliver, S., Lymburner, L., Evans, B., Wyborn, L., Mueller, N., Raevksi, G., Hooke, J., Woodcock, R., Sixsmith, J., Wu, W., Tan, P., Li, F., Killough, B., Minchin, S., Roberts, D., Ayers, D., Bala, B., Dwyer, J., Dekker, A., Dhu, T., Hicks, A., Ip, A., Purss, M., Richards, C., Sagar, S., Trenham, C.,

Wang, P. & Wang, L.-W. (2017). The Australian Geoscience Data Cube — Foundations and lessons learned. *Remote Sensing of Environment*, 202, 276–292. http://doi.org/10.1016/j.rse.2017.03.015

39. Loveland, T. R., & Dwyer, J. L. (2012). Landsat: Building a strong future. *Remote Sensing of Environment*, *122*, 22–29. http://doi.org/10.1016/j.rse.2011.09.022

40. Lu, D., & Weng, Q. (2004). Spectral Mixture Analysis of the Urban Landscape in Indianapolis with Landsat ETM Imagery. *Photogrammetric Engineering & Remote Sensing*, 70(9), 1053–1062. http://doi.org/10.14358/pers.70.9.1053

41. Marceau, D., Howarth, P., Dubois, J., & Gratton, D. (1990). Evaluation Of The Grey-level Co-occurrence Matrix Method For Land-cover Classification Using Spot Imagery. *IEEE Transactions on Geoscience and Remote Sensing*, 28(4), 513–519. http://doi.org/10.1109/tgrs.1990.572937

42. Masek, J. G., Huang, C., Wolfe, R., Cohen, W., Hall, F., Kutler, J., & Nelson, P. (2008). North American forest disturbance mapped from a decadal Landsat record. *Remote Sensing of Environment*, 112(6), 2914–2926. http://doi.org/10.1016/j.rse.2008.02.010

43. Markham, B. L., & Helder, D. L. (2012). Forty-year calibrated record of earth-reflected radiance from Landsat: A review. *Remote Sensing of Environment*, 122, 30–40. http://doi.org/10.1016/j.rse.2011.06.026

44. Melaas, E. K., Friedl, M. A., & Zhu, Z. (2013). Detecting interannual variation in deciduous broadleaf forest phenology using Landsat TM/ETM data. *Remote Sensing of Environment*, 132, 176–185. http://doi.org/10.1016/j.rse.2013.01.011

45. Ollinger, S.V. (2010). Sources of variability in canopy reflectance and the convergent properties of plants. *New Phytologist*, *189*(2), 375–394. http://doi.org/10.1111/j.1469-8137.2010.03536.x

46. Pasquarella, V., Bradley, B., & Woodcock, C. (2017). Near-Real-Time Monitoring of Insect Defoliation Using Landsat Time Series. *Forests*, 8(8), 275. http://doi.org/10.3390/f8080275

47. Pasquarella, V.J., Holden, C.E., Kaufman, L. & Woodcock, C.E. (2016) From imagery to ecology: leveraging time series of all available Landsat observations to map and monitor ecosystem state and dynamics. *Remote Sensing in Ecology and Conservation*, 2, 152–170. https://doi.org/10.1002/rse2.24

48. Pettorelli, N., Vik, J. O., Mysterud, A., Gaillard, J.-M., Tucker, C. J., & Stenseth, N. C. (2005). Using the satellite-derived NDVI to assess ecological responses to environmental change. *Trends in Ecology & Evolution*, *20*(9), 503–510. http://doi.org/10.1016/j.tree.2005.05.011

49. Price, J.C. (1994). How Unique Are Spectral Signatures. *Remote Sensing of Environment*, *49*(3), 181–186. https://doi.org/10.1016/0034-4257(94)90013-2

50. Ridd, M. K. (1995). Exploring a V-I-S (vegetation-impervious surface-soil) model for urban ecosystem analysis through remote sensing: comparative anatomy for cities. *International Journal of Remote Sensing*, *16*(12), 2165–2185. https://doi.org/10.1080/01431169508954549

51. Song, C., Schroeder, T., & Cohen, W. (2007). Predicting temperate conifer forest successional stage distributions with multitemporal Landsat Thematic Mapper imagery. *Remote Sensing of Environment*, 106(2), 228–237. http://doi.org/10.1016/j.rse.2006.08.008

52. Song, C., Woodcock, C. E., & Li, X. (2002). The spectral/temporal manifestation of forest succession in optical imagery. *Remote Sensing of Environment*, 82(2-3), 285–302. http://doi.org/10.1016/s0034-4257(02)00046-9

53. Tucker, C. J. (1979). Red and photographic infrared linear combinations for monitoring vegetation. *Remote Sensing of Environment*, *8*(2), 127–150. http://doi.org/10.1016/0034-4257(79)90013-0

54. US Geological Survey (USGS). (2018). U.S. Landsat Analysis Ready Data (ARD) Data Format Control Book (DFCB). LSDS-1873 Version 4.0 https://landsat.usgs.gov/sites/default/files/documents/LSDS-1873_US_Landsat_ARD_DFCB.pdf. Accessed 14 Feb 2018.

55. Verbesselt, J., Hyndman, R., Newnham, G., & Culvenor, D. (2010). Detecting trend and seasonal changes in satellite image time series. *Remote Sensing of*

Environment, 114(1), 106-115. https://doi.org/10.1016/j.rse.2009.08.014

56. Vogelmann, J. E., Xian, G., Homer, C., & Tolk, B. (2012). Monitoring gradual ecosystem change using Landsat time series analyses: Case studies in selected forest and rangeland ecosystems. *Remote Sensing of Environment*, 122, 92–105. http://doi.org/10.1016/j.rse.2011.06.027
57. Woodcock, C.E., Allen, R., Anderson, M., Belward, A., Bindschadler, R., Cohen, W., Gao, F., Goward, S.N., Helder, D., Helmer, E., & Nemani, R.(2008). Free Access to Landsat Imagery. *Science*, *320*(5879). http://doi.org/10.1126/science.320.5879.1011a
58. Woodcock, C., & Harward, V. J. (1992). *Nested-hierarchical scene models and image segmentation. International Journal of Remote Sensing*, 13(16), 3167–3187. http://doi.org/10.1080/01431169208904109
59. Woodcock, C. & Strahler, A. (1987). The factor of scale in remote sensing. *Remote Sensing of Environment*, *21*(3), 311–332. https://doi.org/10.1016/0034-4257(87)90015-0
60. Woodcock, C. E., Strahler, A. H., & Jupp, D. L. (1988). The use of variograms in remote sensing: I. Scene models and simulated images. *Remote Sensing of Environment*, 25(3), 323–348. http://doi.org/10.1016/0034-4257(88)90108-3
61. Wulder, M. A., Masek, J. G., Cohen, W. B., Loveland, T. R., & Woodcock, C. E. (2012). Opening the archive: How free data has enabled the science and

monitoring promise of Landsat. Remote Sensing of Environment, 122, 2–10. http://doi.org/10.1016/j.rse.2012.01.010

62. Wulder, M.A., White, J.C., Goward, S.N., Masek, J.G., Irons, J.R., Herold, M., Cohen, W.B., Loveland, T.R., & Woodcock, C.E. (2008). Landsat continuity: Issues and opportunities for land cover monitoring. *Remote Sensing of Environment*, *112*(3), 955–969. http://doi.org/10.1016/j.rse.2007.07.004
63. Wulder, M.A., White, J.C., Loveland, T.R., Woodcock, C.E., Belward, A.S., Cohen, W.B., Fosnight, E.A., Shaw, J., Masek, J.G., & Roy, D.P., 2016. The global Landsat archive: Status, consolidation, and direction. *Remote Sensing of Environment*, 185, 271-283. http://doi.org/10.1016/j.rse.2015.11.032
64. Zhu, Z. (2017) Change detection using landsat time series: A review of frequencies, preprocessing, algorithms, and applications. *ISPRS Journal of Photogrammetry and Remote Sensing*, 130, 370–384. https://doi.org/10.1016/j.isprsjprs.2017.06.013
65. Zhu, Z., Gallant, A.L., Woodcock, C.E., Pengra, B., Olofsson, P., Loveland, T.R., Jin, S., Dahal, D., Yang, L. & Auch, R.F. (2016). Optimizing selection of training and auxiliary data for operational land cover classification for the LCMAP initiative. *ISPRS Journal of Photogrammetry and Remote Sensing*, 122, 206–221. http://doi.org/10.1016/j.isprsjprs.2016.11.004
66. Zhu, Z., & Woodcock, C. E. (2012). Object-based cloud and cloud shadow

detection in Landsat imagery. *Remote Sensing of Environment*, 118, 83–94. http://doi.org/10.1016/j.rse.2011.10.028

67. Zhu, Z., & Woodcock, C. E. (2014). Continuous change detection and classification of land cover using all available Landsat data. *Remote Sensing of Environment*, 144, 152–171. http://doi.org/10.1016/j.rse.2014.01.011
68. Zhu, Z., Woodcock, C. E., Holden, C., & Yang, Z. (2015). Generating synthetic Landsat images based on all available Landsat data: Predicting Landsat surface reflectance at any given time. *Remote Sensing of Environment*, 162, 67–83. http://doi.org/10.1016/j.rse.2015.02.009

Chapters 2 and 3

1. Ahlgren, P., Jarneving, B., Rousseau, R. (2003). Requirements for a cocitation similarity measure, with special reference to Pearson's correlation coefficient. *Journal of the American Society for Information Science and Technology*, *54*(6), 550–560. http://doi.org/10.1002/asi.10242
2. Andel, J. van., Aronson, J. (2012). *Restoration Ecology. ; The New Frontier*. John Wiley Sons, Incorporated.
3. Baker, C., Lawrence, R. L., Montagne, C., Patten, D. (2007). Change detection of wetland ecosystems using Landsat imagery and change vector analysis. *Wetlands*, *27*(3), 610–619. http://doi.org/10.1672/0277-5212(2007)27[610:cdoweu]2.0.co;2

4. Baker, C., Lawrence, R., Montagne, C., Patten, D. (2006). Mapping wetlands and riparian areas using Landsat ETM imagery and decision-tree-based models. *Wetlands*, *26*(2), 465–474. http://doi.org/10.1672/0277-5212(2006)26[465:mwarau]2.0.co;2
5. Beeri, O., Phillips, R. L. (2007). Tracking palustrine water seasonal and annual variability in agricultural wetland landscapes using Landsat from 1997 to 2005. *Global Change Biology*. http://doi.org/10.1111/j.1365-2486.2006.01306.x
6. Belgiu, M., Drăguț, L. (2016). Random forest in remote sensing: A review of applications and future directions. *ISPRS Journal of Photogrammetry and Remote Sensing*, *114*, 24–31. http://doi.org/10.1016/j.isprsjprs.2016.01.011
7. Brinson, M. M. (1993). Changes in the functioning of wetlands along environmental gradients. *Wetlands*, *13*(2), 65–74. http://doi.org/10.1007/bf03160866
8. Brinson, M. M., Bradshaw, H. D., Holmes, R. N., Elkins, J. B. (1980). Litterfall, Stemflow, and Throughfall Nutrient Fluxes in an Alluvial Swamp Forest. *Ecology*, *61*(4), 827–835. http://doi.org/10.2307/1936753
9. Brooks, E. B., Wynne, R. H., Thomas, V. A., Blinn, C. E., Coulston, J. W. (2014). On-the-Fly Massively Multitemporal Change Detection Using Statistical Quality Control Charts and Landsat Data. *IEEE Transactions on Geoscience and Remote Sensing*, *52*(6), 3316–3332.

http://doi.org/10.1109/tgrs.2013.2272545

10. Cowardin, L. M. (1979). Classification of wetlands and deepwater habitats of the United States / by Lewis M. Cowardin ... [et al.]. http://doi.org/10.5962/bhl.title.4108
11. Cohen, W. B., Goward, S. N. (2004). Landsat's Role in Ecological Applications of Remote Sensing. *BioScience*, *54*(6), 535. http://doi.org/10.1641/0006-3568(2004)054[0535:lrieao]2.0.co;2
12. Cole, C. A., Brooks, R. P., Wardrop, D. H. (1997). Wetland hydrology as a function of hydrogeomorphic (HGM) subclass. *Wetlands*, *17*(4), 456–467. http://doi.org/10.1007/bf03161511
13. Coulter, L. L., Stow, D. A., Tsai, Y.-H., Ibanez, N., Shih, H.-C., Kerr, A., … Mensah, F. (2016). Classification and assessment of land cover and land use change in southern Ghana using dense stacks of Landsat 7 ETM imagery. *Remote Sensing of Environment*, *184*, 396–409. http://doi.org/10.1016/j.rse.2016.07.016
14. Crist, E. P. (1985). A TM Tasseled Cap equivalent transformation for reflectance factor data. *Remote Sensing of Environment*, *17*(3), 301–306. http://doi.org/10.1016/0034-4257(85)90102-6
15. Daly, C., Halbleib, M., Smith, J. I., Gibson, W. P., Doggett, M. K., Taylor, G. H., … Pasteris, P. P. (2008). Physiographically sensitive mapping of climatological temperature and precipitation across the conterminous United

States. *International Journal of Climatology*, *28*(15), 2031–2064. http://doi.org/10.1002/joc.1688

16. Daniels, A. E. (2006). Incorporating domain knowledge and spatial relationships into land cover classifications: a rule‐based approach. *International Journal of Remote Sensing*, *27*(14), 2949–2975. http://doi.org/10.1080/01431160600567753
17. Defries, R. S., Field, C. B., Fung, I., Justice, C. O., Los, S., Matson, P. A., … Vitousek, P. M. (1995). Mapping the land surface for global atmosphere-biosphere models: Toward continuous distributions of vegetation's functional properties. *Journal of Geophysical Research*, *100*(D10), 20867. http://doi.org/10.1029/95jd01536
18. Devries, B., Pratihast, A. K., Verbesselt, J., Kooistra, L., Herold, M. (2016). Characterizing Forest Change Using Community-Based Monitoring Data and Landsat Time Series. *Plos One*, *11*(3). http://doi.org/10.1371/journal.pone.0147121
19. Devries, B., Decuyper, M., Verbesselt, J., Zeileis, A., Herold, M., Joseph, S. (2015). Tracking disturbance-regrowth dynamics in tropical forests using structural change detection and Landsat time series. *Remote Sensing of Environment*, *169*, 320–334. http://doi.org/10.1016/j.rse.2015.08.020
20. Dvorett, D., Davis, C., Papeş, M. (2016). Mapping and Hydrologic Attribution of Temporary Wetlands Using Recurrent Landsat Imagery.

Wetlands, *36*(3), 431–443. http://doi.org/10.1007/s13157-016-0752-9

21. Díaz-Delgado, R., Aragonés, D., Afán, I., Bustamante, J. (2016). Long-Term Monitoring of the Flooding Regime and Hydroperiod of Doñana Marshes with Landsat Time Series (1974–2014). *Remote Sensing*, *8*(9), 775. http://doi.org/10.3390/rs8090775
22. Farr, T. G., Rosen, P. A., Caro, E., Crippen, R., Duren, R., Hensley, S., … Alsdorf, D. (2007). The Shuttle Radar Topography Mission. *Reviews of Geophysics*, *45*(2). http://doi.org/10.1029/2005rg000183
23. Fernandez-Illescas, C. P., Rodriguez-Iturbe, I. (2003). Hydrologically Driven Hierarchical Competition–Colonization Models: The Impact Of Interannual Climate Fluctuations. *Ecological Monographs*, *73*(2), 207–222. http://doi.org/10.1890/0012-9615(2003)073[0207:hdhcmt]2.0.co;2
24. Fickas, K. C., Cohen, W. B., Yang, Z. (2015). Landsat-based monitoring of annual wetland change in the Willamette Valley of Oregon, USA from 1972 to 2012. *Wetlands Ecology and Management*, *24*(1), 73–92. http://doi.org/10.1007/s11273-015-9452-0
25. Foga, S., Scaramuzza, P. L., Guo, S., Zhu, Z., Dilley, R. D., Beckmann, T., … Laue, B. (2017). Cloud detection algorithm comparison and validation for operational Landsat data products. *Remote Sensing of Environment*, *194*, 379–390. http://doi.org/10.1016/j.rse.2017.03.026
26. Fraser, L. H., Keddy, P. A. (2009). *The world's largest wetlands: ecology and*

conservation. Cambridge University Press.

27. Friedl, M. A., Muchoney, D., Mciver, D., Gao, F., Hodges, J. C. F., Strahler, A. H. (2000). Characterization of North American land cover from NOAA-AVHRR data using the EOS MODIS Land Cover Classification Algorithm. *Geophysical Research Letters*, *27*(7), 977–980. http://doi.org/10.1029/1999gl011010
28. Frohn, R. C., Reif, M., Lane, C., Autrey, B. (2009). Satellite remote sensing of isolated wetlands using object-oriented classification of Landsat-7 data. *Wetlands*, *29*(3), 931–941. http://doi.org/10.1672/08-194.1
29. Gallucci, V. F. (1973). On the Principles of Thermodynamics in Ecology. *Annual Review of Ecology and Systematics*, *4*(1), 329–357. http://doi.org/10.1146/annurev.es.04.110173.001553
30. Genuer, R., Poggi, J.-M., Tuleau-Malot, C. (2010). Variable selection using random forests. *Pattern Recognition Letters*, *31*(14), 2225–2236. http://doi.org/10.1016/j.patrec.2010.03.014
31. Gibbs, J. P. (2000). Wetland Loss and Biodiversity Conservation. *Conservation Biology*, *14*(1), 314–317. http://doi.org/10.1046/j.1523-1739.2000.98608.x
32. Gorelick, N., Hancher, M., Dixon, M., Ilyushchenko, S., Thau, D., Moore, R. (2017). Google Earth Engine: Planetary-scale geospatial analysis for everyone. *Remote Sensing of Environment*, *202*, 18–27.

http://doi.org/10.1016/j.rse.2017.06.031

33. Griffin, E. R., Smith, J. D. (2004). Floodplain stabilization by woody riparian vegetation during an extreme flood. *Riparian Vegetation and Fluvial Geomorphology Water Science and Application*, 221–236. http://doi.org/10.1029/008wsa16

34. Guyot, G. (1990). Optical Properties Of Vegetation Canopies. *Applications of Remote Sensing in Agriculture*, 19–43. http://doi.org/10.1016/b978-0-408-04767-8.50007-4

35. Gómez, C., White, J. C., Wulder, M. A. (2016). Optical remotely sensed time series data for land cover classification: A review. *ISPRS Journal of Photogrammetry and Remote Sensing*, *116*, 55–72. http://doi.org/10.1016/j.isprsjprs.2016.03.008

36. Halabisky, M., Moskal, L. M., Gillespie, A., Hannam, M. (2016). Reconstructing semi-arid wetland surface water dynamics through spectral mixture analysis of a time series of Landsat satellite images (1984–2011). *Remote Sensing of Environment*, *177*, 171–183. http://doi.org/10.1016/j.rse.2016.02.040

37. Healey, S., Cohen, W., Zhiqiang, Y., Krankina, O. (2005). Comparison of Tasseled Cap-based Landsat data structures for use in forest disturbance detection. *Remote Sensing of Environment*, *97*(3), 301–310. http://doi.org/10.1016/j.rse.2005.05.009

38. Hermosilla, T., Wulder, M. A., White, J. C., Coops, N. C., Hobart, G. W. (2018). Disturbance-Informed Annual Land Cover Classification Maps of Canada's Forested Ecosystems for a 29-Year Landsat Time Series. *Canadian Journal of Remote Sensing*, *44*(1), 67–87. http://doi.org/10.1080/07038992.2018.1437719

39. Huang, C., Goward, S. N., Masek, J. G., Thomas, N., Zhu, Z., Vogelmann, J. E. (2010). An automated approach for reconstructing recent forest disturbance history using dense Landsat time series stacks. *Remote Sensing of Environment*, *114*(1), 183–198. http://doi.org/10.1016/j.rse.2009.08.017

40. Huete, A., Didan, K., Miura, T., Rodriguez, E., Gao, X., Ferreira, L. (2002). Overview of the radiometric and biophysical performance of the MODIS vegetation indices. *Remote Sensing of Environment*, *83*(1-2), 195–213. http://doi.org/10.1016/s0034-4257(02)00096-2

41. Jin, S., Yang, L., Danielson, P., Homer, C., Fry, J., Xian, G. (2013). A comprehensive change detection method for updating the National Land Cover Database to circa 2011. *Remote Sensing of Environment*, *132*, 159–175. http://doi.org/10.1016/j.rse.2013.01.012

42. Johnston, C. A. (2013). Wetland Losses Due to Row Crop Expansion in the Dakota Prairie Pothole Region. *Wetlands*, *33*(1), 175–182. http://doi.org/10.1007/s13157-012-0365-x

43. Johnston, R., Barson, M. (1993). Remote sensing of Australian wetlands: An

evaluation of Landsat TM data for inventory and classification. *Marine and Freshwater Research*, *44*(2), 235. http://doi.org/10.1071/mf9930235

44. Kayastha, N., Thomas, V., Galbraith, J., Banskota, A. (2012). Monitoring Wetland Change Using Inter-Annual Landsat Time-Series Data. *Wetlands*, *32*(6), 1149–1162. http://doi.org/10.1007/s13157-012-0345-1
45. Keddy, P. A. (2014). *Wetland ecology principles and conservation*. Cambridge Univ. Press.
46. Kendall, M. G. (1938). A New Measure of Rank Correlation. *Biometrika*, *30*(1/2), 81. http://doi.org/10.2307/2332226
47. Kudray, G. M., Gale, M. R. (2000). Evaluation of National Wetland Inventory maps in a heavily forested region in the upper Great Lakes. *Wetlands*, *20*(4), 581–587. http://doi.org/10.1672/0277-5212(2000)020[0581:eonwim]2.0.co;2
48. Lehner, B., Döll, P. (2004). Development and validation of a global database of lakes, reservoirs and wetlands. *Journal of Hydrology*, *296*(1-4), 1–22. http://doi.org/10.1016/j.jhydrol.2004.03.028
49. *Malheur National Wildlife Refuge: comprehensive conservation plan*. (2013). U.S. Department of the Interior, U.S. Fish and Wildlife Service, Malheur National Wildlife Refuge.
50. Melaas, E. K., Friedl, M. A., Zhu, Z. (2013). Detecting interannual variation in deciduous broadleaf forest phenology using Landsat TM/ETM data.

Remote Sensing of Environment, *132*, 176–185. http://doi.org/10.1016/j.rse.2013.01.011

51. Mitsch, W. J., Gosselink, J. G. (2000). *Wetlands*. John Wiley.
52. Mitsch, W. J., Gosselink, J. G. (2015). *Wetlands*. John Wiley Sons.
53. Nelli, F. (2015). Machine Learning with scikit-learn. *Python Data Analytics*, 237–264. http://doi.org/10.1007/978-1-4842-0958-5_8
54. Nicholls, R. J. (2004). Coastal flooding and wetland loss in the 21st century: changes under the SRES climate and socio-economic scenarios. *Global Environmental Change*, *14*(1), 69–86. http://doi.org/10.1016/j.gloenvcha.2003.10.007
55. Nielsen, E. M., Prince, S. D., Koeln, G. T. (2008). Wetland change mapping for the U.S. mid-Atlantic region using an outlier detection technique. *Remote Sensing of Environment*, *112*(11), 4061–4074. http://doi.org/10.1016/j.rse.2008.04.017
56. Omernik, J. M., Griffith, G. E. (2014). Ecoregions of the Conterminous United States: Evolution of a Hierarchical Spatial Framework. *Environmental Management*, *54*(6), 1249–1266. http://doi.org/10.1007/s00267-014-0364-1
57. Pal, M. (2005). Random forest classifier for remote sensing classification. *International Journal of Remote Sensing*, *26*(1), 217–222. http://doi.org/10.1080/01431160412331269698
58. Pasquarella, V. J., Holden, C. E., Kaufman, L., Woodcock, C. E. (2016).

From imagery to ecology: leveraging time series of all available Landsat observations to map and monitor ecosystem state and dynamics. *Remote Sensing in Ecology and Conservation*, *2*(3), 152–170. http://doi.org/10.1002/rse2.24

59. Pasquarella, V. J., Holden, C. E., Woodcock, C. E. (2018). Improved mapping of forest type using spectral-temporal Landsat features. *Remote Sensing of Environment*, *210*, 193–207. http://doi.org/10.1016/j.rse.2018.02.064
60. Pekel, J.-F., Cottam, A., Gorelick, N., Belward, A. S. (2016). High-resolution mapping of global surface water and its long-term changes. *Nature*, *540*(7633), 418–422. http://doi.org/10.1038/nature20584
61. Pengra, B., Gallant, A., Zhu, Z., Dahal, D. (2016). Evaluation of the Initial Thematic Output from a Continuous Change-Detection Algorithm for Use in Automated Operational Land-Change Mapping by the U.S. Geological Survey. *Remote Sensing*, *8*(10), 811. http://doi.org/10.3390/rs8100811
62. Potapov, P. V., Turubanova, S. A., Hansen, M. C., Adusei, B., Broich, M., Altstatt, A., … Justice, C. O. (2012). Quantifying forest cover loss in Democratic Republic of the Congo, 2000–2010, with Landsat ETM data. *Remote Sensing of Environment*, *122*, 106–116. http://doi.org/10.1016/j.rse.2011.08.027
63. Rodriguez-Galiano, V., Ghimire, B., Rogan, J., Chica-Olmo, M.,

Rigol-Sanchez, J. (2012). An assessment of the effectiveness of a random forest classifier for land-cover classification. *ISPRS Journal of Photogrammetry and Remote Sensing*, *67*, 93–104. http://doi.org/10.1016/j.isprsjprs.2011.11.002

64. Sagar, S., Roberts, D., Bala, B., Lymburner, L. (2017). Extracting the intertidal extent and topography of the Australian coastline from a 28 year time series of Landsat observations. *Remote Sensing of Environment*, *195*, 153–169. http://doi.org/10.1016/j.rse.2017.04.009
65. Sagar, S., Phillips, C., Bala, B., Roberts, D., Lymburner, L. (2018). Generating Continental Scale Pixel-Based Surface Reflectance Composites in Coastal Regions with the Use of a Multi-Resolution Tidal Model. *Remote Sensing*, *10*(3), 480. http://doi.org/10.3390/rs10030480
66. Schmidt, K., Skidmore, A. (2003). Spectral discrimination of vegetation types in a coastal wetland. *Remote Sensing of Environment*, *85*(1), 92–108. http://doi.org/10.1016/s0034-4257(02)00196-7
67. Schroeder, T. A., Wulder, M. A., Healey, S. P., Moisen, G. G. (2011). Mapping wildfire and clearcut harvest disturbances in boreal forests with Landsat time series data. *Remote Sensing of Environment*, *115*(6), 1421–1433. http://doi.org/10.1016/j.rse.2011.01.022
68. Smith, L. M., Pederson, R. L., Kaminski, R. M. (1989). *Habitat management for migrating and wintering waterfowl in North America*. Texas Tech

University Press.

69. Snodgrass, J. W., Komoroski, M. J., Bryan, A. L., Burger, J. (2000). Relationships among Isolated Wetland Size, Hydroperiod, and Amphibian Species Richness: Implications for Wetland Regulations. *Conservation Biology*, *14*(2), 414–419. http://doi.org/10.1046/j.1523-1739.2000.99161.x
70. Stolt, M. H., Baker, J. C. (1995). Evaluation of national wetland inventory maps to inventory wetlands in the southern Blue Ridge of Virginia. *Wetlands*, *15*(4), 346–353. http://doi.org/10.1007/bf03160889
71. Todd, M. J., Muneepeerakul, R., Pumo, D., Azaele, S., Miralles-Wilhelm, F., Rinaldo, A., Rodriguez-Iturbe, I. (2010). Hydrological drivers of wetland vegetation community distribution within Everglades National Park, Florida. *Advances in Water Resources*, *33*(10), 1279–1289. http://doi.org/10.1016/j.advwatres.2010.04.003
72. Townsend, P., Foster, J. Assessing flooding and vegetation structure in forested wetlands using Radarsat SAR imagery. *IEEE International Geoscience and Remote Sensing Symposium*. http://doi.org/10.1109/igarss.2002.1025811
73. Verbesselt, J., Hyndman, R., Newnham, G., Culvenor, D. (2010). Detecting trend and seasonal changes in satellite image time series. *Remote Sensing of Environment*, *114*(1), 106–115. http://doi.org/10.1016/j.rse.2009.08.014
74. Vogelmann, J. E., Sohl, T. L., Campbell, P. V., Shaw, D. M. (1998). Regional

Land Cover Characterization Using Landsat Thematic Mapper Data and Ancillary Data Sources. *Monitoring Ecological Condition at Regional Scales*, 415–428. http://doi.org/10.1007/978-94-011-4976-1_32

75. Vogelmann, J. E., Xian, G., Homer, C., Tolk, B. (2012). Monitoring gradual ecosystem change using Landsat time series analyses: Case studies in selected forest and rangeland ecosystems. *Remote Sensing of Environment*, *122*, 92–105. http://doi.org/10.1016/j.rse.2011.06.027
76. Wilen, B. O., Bates, M. K. (1995). The US Fish and Wildlife Service's National Wetlands Inventory Project. *Classification and Inventory of the World's Wetlands*, 153–169. http://doi.org/10.1007/978-94-011-0427-2_13
77. Wright, C., Gallant, A. (2007). Improved wetland remote sensing in Yellowstone National Park using classification trees to combine TM imagery and ancillary environmental data. *Remote Sensing of Environment*, *107*(4), 582–605. http://doi.org/10.1016/j.rse.2006.10.019
78. Yuan, L., Zhang, L.-Q. (2008). Mapping large-scale distribution of submerged aquatic vegetation coverage using remote sensing. *Ecological Informatics*, *3*(3), 245–251. http://doi.org/10.1016/j.ecoinf.2008.01.004
79. Zhang, Q., Li, L., Wang, Y.-G., Werner, A. D., Xin, P., Jiang, T., Barry, D. A. (2012). Has the Three-Gorges Dam made the Poyang Lake wetlands wetter and drier? *Geophysical Research Letters*, *39*(20). http://doi.org/10.1029/2012gl053431

80. Zhang, Q., Chen, K., Jing, Q., Chen, X. (2016). Automatic invalid Landsat image pixel screening on the Google Earth engine platform. *2016 IEEE International Geoscience and Remote Sensing Symposium (IGARSS)*. http://doi.org/10.1109/igarss.2016.7729615

81. Zhu, Z., Woodcock, C. E. (2014). Continuous change detection and classification of land cover using all available Landsat data. *Remote Sensing of Environment*, *144*, 152–171. http://doi.org/10.1016/j.rse.2014.01.011

82. Zhu, Z., Woodcock, C. E. (2012). Object-based cloud and cloud shadow detection in Landsat imagery. *Remote Sensing of Environment*, *118*, 83–94. http://doi.org/10.1016/j.rse.2011.10.028

83. Zomer, R., Trabucco, A., Ustin, S. (2009). Building spectral libraries for wetlands land cover classification and hyperspectral remote sensing. *Journal of Environmental Management*, *90*(7), 2170–2177. http://doi.org/10.1016/j.jenvman.2007.06.028